

Juan Vicente Alegre Requena

Synthesis of squaramides and
their application in
organocatalysis: computational
and experimental studies

Departamento
Química Orgánica

Director/es
Marqués López, M^a Eugenia
Pérez Herrera, Raquel

EXTRACTO

<http://zaguan.unizar.es/collection/Tesis>

El presente documento es un extracto de la tesis original depositada en el Archivo Universitario.

En cumplimiento del artículo 14.6 del Real Decreto 99/2011, de 28 de enero, por el que se regulan las enseñanzas oficiales de doctorado, los autores que puedan verse afectados por alguna de las excepciones contempladas en la normativa citada deberán solicitar explícitamente la no publicación del contenido íntegro de su tesis doctoral en el repositorio de la Universidad de Zaragoza. Las situaciones excepcionales contempladas son:

- Que la tesis se haya desarrollado en los términos de un convenio de confidencialidad con una o más empresas o instituciones.
- Que la tesis recoja resultados susceptibles de ser patentados.
- Alguna otra circunstancia legal que impida su difusión completa en abierto.



Reconocimiento – NoComercial – SinObraDerivada (by-nc-nd): No se permite un uso comercial de la obra original ni la generación de obras derivadas.

© Universidad de Zaragoza
Servicio de Publicaciones

ISSN 2254-7606

Tesis Doctoral [Extracto]

SYNTHESIS OF SQUARAMIDES AND THEIR
APPLICATION IN ORGANOCATALYSIS:
COMPUTATIONAL AND EXPERIMENTAL STUDIES

Autor

Juan Vicente Alegre Requena

Director/es

Marqués López, M^a Eugenia
Pérez Herrera, Raquel

UNIVERSIDAD DE ZARAGOZA

Química Orgánica

2017



Universidad
Zaragoza



SYNTHESIS OF SQUARAMIDES AND THEIR APPLICATION IN ORGANOCATALYSIS: COMPUTATIONAL AND EXPERIMENTAL STUDIES

Doctoral Thesis

Directors:

Dr. Raquel Pérez Herrera

Dr. María Eugenia Marqués López

Department of Organic Chemistry

Faculty of Science

University of Zaragoza

20 September 2017

Juan Vicente Alegre Requena



Departamento de
Química Orgánica
Universidad Zaragoza



This doctoral thesis is presented as a thesis by publications (*compendio de publicaciones*). The four papers included are interrelated with each other and focus on the synthesis of squaramides and their use to catalyze the Henry reaction.

1. a) Alegre-Requena, J. V.; Marqués-López, E.; Herrera, R. P. One-Pot Synthesis of Unsymmetrical Squaramides. *RSC Adv.* **2015**, 5, 33450-33462.

IF(2015) = 3.289. Q2 (49/163 in Chemistry, Multidisciplinary).

- b) Alegre-Requena, J. V.; Marqués-López, E.; Herrera, R. P. One-Pot Synthesis of Squaramides. WO2016005407 A1, January 14, 2016.

International (PCT) patent.

Chapter 2.

2. Alegre-Requena, J. V.; Marqués-López, E.; Herrera, R. P. Trifunctional Squaramide Catalyst for Efficient Enantioselective Henry Reaction Activation. *Adv. Synth. Catal.* **2016**, 358, 1801-1809.

IF(2016) = 5.646. Q1 (2/72 in Chemistry, Applied).

Highlighted in *Synfacts* **2016**, 12, 743.

Chapter 3.

3. Alegre-Requena, J. V.; Marqués-López, E.; Herrera, R. P. Optimizing Accuracy and Computational Cost in Theoretical Squaramide Catalysis: the Henry Reaction. *Chem. Eur. J.* **2017**, DOI: 10.1002/chem.201702841.

IF(2016) = 5.317. Q1 (29/166 in Chemistry, Multidisciplinary).

Frontispiece cover, hot paper.

Chapter 4.

4. Alegre-Requena, J. V.; Marqués-López, E.; Herrera, R. P. "Push-Pull π^+/π^- " (PP $\pi\pi$) Systems in Catalysis. *ACS Catal.* **2017**, 7, 6430-6439.

IF(2016) = 10.614. Q1 (11/145 in Chemistry, Physical).

Main cover.

Chapter 5.

INFORME DE LAS DIRECTORAS

La Dra. María Eugenia Marqués López, Profesora Contratado Doctor y la Dra. Raquel Pérez Herrera, Científico Titular, ambas del Departamento de Química Orgánica de la Universidad de Zaragoza,

AUTORIZAN

La presentación en la modalidad de *Compendio de publicaciones* de la memoria titulada:

SYNTHESIS OF SQUARAMIDES AND THEIR APPLICATION IN ORGANOCATALYSIS: COMPUTATIONAL AND EXPERIMENTAL STUDIES

SÍNTESIS DE ESCUARAMIDAS Y SU APLICACIÓN EN ORGANOCATÁLISIS: ESTUDIOS EXPERIMENTALES Y COMPUTACIONALES

presentada por D. Juan Vicente Alegre Requena para optar al grado de Doctor por la Universidad de Zaragoza y certifican que ha sido realizada bajo su dirección en el Laboratorio de Organocatálisis Asimétrica del Departamento de Química Orgánica.

Y para que así conste, expiden la presente autorización

en Zaragoza, a 20 de Septiembre de 2017



Fdo. Raquel Pérez Herrera



Fdo. M^a Eugenia Marqués López

JUSTIFICACIÓN DE LA CONTRIBUCIÓN DEL DOCTORANDO

La Dra. María Eugenia Marqués López, Profesora Contratado Doctor y la Dra. Raquel Pérez Herrera, Científico Titular, ambas del Departamento de Química Orgánica de la Universidad de Zaragoza, y directoras de la presente Tesis Doctoral,

CERTIFICAN

Que D. Juan Vicente Alegre Requena ha llevado a cabo la mayor parte del trabajo experimental en todos los trabajos. Asimismo, también ha realizado la caracterización e interpretación de resultados necesaria para finalizar con éxito los distintos estudios.

Por otra parte, el doctorando es primer autor en todas las publicaciones y no hay otros co-autores además de las directoras. Por ello, no existe la posibilidad de que los trabajos recogidos en esta Tesis Doctoral puedan ser usados en otras tesis.

Y para que así conste, expiden el presente certificado

en Zaragoza, a 20 de Septiembre de 2017

Fdo. Raquel Pérez Herrera

Fdo. M^a Eugenia Marqués López

Abbreviations

BMIM = 1-butyl-3-methylimidazolium

C = concentration

DFT = density functional theory

E = electronic energy

ee = enantiomeric excess

EHB = hydrogen bond energy

Eint = electronic interaction energy

eq = equivalent

ESP = electrostatic potential

EtOAc = ethyl acetate

G = Gibbs free energy

Hex = hexane

HPLC = high performance liquid chromatography

HR = hindered rotor corrections

ⁱPrOH = isopropanol

NCI = non-covalent interaction

n.d. = not determined

NMR = nuclear magnetic resonance

n.r. = no reaction observed

QHA = quasi-harmonic approximation

Rac. = racemic mixture

SMD = solvation model based on density

^tBu = *tert*-butyl

TLC = thin layer chromatography

Tos = tosyl

UF = ultrafine

V(rcp) = potential energy density at critical points of hydrogen bonds

[α] = specific rotation

$\Delta\Delta G^\ddagger$ = difference of G between the **TS1** of pathways **P1** and **P3** ($G^{\text{TS1(P1)}} - G^{\text{TS1(P3)}}$)

λ = wavelength

ρ = electron density

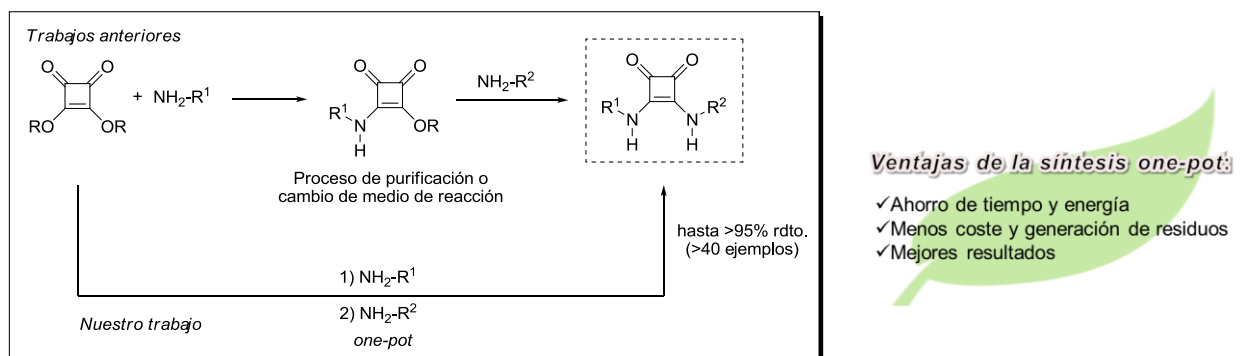
τ = elution time

$\nabla^2\rho$ = Laplacian of the electron density

RESUMEN DE LA TESIS EN ESPAÑOL

Las escuaramidas han resultado ser compuestos de marcado interés en distintas ramas de la química.^[1] El uso de las escuaramidas quirales como organocatalizadores es interesante ya que, usando la escuaramida adecuada, se crean entornos quirales ideales para la obtención de productos enriquecidos enantioméricamente mediante la formación de enlaces de hidrógeno con los sustratos. Una de las líneas principales de investigación de nuestro grupo es la síntesis y la aplicación organocatalítica de este tipo de compuestos, lo que nos ha llevado a desarrollar durante esta tesis doctoral reacciones quirales poco exploradas anteriormente en esta área.

En primer lugar, es muy importante disponer de un método eficaz de síntesis de escuaramidas, motivos estructurales centro de investigaciones posteriores. La síntesis tradicional de escuaramidas consta de dos reacciones independientes de adición de aminas. Sin embargo, a través del diseño de un método de síntesis *one-pot*, conseguimos sintetizar las escuaramidas empleando un único reactor, con las ventajas asociadas de ahorro de tiempo, energía, dinero, menor generación de residuos, etc. (Esquema 1).^[2]



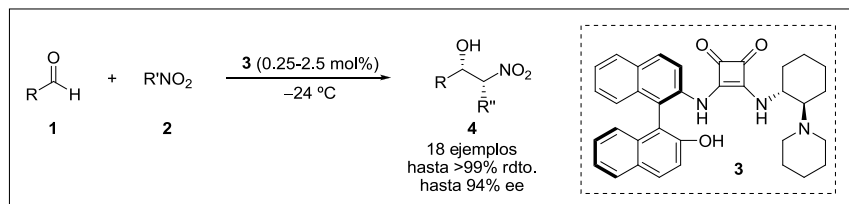
Esquema 1. Síntesis *one-pot* de escuaramidas no simétricas.

Una de nuestras mayores prioridades dentro de esta tesis ha sido el desarrollo de reacciones organocatalíticas usando escuaramidas que dan lugar a productos enantioméricamente enriquecidos con potencial actividad biológica. A lo largo de esta tesis doctoral, desarrollamos la reacción de Henry catalizada por la escuaramida **3**, obteniéndose los correspondientes β -nitroalcoholes (**4**) con muy buenos rendimientos y enantioselectividades

[1] a) Schmidt, A. H. *Synthesis* **1980**, 961; b) Alemán, J.; Parra, A.; Jiang, H.; Jørgensen, K. A. *Chem. Eur. J.* **2011**, *17*, 6890; c) Storer, R. I.; Aciro, C.; Jones, L. H. *Chem. Soc. Rev.* **2011**, *40*, 2330; d) Wurm, F. R.; Klok, H.-A. *Chem. Soc. Rev.* **2013**, *42*, 8220; e) Alegre-Requena, J. V. *Synlett* **2014**, 25, 298.

[2] Alegre-Requena, J. V.; Marqués-López, E.; Herrera, R. P. *RSC Adv.* **2015**, *5*, 33450.

(Esquema 2).^[3] Además, en algunos casos la carga catalítica requerida fue de tan sólo 0.25 mol%, siendo la más baja conocida para esta reacción en el campo de la organocatálisis.



Esquema 2. Reacción quiral de Henry desarrollada durante esta tesis doctoral.

Asimismo, también estudiamos el mecanismo de la reacción de Henry catalizada con la escuaramida **3** anteriormente descrita.^[4] Para ello, realizamos distintos estudios computacionales en combinación con los propios datos experimentales. Además, estudiamos distintas combinaciones de métodos y conjuntos de funciones de base para averiguar cuál de ellas llevaba a los mejores resultados. En este estudio, la combinación más precisa fue la formada por el funcional ω B97X-D y el conjunto de funciones 6-311G(d). Este análisis representa el primer ejemplo en el cual se compara la eficiencia de distintas aproximaciones computacionales en la catálisis con escuaramidas.

Además, se observó que en esta reacción existe un modo de interacción peculiar que nunca antes se había visto en catálisis, llamado “push-pull π +/ π -”.^[5] Este modo consiste en dos interacciones π creadas por los anillos aromáticos de un grupo naftilo del catalizador **3** con dos átomos del grupo aldehído, uno δ^+ (su átomo de hidrógeno) y el otro δ^- (su átomo de oxígeno) (Figura 1).

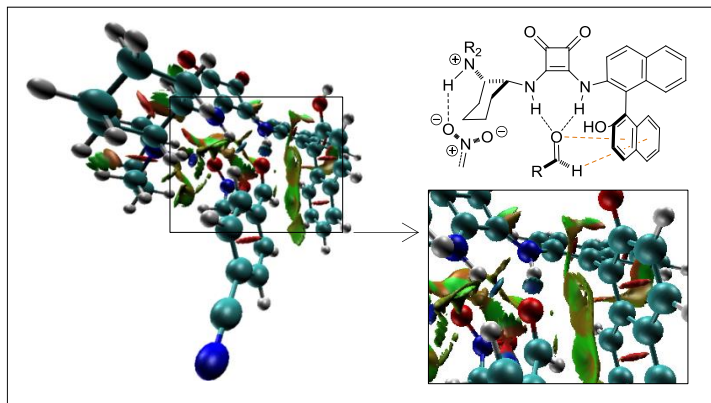


Figura 1. Ejemplo de interacciones π formadas en el sistema “push-pull π +/ π -” generado en la reacción de Henry estudiada.

[3] Alegre-Requena, J. V.; Marqués-López, E.; Herrera, R. P. *Adv. Synth. Catal.* **2016**, 358, 1801. Destacado en *Synfacts* **2016**, 12, 743.

[4] Alegre-Requena, J. V.; Marqués-López, E.; Herrera, R. P. *Chem. Eur. J.* **2017**, DOI: 10.1002/chem.201702841.

[5] Alegre-Requena, J. V.; Marqués-López, E.; Herrera, R. P. *ACS Catal.* **2017**, 7, 6430.

Table of Contents

1. GENERAL INTRODUCTION		1
1.1 Enantioselective Organocatalysis and Squaramides	1	
1.2 Properties of Squaramides	2	
1.3 Squaramide Organocatalysts	4	
1.4 References	6	
2. ONE-POT SYNTHESIS OF UNSYMMETRICAL SQUARAMIDES		9
2.1 Introduction	9	
2.2 Objectives	10	
2.3 Results and Discussion	11	
2.4 Conclusions	22	
2.5 References	22	
2.6 Article	25	
2.7 Supporting Information	39	
3. TRIFUNCTIONAL SQUARAMIDE CATALYST FOR EFFICIENT ENANTIOSELECTIVE HENRY REACTION ACTIVATION		41
3.1 Introduction	41	
3.2 Objectives	43	
3.3 Results and Discussion	43	
3.4 Conclusions	50	
3.5 References	51	
3.6 Article	53	
3.7 Supporting Information	63	
4. OPTIMIZING ACCURACY AND COMPUTATIONAL COST IN THEORETICAL SQUARAMIDE CATALYSIS: THE HENRY REACTION		71
4.1 Introduction	71	
4.2 Objectives	72	
4.3 Results and Discussion	72	
4.4 Conclusions	91	
4.5 References	92	
4.6 Article	97	
4.7 Supporting Information	111	
5. "PUSH-PULL π^+/π^-" (PP$\pi\pi$) SYSTEMS IN CATALYSIS		119
5.1 Introduction	119	
5.2 Objectives	119	
5.3 Results and Discussion	120	
5.4 Conclusions	134	
5.5 References	135	
5.6 Article	137	
5.7 Supporting Information	147	
6. CONCLUSIONES GENERALES		149
ANNEX 1. PUBLICATIONS AND CONFERENCES		151
A1.1 Publications that Are Related to the Content of this Thesis	151	
A1.2 Complete List of Publications	153	
A1.3 Complete List of Patents	154	
A1.2 Complete List of Conferences	155	

1

GENERAL INTRODUCTION

1.1 Enantioselective Organocatalysis and Squaramides

The development of new enantioselective processes is an area that has a tremendous impact in the synthesis of new chiral compounds with commercial applications.^[1] In this field, catalysis plays a key role, since catalyzed reactions improve significantly the efficiency and selectivity of chiral transformations while they only require low amounts of catalysts. For this reason, the development of more effective catalysts has become crucial within the scientific community, since it is in line with the growing trend to design chemical transformations that entail minimal repercussions in the environment.

Traditionally, researchers just employed two main groups of catalysts, metal catalysts and enzymes; however, quite recently, a new type of catalysis emerged and quickly attracted the attention of a wide audience: organocatalysis. Currently, enantioselective organocatalysis has become a suitable alternative for carrying out relevant processes that classically have been dominated by the other two types of catalysis,^[2] including the synthesis of natural products with significant biological activity.^[3] Some of the most important families of catalysts in this area are proline derivatives (**1**), cinchona alkaloids (**2**), phase transfer catalysts (**3**), phosphoric acids (**4**), (thio)ureas (**5**) and squaramides (**6**), among others (Figure 1.1).

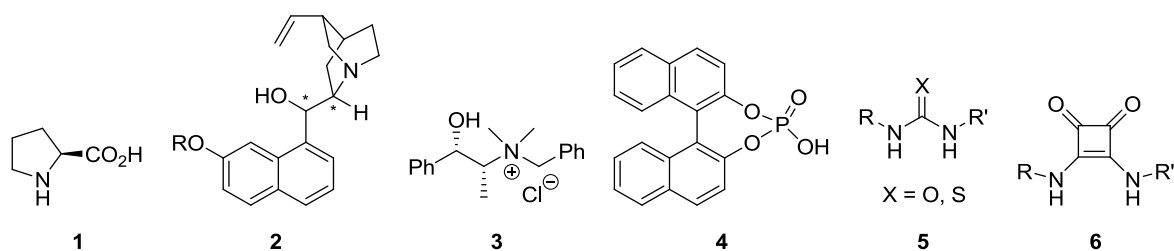


Figure 1.1. Some of the most relevant families of organocatalysts.

Within these families, squaramides are compounds that are breaking new ground in the field of organocatalysis. They have been successfully used in other areas of Chemistry,^[4] but that success pales in comparison to the results they have had in organocatalysis.^[5] This is mainly due to the interesting combination of using hydrogen bond catalysis together with chiral bifunctional structures. Their importance in organocatalysis is shown in the increasing number of reactions that are being developed using squaramides. Also, despite they were introduced very recently, diverse squaramide-catalyzed reactions have been employed in the synthesis of relevant natural products (Figure 1.2).

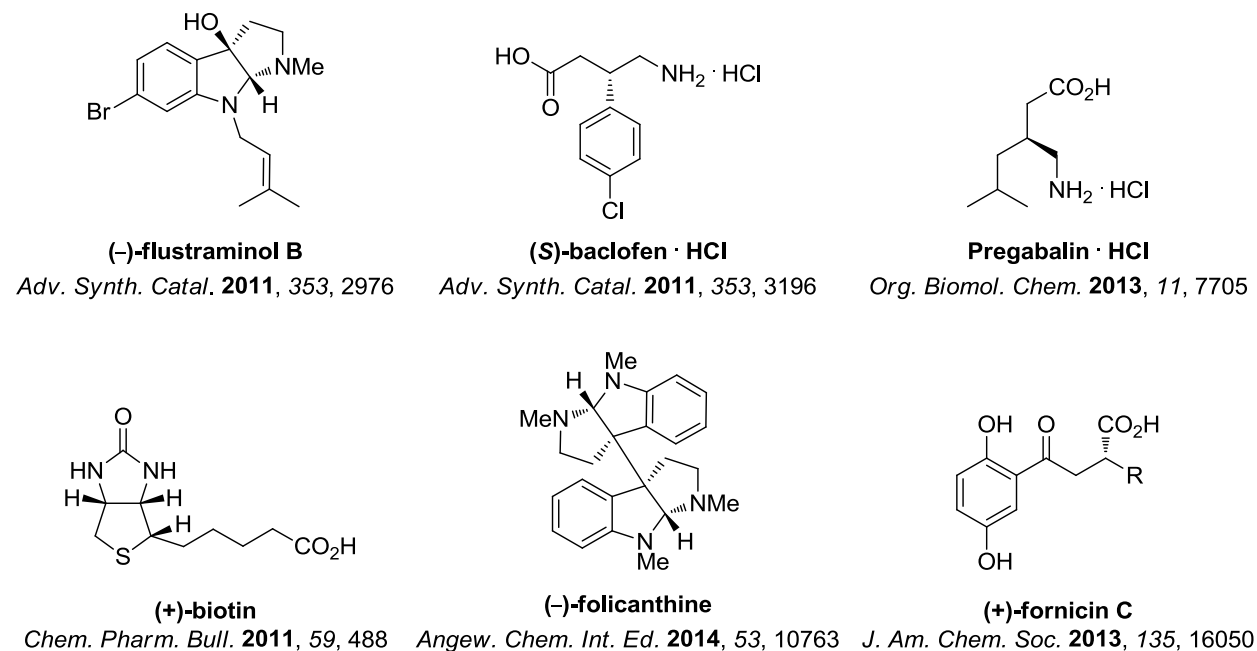


Figure 1.2. Examples of biologically active products synthesized with squaramide organocatalysts.

1.2 Properties of Squaramides

Squaramides are compounds that have shown properties that are as intriguing as they are appealing. One of the most important characteristic of these compounds is that their cyclobutene core is aromatic. This has a significant repercussion in the structural features as well as in the acidity of the hydrogen atoms of squaramides. Aromaticity of the cyclobutene ring in squaramides was initially studied by Frontera and coworkers.^[6] In these pioneering computational studies, the authors determined not only that squaramide moieties were aromatic, but also that their aromaticity increased when these structures formed hydrogen bonds with different substrates. The increase in the aromaticity of the cyclobutene rings is a factor that strengthens the hydrogen bonds formed between the NH bonds or the carbonyl groups of the squaramide and different substrates.

Another relevant feature of squaramides is that the lone electron pairs of the nitrogen atoms are delocalized throughout the cyclobutenedione system (Figure 1.3, A).^[7] One consequence of this electron delocalization is that the two nitrogen atoms of the squaramide group show sp^2 hybridization, which make the squaramide group (cyclobutene ring, ketone and amine groups) planar.

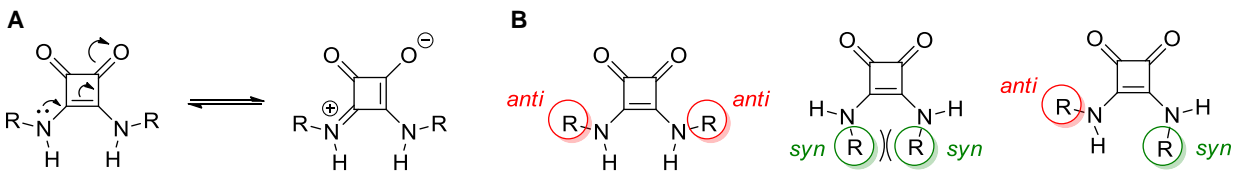


Figure 1.3. Structural features of squaramides. (A) Example of a resonant structure in the delocalization of the lone electron pair of a nitrogen atom throughout the squaramide group. (B) Different dispositions that the substituents can adopt in squaramide molecules.

The amide-like conformation of the nitrogen atoms also induces the formation of two different positions that the nitrogen substituents can adopt: *syn* and *anti* (Figure 1.3, B).^[8] Depending on the substituents and the media conditions, the positions of the substituents can be modulated with precision. This is a property that results crucial to understand why squaramides have shown outstanding results in diverse organocatalyzed reactions. In this field, structures with rigid cores without many possible conformations are highly desired for the catalysts. The vast majority of the squaramide catalysts employed, which contain disubstituted nitrogen atoms, adopt the *anti/anti* conformation in solids and they do not show significant amounts of the isomers *anti/syn* and *syn/syn* in their ¹H-NMR spectra in DMSO.^[9]

Within all the features that these compounds exhibit, the property that has made these compounds more appealing for organocatalysis has probably been the acidity of the squaramide NH hydrogens. These hydrogen atoms are generally more acidic than the hydrogen atoms of their analogous thioureas and ureas (Figure 1.4).^[10] This influences the activity of the catalysts, which normally bind more tightly to the substrates and activate the reactions in a greater extent. The superior acidity of squaramides compared to the acidities of their analogous thioureas opens promising unexplored possibilities, such as obtaining higher performances than thioureas in reactions where the acidity of NH hydrogens plays an important role.^[11]

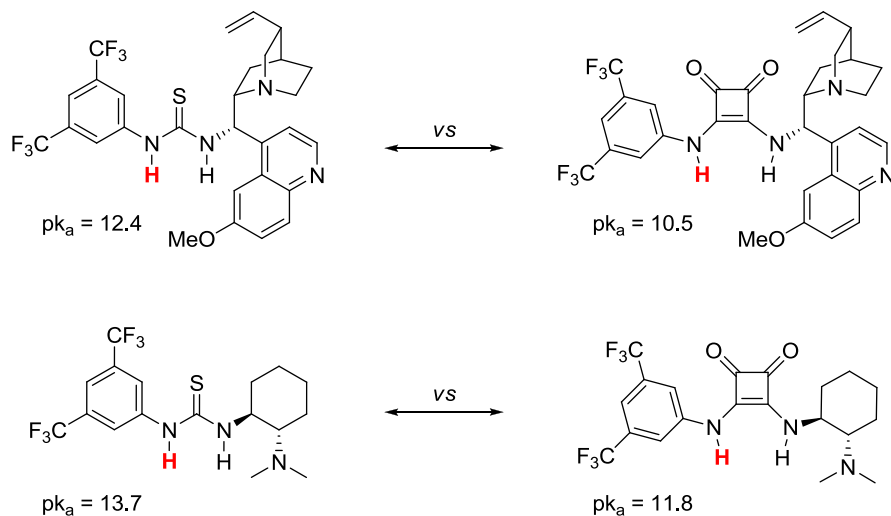
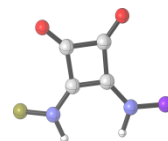


Figure 1.4. p_{K_a} values of the most acidic NH hydrogen of relevant thiourea-based organocatalysts and their equivalent squaramides.^[10,12]



Even though the structure of squaramide groups may initially resemble that of ureas and thioureas, there are significant differences between their structures. For example, the distance between the two NH hydrogen atoms is considerably larger in squaramides than in ureas (Figure 1.5, A).^[4a,13] Also, the distance between these atoms and the oxygen of the carbonyl groups is longer in squaramides. Furthermore, the position and direction of the NH bonds vary depending on the type of compound: while the NH bonds of (thio)ureas are parallel and their directions are the same, these bonds are not parallel and their orientation is different in squaramides (Figure 1.5, B).^[5a] This is a critical structural characteristic of organocatalysts, since the positions and directions of the NH bonds in these molecules significantly influence the strength of the hydrogen bonds formed with the substrates of a reaction.

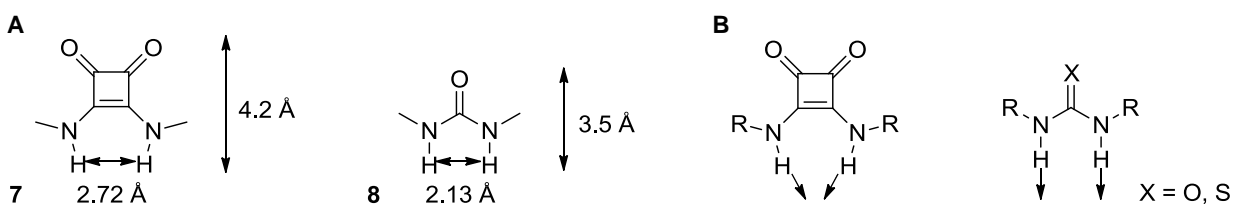
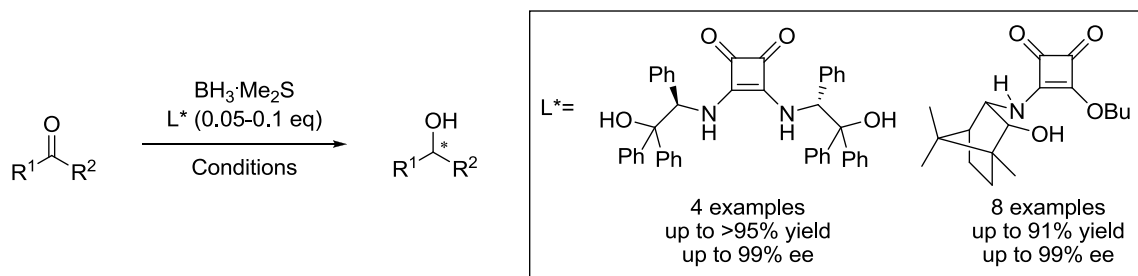


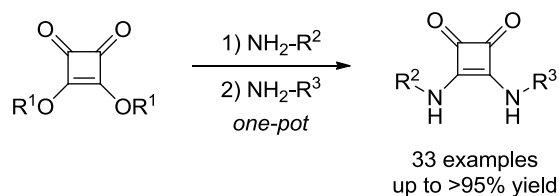
Figure 1.5. Structural features of squaramides and (thio)ureas. (A) Representative distances of squaramide **7** and its analogous urea **8**. (B) Direction of the NH bonds of squaramides and (thio)ureas.

1.3 Squaramide Organocatalysts

Before the discovery of the promising and useful properties that squaramides have shown in the field of hydrogen bond organocatalysis, they were used as ligands for different hydroboration reactions. The pioneering studies in this area were carried out by Xie and coworkers in 2001.^[14] In this year, this research group developed various hydroboration reactions (Scheme 1.1), paving the way for other investigations that were developed in the following years.^[15] In Xie and coworkers' studies, the authors did not propose any transition state where hydrogen bonds were generated between the hydrogens of the squaramide moieties and the substrates.^[15b] However, this kind of interaction might have played an important role since many of the squaramides used in these reactions had acidic hydrogens capable of forming hydrogen bonds with ketones.

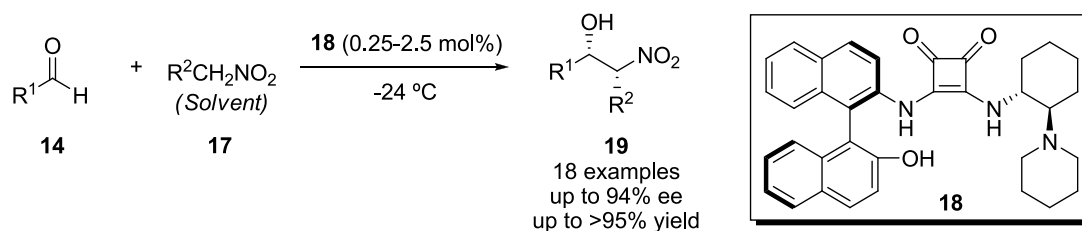


Scheme 1.1. Examples of squaramides used as ligands in hydroboration reactions.



Scheme 1.4. One-pot synthesis of squaramides developed at the beginning of this PhD dissertation.

With this one-pot synthetic method, we generated a great number of new squaramides whose structures were designed to promote diverse asymmetric reactions. One of them, squaramide **18**, showed very good results in the Henry reaction (Scheme 1.5), which encouraged us to study in detail the reaction mechanism using computational and experimental chemistry.



Scheme 1.5. Henry reaction catalyzed by squaramide **18**.

The mechanistic study revealed many unexplored features about this reaction, such as the structures of the catalyst-substrate complexes and the energy profiles of the reaction pathways. Interestingly, the catalyst and the substrates created a new interaction system that had not been observed previously in catalysis: a P Π Π system.

1.4 References

[1] a) Jacobsen, E. N.; Pfaltz, A.; Yamamoto, H. (Eds.) *Comprehensive Asymmetric Catalysis*. 2^a ed. Springer-Verlag: Berlin-Heidelberg, **2004**; b) Mikami, K.; Lautens, M. (Eds.) *Asymmetric Catalysis*. Wiley: Hoboken-New Jersey, **2007**.

[2] a) Berkessel, A.; Gröger, H. (Eds.) *Asymmetric Organocatalysis*. Wiley-VCH: Weinheim, **2005**; b) Dalko, P. I. (Ed.) *Enantioselective Organocatalysis: Reaction and Experimental Procedures*. Wiley & Sons: New York, **2007**; c) Dalko, P. (Ed.) *Comprehensive Enantioselective Organocatalysis*. Wiley-VCH: Weinheim, **2013**.

[3] a) de Figueiredo, R. M.; Christmann, M. *Eur. J. Org. Chem.* **2007**, 2575; b) Marqués-López, E.; Herrera, R. P.; Christmann, M. *Nat. Prod. Rep.* **2010**, 27, 1138; c) Marqués-López, E.; Herrera, R. P. in *Comprehensive Enantioselective Organocatalysis*. Dalko, P. (Ed.). Wiley-VCH: Weinheim, **2013**, pp 1359-1383.

[4] a) Storer, R. I.; Aciro, C.; Jones, L. H. *Chem. Soc. Rev.* **2011**, *40*, 2330; b) Wurm, F. R.; Klok, H.-A. *Chem. Soc. Rev.* **2013**, *42*, 8220.

[5] a) Alemán, J.; Parra, A.; Jiang, H.; Jørgensen, K. A. *Chem. Eur. J.* **2011**, *17*, 6890; b) Tsakos, M.; Kokotos, C. G. *Tetrahedron* **2013**, *69*, 10199; c) Auvil, T. J.; Schafer, A. G.; Mattson, A. E. *Eur. J. Org. Chem.* **2014**, 2633; d) Alegre-Requena, J. V. *Synlett* **2014**, *25*, 298; e) Chauhan, P.; Mahajan, S.; Kaya, U.; Hack, D.; Enders, D. *Adv. Synth. Catal.* **2015**, *357*, 253.

[6] a) Quiñonero, D.; Frontera, A.; Ballester, P.; Deyà, P. M. *Tetrahedron Lett.* **2000**, *41*, 2001; b) Quiñonero, D.; Garau, C.; Frontera, A.; Ballester, P.; Costa, A.; Deyà, P. M. *Chem. Eur. J.* **2002**, *8*, 433; c) Quiñonero, D.; Prohens, R.; Garau, C.; Frontera, A.; Ballester, P.; Costa, A.; Deyà, P. M. *Chem. Phys. Lett.* **2002**, *351*, 115; d) Frontera, A.; Orell, M.; Garau, C.; Quiñonero, D.; Molins, E.; Mata, I.; Morey, J. *Org. Lett.* **2005**, *7*, 1437.

[7] Deyà, P. M.; Frontera, A.; Suñer, G. A.; Quiñonero, D.; Garau, C.; Costa, A.; Ballester, P. *Theor. Chem. Acc.* **2002**, *108*, 157.

[8] Rotger, M. C.; Piña, M. N.; Frontera, A.; Martorell, G.; Ballester, P.; Deyà, P. M.; Costa, A. *J. Org. Chem.* **2004**, *69*, 2302.

[9] For structures of squaramide crystals, see: a) Prohens, R.; Portell, A.; Puigjaner, C.; Tomàs, S.; Fujii, K.; Harris, K. D. M.; Alcobé, X.; Font-Bardia, M.; Barbas, R. *Cryst. Growth Des.* **2011**, *11*, 3725. For examples of ¹H-NMR spectra in DMSO, see: b) Alegre-Requena, J. V.; Marqués-López, E.; Herrera, R. P. *RSC Adv.* **2015**, *5*, 33450.

[10] Ni, X.; Li, X.; Wang, Z.; Cheng, J.-P. *Org. Lett.* **2014**, *16*, 1786.

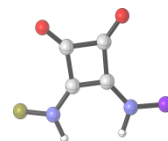
[11] For examples where pK_a values play an important role on the reactivity and/or enantioselectivity, see: a) Li, X.; Deng, H.; Zhang, B.; Li, J.; Zhang, L.; Luo, S.; Cheng, J.-P. *Chem. Eur. J.* **2010**, *16*, 450; b) Marqués-López, E.; Alcaine, A.; Tejero, T.; Herrera, R. P. *Eur. J. Org. Chem.* **2011**, 3700; c) Kaupmees, K.; Tolstoluzhsky, N.; Raja, S.; Rueping, M.; Leito, I. *Angew. Chem. Int. Ed.* **2013**, *52*, 11569; d) Auvil, T. J.; Schafer, A. G.; Mattson, A. E. *Eur. J. Org. Chem.* **2014**, 2633.

[12] Jakab, G.; Tancon, C.; Zhang, Z.; Lippert, K. M.; Schreiner, P. R. *Org. Lett.* **2012**, *14*, 1724.

[13] Malerich, J. P.; Hagihara, K.; Rawal, V. H. *J. Am. Chem. Soc.* **2008**, *130*, 14416.

[14] a) Zhou, H.-B.; Zhang, J.; Lü, S.-M.; Xie, R.-G.; Zhou, Z.-Y.; Choi, M. C. K.; Chan, A. S. C.; Yang, T.-K. *Tetrahedron* **2001**, *57*, 9325; b) Zhang, J.; Zhou, H.-B.; Lü, S.-M.; Luo, M.-M.; Xie, R.-G.; Choi, M. C. K.; Zhou, Z.-Y.; Chan, A. S. C.; Yang, T.-K. *Tetrahedron: Asymmetry* **2001**, *12*, 1907; c) Zhou, H.; Lü, S.; Xie, R.; Chan, A. S. C.; Yang, T.-K. *Tetrahedron Lett.* **2001**, *42*, 1107.

[15] a) Zhou, H.-B.; Zhang, J.; Lü, S.-M.; Xie, R.-G.; Zhou, Z.-Y.; Choi, M. C. K.; Chan, A. S. C.; Yang, T.-K. *Tetrahedron* **2001**, *57*, 9325; b) Zou, H.-H.; Hu, J.; Zhang, J.; You, J.-S.; Ma, D.; Lü, D.; Xie, R.-G. *J. Mol. Catal. A: Chem.* **2005**, *242*, 57.



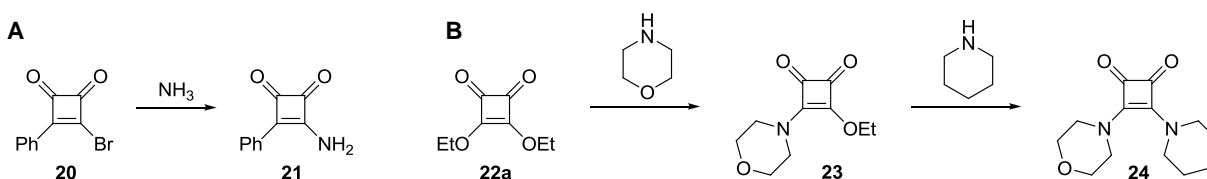
[16] Alegre-Requena, J. V.; Marqués-López, E.; Miguel, P. J. S.; Herrera, R. P. *Org. Biomol. Chem.* **2014**, *12*, 1258.

2

ONE-POT SYNTHESIS OF UNSYMMETRICAL SQUARAMIDES

2.1 Introduction

The first squaramide derivative (**21**) was synthesized by Smutny and Roberts in 1955.^[17] This pioneering squaramide consisted in a 1,2-cyclobutenedione ring bearing a phenyl group and a primary amine. This was achieved by adding ammonia to compound **20**, which had a bromine atom that acted as the leaving group in the amine addition (Scheme 2.1, A). In 1965, Maahs and Hegenberg designed the first synthesis of squaramides that consisted in the substitution of ethoxy groups for amines (Scheme 2.1, B).^[18]



Scheme 2.1. First synthetic protocols designed to obtain squaramides.

The discovery of the latter synthetic strategy starting from dialkyl squarates resulted crucial for the development of squaramides, since it has been the most followed synthetic route to synthesize squaramides up to date. This synthesis starts with the addition of an amine to a dialkyl squarate, normally dimethoxy or diethoxy (**22a**) squarate, to form squaramide monoamines, such as compound **23** (Scheme 2.1, B). Then, the squaramide monoamine is isolated and another amine is added to form the target squaramide. This method is very versatile and leads, generally, to good results.

The design of more efficient and straightforward synthetic protocols is a crucial factor in the development of any field in Chemistry, since the products obtained using these protocols become more accessible to the scientific community. In this context, one-pot syntheses, in which at least two sequential reactions are carried out in a single flask, have been on the spotlight in the last years.^[19] The growing interest that these syntheses have is related to the increasing importance that green chemistry principles, such as saving resources and reducing waste generation, have among scientists.

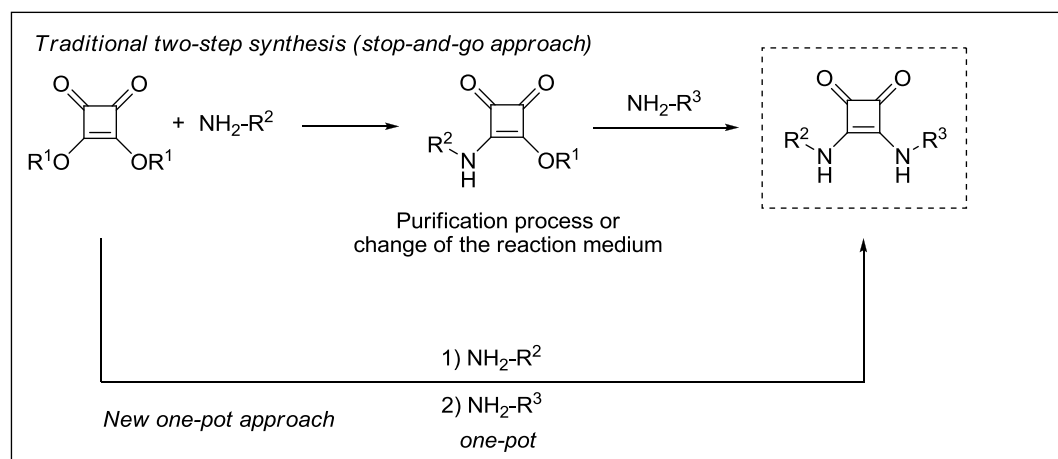
In syntheses with multiple steps, after each chemical transformation the process is stopped to purify and isolate the reaction intermediates before the following reaction is carried out. The purification processes are, in many cases, where more time and resources are consumed. Therefore, the change of multi-step processes for one-pot approaches will reduce precious manipulation time, costs, resources and waste generation, since these processes do

not require purification of the intermediate products between individual reaction steps. Another important benefit of one-pot syntheses is that they normally reduce the loss of products related to the purification processes and, consequently, increase the overall yield of the complete synthetic process.^[20]

To the best of our knowledge, the synthesis of unsymmetrical squaramides had always been carried out in, at least, two individual reactions. Therefore, the implementation of a one-pot methodology to generate squaramides would strongly impact on the development of these compounds.

2.2 Objectives

The main goal of this investigation was to develop a more efficient synthetic methodology for squaramides compared to previous approaches. This will bring squaramides closer to a broader audience and make them more appealing for industry. For this, we designed a one-pot protocol that would be faster, more efficient and cleaner than the previous synthetic methods since the purification of squaramide monoamines is avoided (Scheme 2.2). Furthermore, the yields obtained will be compared with the analogous yields observed using the multi-step protocol to ensure that they improve when there is no loss of products coming from the purification processes.



Scheme 2.2. Description of the traditional two-step and our new one-pot synthesis of squaramides.

This synthetic methodology should be suitable for the synthesis of many squaramides with different structures. For this, a wide collection of amines with substituents bearing diverse functional groups is necessary for testing the one-pot synthesis of squaramides. In this substrate screening, various products with notorious interest will be included, such as the only commercially available chiral squaramide **15** and biologically active compounds **25**, **26** and **27** (Figure 2.1).

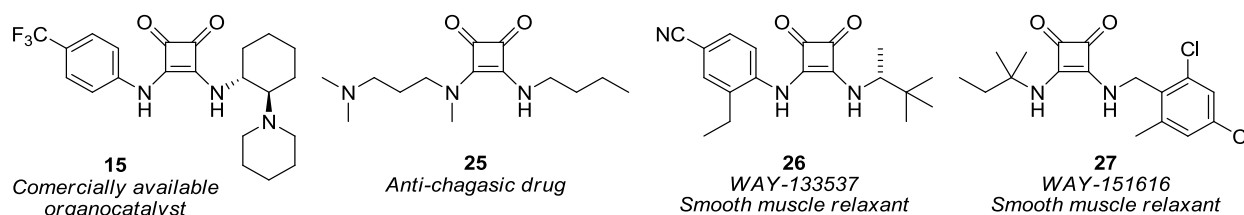
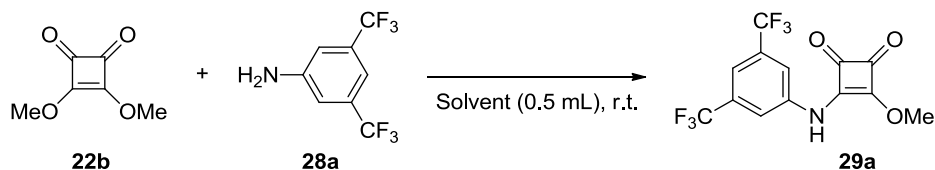


Figure 2.1. Structure of the only chiral squaramide organocatalyst on the market (**15**) and relevant biologically active squaramides (**25**, **26** and **27**).

2.3 Results and Discussion

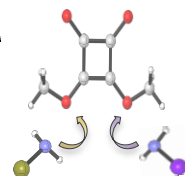
We started investigating the first step of the one-pot process by performing an initial screening of solvents and concentrations of the model reaction (Table 2.1). In this screening, the yields obtained in the synthesis of **29a** were analyzed for different solvents. This is the first reaction in the equivalent “stop-and-go” syntheses and, therefore, **29a** is the first intermediate formed in the new one-pot approach. During this reaction step, the incomplete formation of intermediate **29a** after the addition of the first amine **28a** might lower the overall yield of the one-pot process. The decrease in the yield occurs because a smaller amount of intermediate **29a** is available for the second amine addition and the remaining squarate **22b** could also react with the second amine. Consequently, the generated amount of intermediate **29a** limits the overall yield of the final squaramides in this one-pot procedure.

Table 2.1. Screening of solvents and concentrations in the synthesis of squaramide monoamine **29a**.



Entry ^[a]	Solvent	t (h)	Yield (%)
1	CHCl ₃	24	47
2	MeOH	24	59
3	EtOH	24	53
4	CH ₃ CN	24	46
5	DMSO	24	n.r. ^[b]
6	DMF	24	n.r. ^[b]
7	1,4-Dioxane	24	n.r. ^[b]
8	Toluene	24	n.r. ^[b]
9 ^[c]	MeOH	24	69
10 ^[c]	MeOH	85	>95

[a] Reaction conditions: Amine **28a** (0.2 mmol) was added to a solution of squarate **22b** (0.2 mmol) dissolved in MeOH (0.5 mL) at r.t. After the corresponding reaction time, conversion was calculated by ¹H-NMR using dimethyl fumarate as the internal standard. [b] No reaction observed. [c] Reaction performed with 0.25 mL of MeOH.

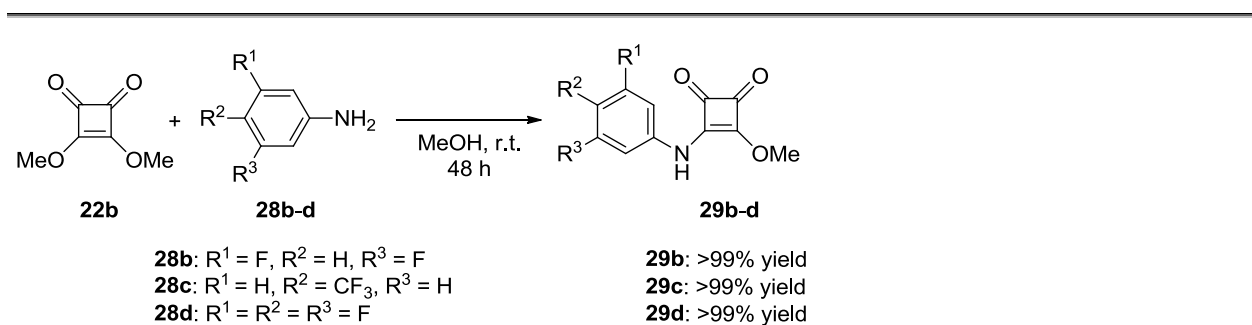


Among all the solvents studied, MeOH was the best choice for the synthesis of intermediate **29a** (Table 2.1, entry 2), whereas no reaction was observed with some aprotic polar solvents such as DMSO, DMF or 1,4-dioxane (Table 2.1, entries 5-7). Aprotic non-polar solvents such as toluene also showed no reaction (Table 2.1, entry 8).

Additionally, Luk and coworkers observed that the addition reaction of the second amine in squaramide synthesis was faster when molecules with hydrogen-bond donor groups were employed as the solvents.^[21] In our screening of solvents, the best results were obtained with MeOH and EtOH (Table 2.1, entries 2-3). Therefore, a similar conclusion can be also stated since the reaction rates observed in the additions of the first amine were higher as the hydrogen-bond donor character of the solvents increased. In fact, the results suggest that (1) there is a direct relation between the hydrogen-bond donor acidities^[22] and the yields obtained and (2) there was no relation between the dielectric constants of the solvents employed and the outcomes of the reactions.

Based on the results, we used water as the solvent in these reactions since this solvent outstands from all the green solvents and has a higher hydrogen-bond donor character than MeOH and EtOH. However, the use of pure water as the solvent was not effective since the formation of the final squaramides was low due to the high insolubility of intermediate **29a** in this medium. Moreover, the hydrolysis of squarate **22b** in water produced different byproducts as observed previously in other studies.^[23]

MeOH showed the best results of all the solvents tested. The design of reactions that employ this solvent is highly desirable since MeOH has been considered one of the preferred green solvents.^[22] In order to test whether or not other reaction conditions could improve the outcomes of the reactions, the concentration of the substrates were changed. The results showed that increasing the concentration of the reaction had a pronounced positive effect on the yield. When using 0.25 mL of MeOH, compound **29a** was obtained in 69% yield, compared to the 59% yield obtained when 0.5 mL of MeOH were used (Table 2.1, entry 9 vs entry 2). Additionally, we observed that the conversion of the reaction increased up to >95% after 85 h of reaction (Table 2.1, entry 10). After this, various anilines (**28b-d**) were also employed in our one-pot approach in order to test whether or not MeOH was compatible with other reagents (Scheme 2.3).



Scheme 2.3. Synthesis of compounds **29b-d** using 0.2 mmol of initial reagents in 0.5 mL of MeOH.

As seen in Scheme 2.3, the addition of amines **28** using MeOH as the solvent showed excellent results for other substrates as well. After this substrate screening, the viability of the one-pot process was tested by incorporating the third reaction component (amines **30**) in the reaction medium after the formation of intermediates **29**. For this, a great number of anilines and amines were used in order to ensure that this new one-pot synthetic protocol was suitable for the synthesis of squaramides with different structural features (Table 2.2). The target squaramides included 15 new structures (Table 2.2, entries 1-16) and 11 squaramides that had previously been employed as organocatalysts (Table 2.2, entries 17-29).^[24]

In this one-pot procedure, first amine **28a-i** was added in one portion into a solution of squarate **22b** in MeOH. Then, after the corresponding reaction time t_1 , we added the second amine **30a-l** dissolved in MeOH. After the time t_2 indicated in Table 2.2, the reactions were stopped. In most of the examples, squaramides **15**, **18** and **31a-x** were isolated by filtration *in vacuo* and washed with cold MeOH, although in a few cases, these products were isolated by column chromatography.

The concentration of each reaction was investigated and optimised individually since the reagents and the final products showed different solubility in MeOH. For this optimization process, only slight modifications in the amounts of MeOH were necessary to find suitable conditions for all the reactions tested (Table 2.2).

This synthetic approach led to squaramides with moderate to very good yields (from 43% to >95% yield). In these approaches, we observed that yields increased as the amount of initial reagents was higher (from 0.2 to 0.4 or 1 mmol of initial reagents, 72% vs 80% in entries 3-4, 45% vs 52% in entries 19-20, and 43% vs 53% in entries 25-26). This mainly occurs because the loss of material in the purification of the products (filtration or chromatography) affects less to the yield when the amount of product is larger. This could attract the attention of researchers from industry, since even better yields could be expected at industrial reaction scales.

In the majority of the examples, the new one-pot procedure led to better outcomes than the previous two-step reactions, showing increases in the yields of up to 23% compared to the highest values previously reported (Table 2.2, entry 28). Squaramides **31q** (Table 2.2, entry 21) and **31r** (Table 2.2, entry 22) were the only compounds that were obtained with slightly lower yields than those previously reported in the “stop-and-go” procedures. This might be caused by the use of smaller amounts of reagents in the one-pot approaches compared to the original examples (0.2 mmol vs 1 mmol) and better results might be obtained when these processes are scaled-up as we have already demonstrated for some examples.

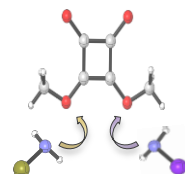
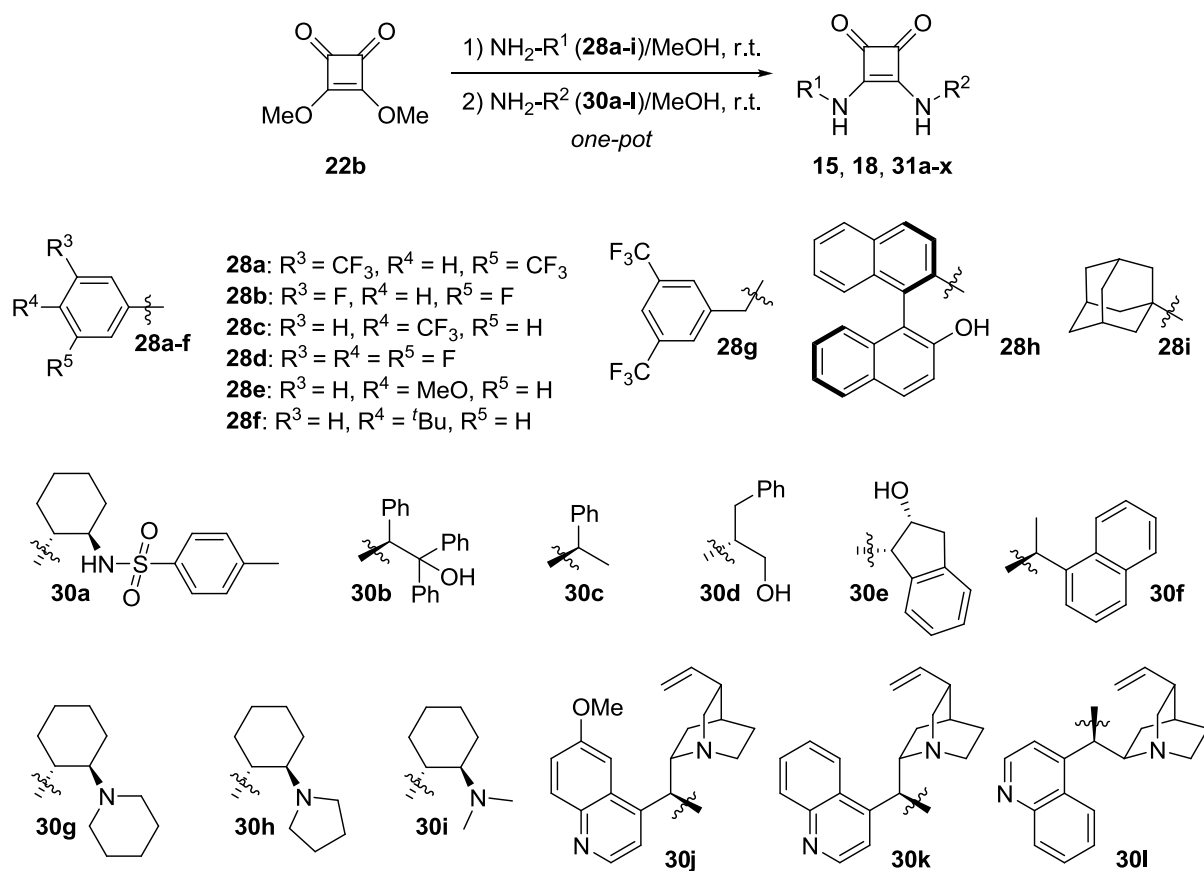
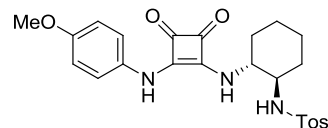
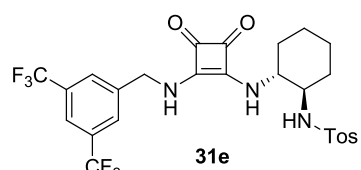
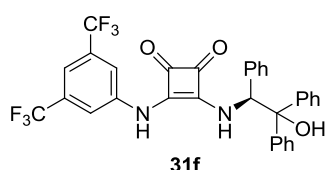
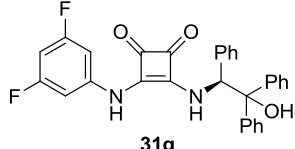
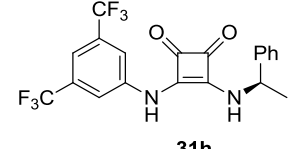
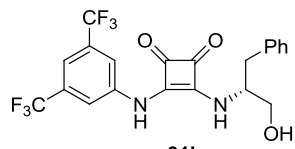
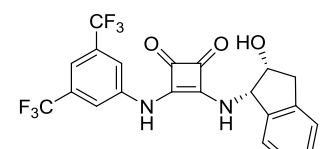
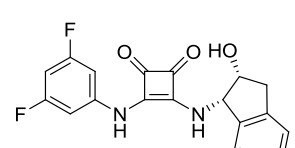
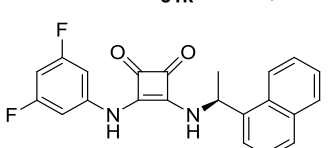
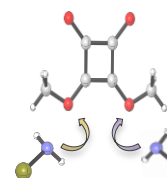


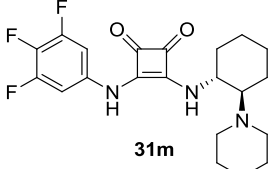
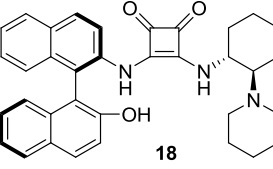
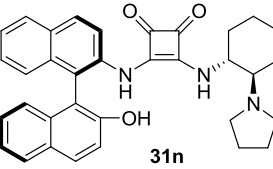
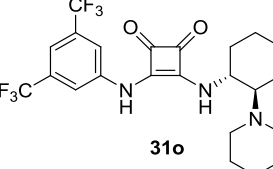
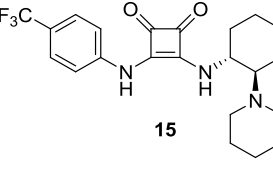
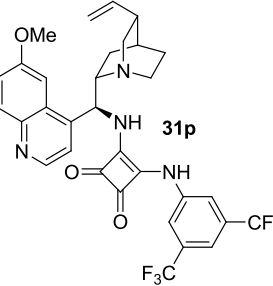
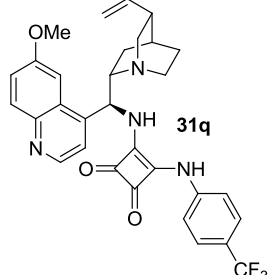
Table 2.2. One-pot synthesis of squaramides **31**.

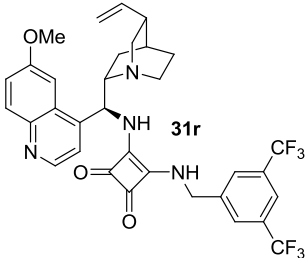
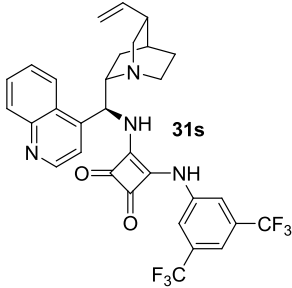
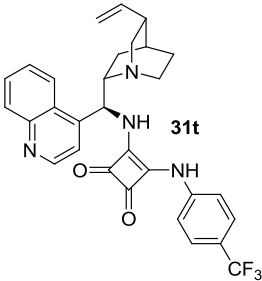
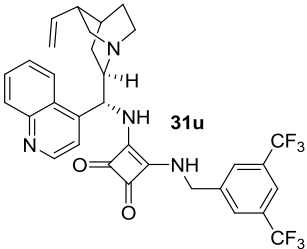
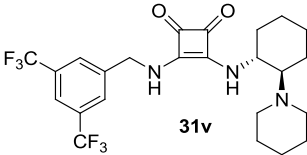
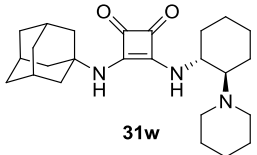
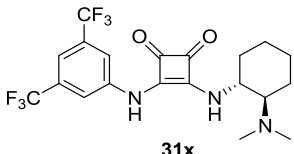
Entry ^[a]	NH ₂ R ¹ (28a-i)/ MeOH (mL)	NH ₂ R ² (30a-l)/ MeOH (mL)	t ₁ (h)	t ₂ (h)	Product	Yield (%) ^[b]
1	28a /0.25	30a /1.75	80	20		75
2	28b /0.5	30a /1.5	26	25		82
3	28f /1	30a /1	2	2		72
4 ^[c]	28f /5	30a /5	2.5	4		80

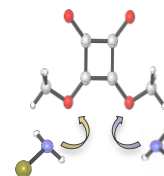
5	28e /0.5	30a /1.5	3	7		85
6	28g /0.5	30a /1.5	20	3		72
7	28a /0.25	30b /1.75	82	10		77
8	28b /0.5	30b /1.5	48	14		>95
9 ^[c]	28a /1.25	30c /5.75	82	3		84
10	28a /0.25	30d /1.75	82	14		60
11	28a /0.25	30e /1.75	49	3		61
12	28b /0.5	30e /1.5	35	5		88
13	28b /0.5	30f /4.5	30	3		82



ONE-POT SYNTHESIS OF UNSYMMETRICAL SQUARAMIDES

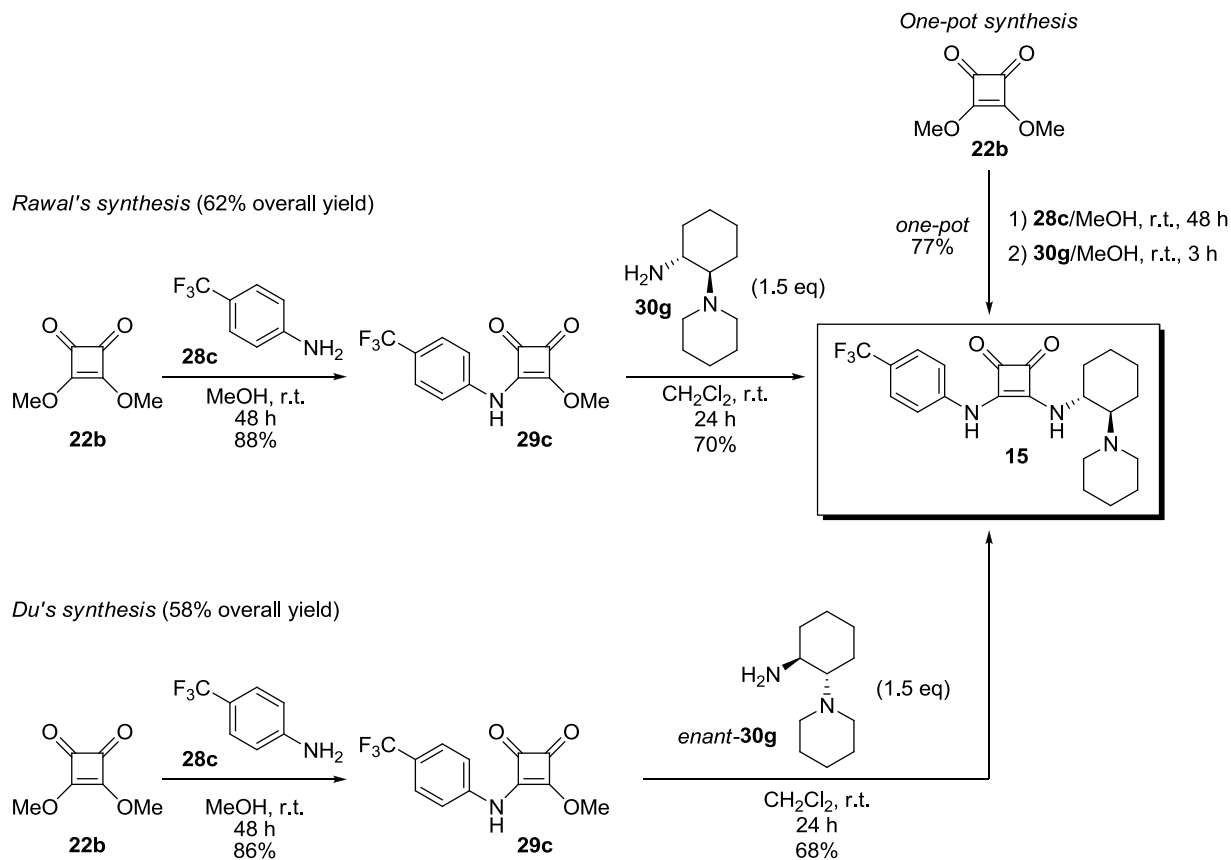
14	28d /0.75	30g /1.25	66	3	 <p>31m</p>	82
15 ^[d]	28h /0.75	30g /1.25	65	23	 <p>18</p>	68 ^[e]
16 ^[d]	28h /0.75	30h /1.25	67	25	 <p>31n</p>	50 ^[f]
17 ^[g]	28a /0.5	30g /3.5	77	2.5	 <p>31o</p>	80 ^[h] (43) ^[25] (62) ^[26]
18 ^[g]	28c /1	30g /3	48	3	 <p>15</p>	77 (58) ^[25] (62) ^[27]
19	28a /0.25	30j /1.75	72	48	 <p>31p</p>	45 ^[i] 52 ^[i] (49) ^[28]
20 ^[g]	28a /0.5	30j /3.5	76	45		
21	28c /0.5	30j /1.5	48	48	 <p>31q</p>	48 or 64 ^[i] (74) ^[28]

22 ^[9]	28g /1	30j /3	26	48	 <chem>CN1CC2(CCN1)C=C2C3=CC=C4C(=C3)N=C(C=C4)OC5=C(C(=O)N5C)C(=O)N6=CC=C(C=C6)C(F)(F)F</chem> 31r	56 or 74 ^[i] (78) ^[29]
23	28a /0.25	30k /1.75	77	25	 <chem>CN1CC2(CCN1)C=C2C3=CC=C4C(=C3)N=C(C=C4)C5=CC=CC=C5N6=CC=CC=C67C=CC=CC=C7C(F)(F)F</chem> 31s	67 ^[i] (49) ^[28]
24	28c /0.5	30k /1.5	48	48	 <chem>CN1CC2(CCN1)C=C2C3=CC=C4C(=C3)N=C(C=C4)C5=CC=CC=C5N6=CC=CC=C67C=CC=C(C=C7)C(F)(F)F</chem> 31t	68 or 78 ^[i] (72) ^[28]
25 26 ^[9]	28g /0.5 28g /1	30l /1.5 30l /3	22 26	48 48	 <chem>CN1CC2(CCN1)C=C2C3=CC=C4C(=C3)N=C(C=C4)C5=CC=CC=C5N6=CC=CC=C67C=CC=C(C=C7)C(F)(F)F</chem> 31u	43 53 or 67 ^[i] (61) ^[13]
27	28g /0.5	30g /1.5	21	3	 <chem>CN1CC2(CCN1)C=C2C3=CC=C4C(=C3)N=C(C=C4)C(=O)N5C(=O)N(C5)C6=CC=C(C=C6)C(F)(F)F</chem> 31v	43 (34) ^[30]
28	28i /1	30g /1	48	23	 <chem>CN1CC2(CCN1)C=C2C3=CC=C4C(=C3)N=C(C=C4)C(=O)N5C(=O)N(C5)C6=CC=C(C=C6)C(F)(F)F</chem> 31w	53 (30) ^[31]
29	28a /0.25	30i /1.75	74	3	 <chem>CN1CC2(CCN1)C=C2C3=CC=C4C(=C3)N=C(C=C4)C(=O)N5C(=O)N(C5)C6=CC=C(C=C6)C(F)(F)F</chem> 31x	60 (29) ^[25] (48) ^[26]



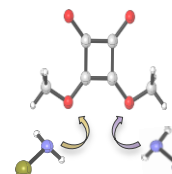
[a] Experimental conditions: To a mixture of squarate **22b** (0.2 mmol) in MeOH (0.25-1 mL), amine **28a-i** (0.2 mmol) was added in one portion at room temperature. After the reaction time t_1 , amine **30a-l** (0.2 mmol) was further added dissolved in MeOH (1-4.5 mL). After t_2 , adducts **15**, **18** and **31a-x** were filtrated under vacuum, placed at -22 °C for 30 mins and the solid was washed with cold MeOH (1 mL). [b] Isolated yield. [c] Reaction performed for 1 mmol of reagents. [d] Reaction performed for 0.15 mmol of reagents. [e] Isolated by column chromatography (from 6:4 Hex:EtOAc to 9:1 EtOAc:MeOH). [f] Isolated by column chromatography (from EtOAc to 7:3 EtOAc:MeOH). [g] Reaction performed for 0.4 mmol of reagents. [h] Isolated by column chromatography (SiO₂ treated with Et₃N, from CH₂Cl₂ to 98:2 CH₂Cl₂:MeOH). [i] Isolated by column chromatography (from 6:4 Hex:EtOAc to 7:3 EtOAc:MeOH).

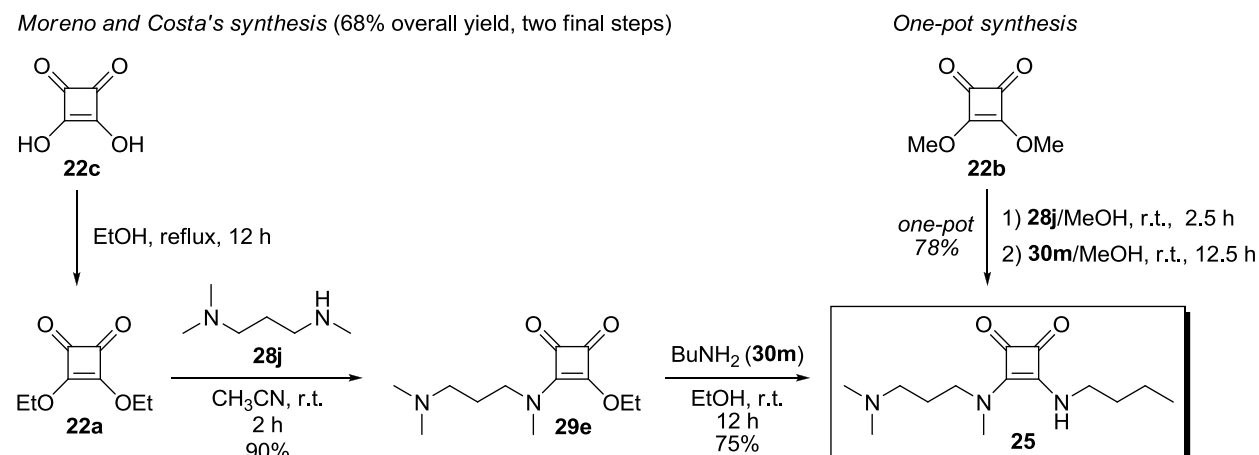
One of our main goals within this research was to synthesize squaramides with special relevance using the one-pot approach proposed. One of the target squaramides was squaramide organocatalyst **15**, since it is the only chiral squaramide organocatalyst that was commercially available at that time. In this investigation, the one-pot approach was successfully employed to synthesize **15**, showing a promising yield of 77%, which was considerably higher than the yield of the two-step synthesis developed by Du's and Rawal's groups (58% and 62%, respectively)^[25,27] (Scheme 2.4 and Table 2.2, entry 18). Additionally, the method showed another important benefit: in the previous procedures, the authors used in the second reaction step an excess of amine **30g** (1.5 eq), the most expensive part of this squaramide, while we performed the reaction using equimolar amounts of each reagent. This reduces greatly the cost of this reaction and makes this process more appealing for real-world applications. Furthermore, amine **30g** was totally consumed after 3 h in the second step of the one-pot reaction, which is a notably shorter time than the reaction times reported in the other procedures (24 h, Scheme 2.4).



Scheme 2.4. Yields of the two-step and one-pot synthesis of commercially available squaramide **15**.

Other interesting targets within the scope of the one-pot synthesis were squaramides with biological activity that might be potential drugs for the pharmaceutical industry. Recently, Moreno, Costa and coworkers discovered an squaramide (**25**) that showed antiparasitic properties (Scheme 2.5).^[32] This was a promising candidate in the preliminary *in vivo* studies on acute and chronic phases of Chagas disease and showed low toxicity. This disease is a tropical parasitic infection that especially affects to the poorest rural areas of Latin America. Even though there are currently treatments for this illness, the design of more efficient and less expensive drugs is highly desired to combat Chagas disease in these extremely poor regions.^[33] In this context, squaramide **25** is a low-cost drug and could be an interesting alternative to the medicines that are currently being used for this disease, which normally present severe side effects and are not effective for chronic patients.





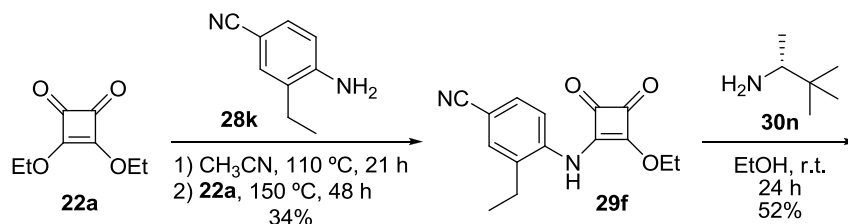
Scheme 2.5. Traditional and one-pot synthesis of anti-chagasic squaramide **25** with their yields.

The one-pot approach showed an improvement in the yield of squaramide **25** compared to the previously reported yield.^[32] In the previous synthesis, the authors obtained an overall yield for the last two synthetic steps 68%, while product **25** was obtained with 78% yield with the new one-pot protocol. In addition, the cost of the reaction became even lower due to the advantages of one-pot processes. This could help to overcome one of the main drawbacks of current treatments of Chagas disease: the high cost of the drugs used to fight it, which makes the treatment inaccessible for many people affected by this illness. This simple and inexpensive method might attract the interest of pharmaceutical companies for the production of this compound at a larger scale.

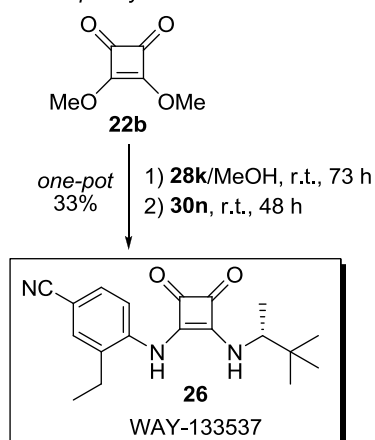
Two other biological active compounds were prepared, WAY-133537 (**26**)^[34] and WAY-151616 (**27**)^[35] which are potent smooth muscle relaxants (Scheme 2.6). These two compounds act as bladder-selective KATP-channel openers^[36] and exhibit remarkable oral efficacy in a rat hypertrophied bladder model of urge urinary incontinency. Urinary incontinency is a disease that affects approximately 10-20% of the global population and causes enormous health care expenses. Currently, the therapeutic drugs that are being used to treat this disease, such as tolterodine, show severe cardiovascular side effects that limit their use. Therefore, it is highly desirable to find new candidates that follow different mechanisms of action and are suitable for a wide range of patients. In this context, squaramides **26** and **27** are potential new drugs to treat urinary incontinency since they show bladder selectivity and do not produce the side effects of the previous drugs used to treat this illness. In addition, squaramides **26** and **27** have been successfully employed in the treatment of other diseases related to smooth muscle contraction, such as hypertension, asthma and premature labor, among others.^[37] Moreover, the synthesis of compound **27** using our one-pot approach was a milestone in this investigation because squaramide **27** is already being produced industrially.

A

Butera's synthesis (18% overall yield)

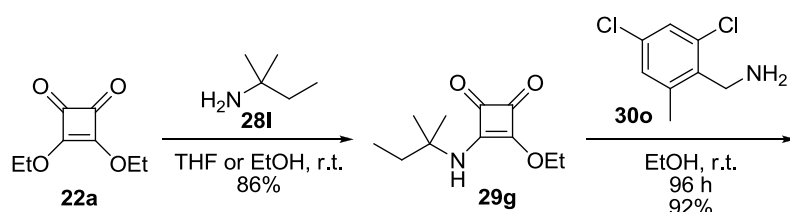


One-pot synthesis

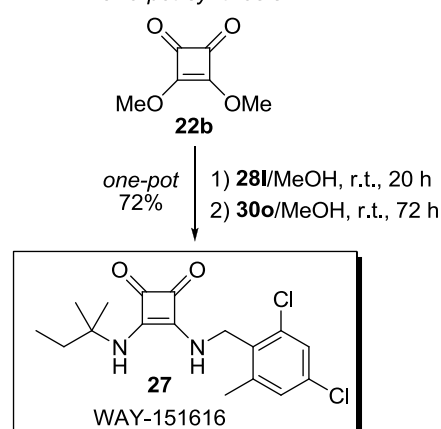


B

Butera's synthesis (79% overall yield)

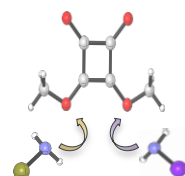


One-pot synthesis

**Scheme 2.6.** Syntheses of biologically active squaramides **26** (A) and **27** (B).

The original synthesis of compound **26** (Scheme 2.6, A) leads to an overall yield of 18%.^[34] The one-pot synthetic method developed in this research was successfully implemented in the synthesis of this drug, giving higher yields than the original synthesis (33%). It is worth noting that we performed the synthesis of **26** at a scale of 0.2 mmol, while the original approach employed 5.88 mmol. Consequently, the difference in the yields obtained using these two approaches might be even greater when the one-pot approach is performed at higher scales.

Butera and coworkers prepared biologically active squaramide **27** (Scheme 2.6, B) with an overall yield of 79%.^[35] When our one-pot method was used, compound **27** was produced in a 72% yield. Again, it is worth to mention that the two methodologies compared were performed in different reaction scales: while the authors performed the original synthesis in a high scale expecting to obtain around 28 g of product, we carried out this reaction on a smaller scale (0.4 mmol of product, 136 mg). Therefore, a higher yield might be obtained when employing our methodology on a larger scale. To emphasize the influence that different scales have in the reaction yields obtained, we performed the synthesis of **27** at a smaller scale (0.2 mmol) and the



final product was obtained with a 62% yield. This strongly stresses how scale influences the yields of the reactions and reinforces the possibility of obtaining better results in the one-pot method when higher amounts of product are synthesized.

2.4 Conclusions

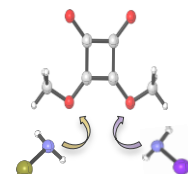
Summarizing, the first one-pot synthesis of squaramides was developed, obtaining yields that were generally superior to those observed in their corresponding two-step traditional synthesis. The one-pot protocol presented is a simpler procedure for obtaining a wide range of squaramide derivatives when compared to the previously developed “stop-and-go” processes. This new synthetic methodology also has the advantages of one-pot procedures, such as great reductions in the energy, time, waste and cost required in the reactions.

The high versatility of our process was demonstrated by expanding the methodology to the synthesis of relevant squaramides in industry and Medicinal Chemistry. For this, the one-pot approach was applied to the production of three biologically active structures as well as a commercially available organocatalyst, improving most of the results observed in the corresponding previous stepwise syntheses. This synthetic method makes the synthesis of squaramides simpler and more economically viable, which could attract the interest of pharmaceutical and chemical companies aiming to produce these compounds at a large scale. We also believe that our investigation could be crucial in accelerating the development of the field of squaramides, since the syntheses of a wide variety of these compounds would become easier and faster to carry out.

2.5 References

- [17] Smutny, E. J.; Roberts, J. D. *J. Am. Chem. Soc.* **1955**, *77*, 3420.
- [18] Maahs, G.; Hegenberg, P. DE1518660 A1, July 9, 1965.
- [19] a) Vaxelaire, C.; Winter, P.; Christmann, M. *Angew. Chem. Int. Ed.* **2011**, *50*, 3605; b) Albrecht, Ł.; Jiang, H.; Jørgensen, K. A. *Angew. Chem. Int. Ed.* **2011**, *50*, 8492; c) Saha, A.; Baig, R. B. N.; Leazer, J.; Varma, R. S. *Chem. Commun.* **2012**, *48*, 8889; d) Baig, R. B. N.; Varma, R. S. *Green Chem.* **2012**, *14*, 625.
- [20] Walji, A. M.; MacMillan, D. W. C. *Synlett*, **2007**, 1477.
- [21] Sejwal, P.; Han, Y.; Shah, A.; Luk, Y.-Y. *Org. Lett.* **2007**, *9*, 4897.
- [22] Reichardt, C.; Welton, T. (Eds.) *Solvents and Solvent Effects in Organic Chemistry*. Wiley-VCH: Weinheim, **2003**.
- [23] Cohen, S.; Cohen, S. G. *J. Am. Chem. Soc.* **1966**, *88*, 1533.

- [24] Marqués-López, E.; Alegre-Requena, J.-V.; Herrera, R. P. WO2016005407 A1, July 07, 2014.
- [25] For the preparation of the opposite enantiomer, see: Yang, W.; Du, D.-M. *Adv. Synth. Catal.* **2011**, 353, 1241.
- [26] Konishi, H.; Lam, T. Y.; Malerich, J. P.; Rawal, V. H. *Org. Lett.* **2010**, 12, 2028.
- [27] Zhu, Y.; Malerich, J. P.; Rawal, V. H. *Angew. Chem. Int. Ed.* **2010**, 49, 153.
- [28] Yang, W.; Du, D.-M. *Org. Lett.* **2010**, 12, 5450.
- [29] Jiang, H.; Paixão, M. W.; Monge, D.; Jørgensen, K. A. *J. Am. Chem. Soc.* **2010**, 132, 2775.
- [30] For the second step (40% yield), see: Baran, R.; Veverková, E.; Škvorcová, A.; Šebesta, R. *Org. Biomol. Chem.* **2013**, 11, 7705. The authors did not detail the yield of the first reaction step and we used the yield that Rawal and coworkers obtained in this step (85% yield), see: Malerich, J. P.; Hagihara, K.; Rawal, V. H. *J. Am. Chem. Soc.* **2008**, 130, 14416.
- [31] For the preparation of the opposite enantiomer, see: Yang, W.; Du, D.-M. *Org. Biomol. Chem.* **2012**, 10, 6876.
- [32] Olmo, F.; Rotger, C.; Ramírez-Macías, I.; Martínez, L.; Marín, C.; Carreras, L.; Urbanová, K.; Vega, M.; Chaves-Lemaur, G.; Sampedro, A.; Rosales, M. J.; Sánchez-Moreno, M.; Costa, A. *J. Med. Chem.* **2014**, 57, 987.
- [33] a) Guedes, P. M. M.; Silva, G. K.; Gutierrez, F. R. S.; Silva, J. S. *Expert Rev. Anti-Infect. Ther.* **2011**, 9, 609; b) Urbina, J. A. *Acta Trop.* **2010**, 115, 55; c) Cerecetto, H.; González, M. *Pharmaceuticals* **2010**, 3, 810.
- [34] a) Butera, J. A.; Antane, S. A. US5506252 A, November 17, 1993; b) Butera, J. A.; Antane, M. M.; Antane, S. A.; Argentieri, T. M.; Freedden, C.; Graceffa, R. F.; Hirth, B. H.; Jenkins, D.; Lennox, J. R.; Matelan, E.; Norton, N. W.; Quagliato, D.; Sheldon, J. H.; Spinelli, W.; Warga, D.; Wojdan, A.; Woods, M. *J. Med. Chem.* **2000**, 43, 1187.
- [35] a) Herbst, D. R.; Antane, M. M.; McFarlane, G. R.; Gundersen, E. G.; Hirth, B. H.; Quagliato, D. A.; Graceffa, R. F.; Butera, J. A. US5763474 A, July 17, 1996; b) Gilbert, A. M.; Antane, M. M.; Argentieri, T. M.; Butera, J. A.; Francisco, G. D.; Freedden, C.; Gundersen, E. G.; Graceffa, R. F.; Herbst, D.; Hirth, B. H.; Lennox, J. R.; McFarlane, G.; Norton, N. W.; Quagliato, D.; Sheldon, J. H.; Warga, D.; Wojdan, A.; Woods, M. *J. Med. Chem.* **2000**, 43, 1203.
- [36] a) Coghlan, M. J.; Carroll, W. A.; Gopalakrishnan, M. *J. Med. Chem.* **2001**, 44, 1627; b) Ashcroft, F. M.; Gribble, F. M. *Trends Neurosci.* **1998**, 21, 288.
- [37] For selected studies using WAY-133537 (**26**), see: a) Wojdan, A.; Freedden, C.; Woods, M.; Oshiro, G.; Spinelli, W.; Colatsky, T. J.; Sheldon, J. H.; Norton, N. W.; Wargan, D.; Antane, M. M.; Antane, S. A.; Butera, J. A.; Argentieri, T. M. *J. Pharmacol. Exp. Ther.* **1999**, 289, 1410; b) Buckner, S. A.; Milicic, I.; Daza, A. V.; Coghlan, M. J.; Gopalakrishnan, M. *Br. J. Pharmacol.*

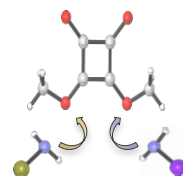


2002, 135, 639; c) Fabiyi, A. C.; Gopalakrishnan, M.; Lynch III, J. J.; Brioni, J. D.; Coghlan, M. J.; Brune, M. E. *BJU Int.* **2003**, 91, 284. For selected studies using WAY-151616 (**27**), see: d) Antane, M. M.; Herbst, D. R.; McFarlane, G. R.; Gundersen, E. G.; Hirth, B. H.; Quagliato, D. A.; Graceffa, R. F.; Butera, J. A.; Gilbert, A. M. WO199802413 A1, July 17, 1996; e) Butera, J. A.; Argentieri, T. M. *Drugs Future* **2000**, 25, 239; f) Gehenne, J.-N. M.; Allue, M. J. R.; Pugliese, M. WO2006000607 A1, June 23, 2004.

2.7 Supporting Information

General Experimental Methods

Purification of reaction products was carried out by filtration or flash chromatography using silica-gel (0.063-0.200 mm). Analytical thin layer chromatography was performed on 0.25 mm silica gel 60-F plates. ESI ionization method and mass analyzer type MicroTof-Q were used for the HRMS measurements. $^1\text{H-NMR}$ spectra were recorded at 400 and 300 MHz. ^{13}C APT-NMR spectra were recorded at 100 and 75 MHz. CDCl_3 and $\text{DMSO-}d_6$ were used as the deuterated solvents. Chemical shifts were reported in the δ scale relative to residual CHCl_3 (7.26 ppm) and DMSO (2.50 ppm) for $^1\text{H-NMR}$ and to the central line of CHCl_3 (77 ppm) and DMSO (39.43 ppm) for ^{13}C APT-NMR. The spectral information of products **18** and **31a-n** is included in the *Experimental Section* of the article presented in this chapter. $^1\text{H-NMR}$ and ^{13}C APT-NMR spectra of squaramides **18** and **31a-n** are included in the annex on the CD (Figures S2.1-S2.15).

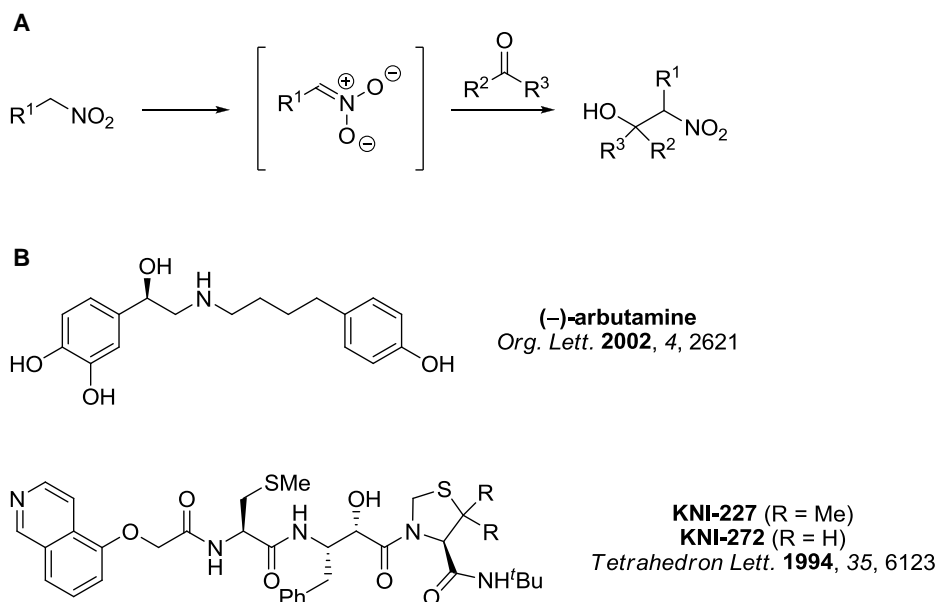


3

TRIFUNCTIONAL SQUARAMIDE CATALYST FOR EFFICIENT ENANTIOSELECTIVE HENRY REACTION ACTIVATION

3.1 Introduction

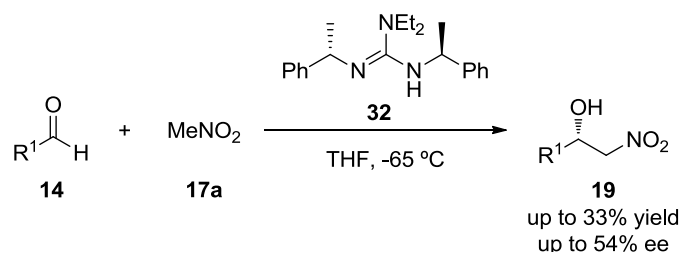
The Henry (nitroaldol) reaction, is an outstanding synthetic tool in Organic Chemistry to create carbon-carbon bonds.^[38] This reaction consists in the addition of an *in situ* generated nitronate on a carbonyl group and has proven to be a valuable synthetic strategy to obtain β -nitro alcohols (Scheme 3.1, A).^[39] This reaction has been successfully employed in the total synthesis of many biologically active molecules (Scheme 3.1, B). One of most appealing features of the Henry reaction in synthesis is that the nitro group of the β -nitro alcohols produced can be transformed into other functional groups, generating different derivatives such as β -amino alcohols and α -hydroxy acids, among others.^[40] Therefore, the development of new asymmetric Henry reactions is crucial for creating useful building blocks in the field of total synthesis.



Scheme 3.1. (A) General mechanism of the Henry reaction. (B) Examples of biologically active compounds obtained through a synthetic route that includes a Henry reaction.

The Henry reaction can be promoted using diverse catalytic systems to obtain chiral β -amino alcohols. Much effort has been taken in the field of Organocatalysis for improving the results of this reaction since the first asymmetric example reported by Nájera and coworkers in 1994 (Scheme 3.2).^[41] In this example, the authors used guanidine **32** as the organocatalyst

and obtained enantioenriched products with up to 54% ee. This example paved the way for other investigations in which different kinds of organocatalysts were successfully used to promote this chemical transformation.^[42,43]



Scheme 3.2. First asymmetric organocatalytic Henry reaction developed by Nájera and coworkers.

The Henry reaction is still a process that has so much margin of improvement, especially in terms of catalyst loading. In the existing organocatalytic versions of this reaction, relatively high catalyst loadings are required (normally from 5 to 20 mol%).^[42] In this context, multifunctional organocatalysts have gained much attention in the last years and there are various examples where trifunctional catalysts promote reactions with outstanding results (Figure 3.1).^[44] The high efficiency achieved in these catalytic systems is due to the creation of complex networks of synergic non-covalent interactions between the catalyst and the substrates of a reaction.^[45] Therefore, multifunctional catalysts^[45] might be promising tools to lower the catalyst loadings required in Organocatalysis, a field where normally the catalyst loadings are larger than in other types of catalysis.^[46]

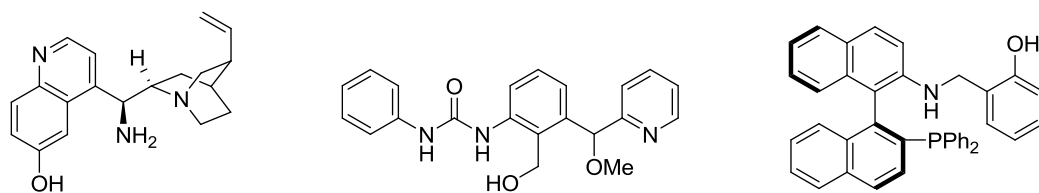
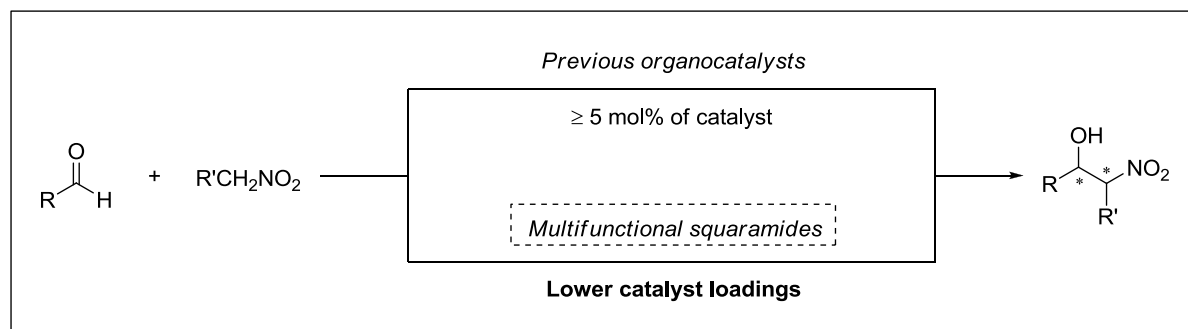


Figure 3.1. Structures of different trifunctional organocatalysts employed previously in other studies.

Different types of non-covalent interactions have coexisted in previous multifunctional catalytic systems, such as hydrogen bonds, electrostatic effects, π -interactions and Van der Waals forces, among others. All these interactions cooperated to decrease the energy of the limiting rate steps in different reactions and, consequently, increased significantly their reaction rates. These interactions could also be a key factor in the improvement of the stereoselectivity of the chemical transformations, since they differently affect the energy of each reaction pathway that comprises the mechanism. This produces an energetic differentiation in the pathways that lead to stereoisomers and could favor the formation of one stereoisomer over the others.

3.2 Objectives

In this research, the main objective was to develop an asymmetric organocatalytic version of the Henry reaction that was highly efficient and needed lower catalyst loadings than the previous organocatalytic examples (Scheme 3.3). Furthermore, this method must have high yields and lead to products with good enantiomeric excesses.



Scheme 3.3. Main goal of the multifunctional squaramide-catalyzed Henry reaction developed in this research.

In previous studies, it was stated that it is very important to use organocatalysts that have a hydrogen-bond donor and a hydrogen-bond acceptor group in the same structure in this reaction. Therefore, in order to achieve our goal, a wide collection of squaramide organocatalysts containing both hydrogen-bond donor and acceptor groups were tested in the Henry reactions. In addition, we included in the investigation a trifunctional squaramide organocatalyst in order to make the MeNO₂ attack on the aldehyde more energetically favorable and, therefore, accelerate the reactions.

3.3 Results and Discussion

The model Henry reaction chosen to start this investigation was the addition of nitromethane (**17a**) to 4-nitrobenzaldehyde (**14a**) using catalyst **15**. These reagents made the optimization process of the reaction conditions more convenient, since all the reagents were readily available. In this optimization step, we initially performed a screening of the reaction medium (Table 3.1).

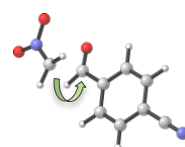
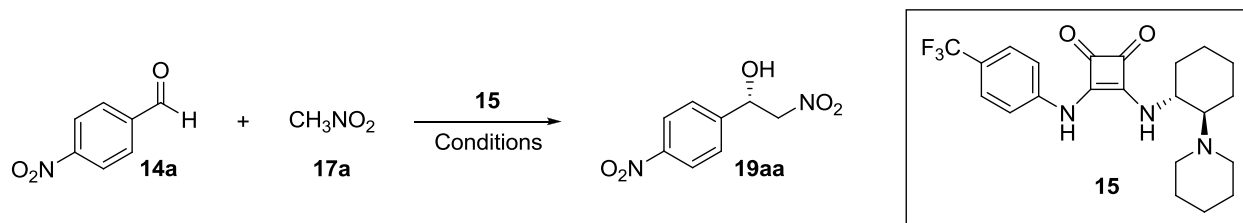


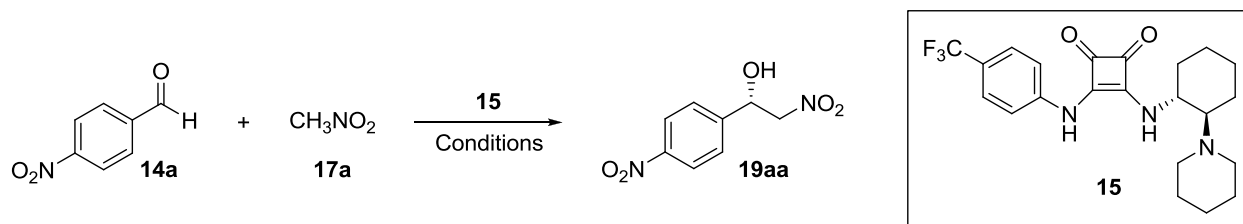
Table 3.1. Screening of solvents using catalyst **15**.

Entry ^[a]	Solvent	15 (mol%)	T (°C)	t (h)	Yield (%) ^[b]	ee (%) ^[c]
1	MeCN	20	r.t.	66	>99	48
2	Dibutylether	20	r.t.	70	95	43
3	1,4-Dioxane	20	r.t.	41	>99	35
4	THF	20	r.t.	41	>99	42
5	CH ₂ Cl ₂	20	r.t.	48	89	Rac.
6	CHCl ₃	20	r.t.	68	75	Rac.
7	Toluene	20	r.t.	70	94	31
8	Xylene	20	r.t.	70	>99	30
9	EtOAc	20	r.t.	62	68	47
10	H ₂ O	20	r.t.	62	>99	Rac.
11	MeCN	10	r.t.	66	>99	44
12	EtOAc	10	r.t.	71	73	51
13	MeCN	10	-24	103	29	59
14	EtOAc	10	-24	103	19	27

[a] Experimental conditions: To a solution of squaramide **15** and aldehyde **14a** (0.1 mmol) in the corresponding solvent (0.5 mL), nitromethane (**17a**) (1 mmol) was added at the temperature indicated in the table. After the reaction time, product **19aa** was isolated by column chromatography (from 9:1 to 7:3 Hex:EtOAc). [b] After isolation by column chromatography. [c] Determined by chiral HPLC analysis.

In all cases, the reaction proceeded smoothly and the only product observed was the nitroaldol adduct **19aa**. The highest values of enantiomeric excess were obtained when using polar aprotic solvents such as MeCN and EtOAc (Table 3.1, entries 1 and 9). When the catalyst load was decreased (10 mol%), similar results were found in MeCN (Table 3.1, entry 11) and EtOAc (entry 12). However, when a lower reaction temperature was employed in the reaction (-24 °C), the outcomes considerably changed. In the case of EtOAc at this temperature, both reactivity and enantioselectivity decreased, while when using MeCN, the reactivity lowered but the enantiomeric excess became higher than the excess obtained at room temperature (Table 3.1, entries 13-14).

In order to improve the results obtained with MeCN in the previous screening, different amounts of MeNO₂ were added in the reaction medium. For this, different MeCN/MeNO₂ mixtures and concentrations were tested at diverse temperatures (Table 3.2).

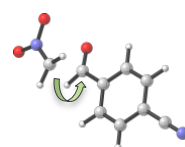
Table 3.2. Results of the Henry reactions using different amounts of MeNO₂.

Entry ^[a]	MeCN (mL)/MeNO ₂ (mL)	15 (mol%)	T (°C)	t (h)	Yield (%) ^[b]	ee (%) ^[c]
1	0.5 / 0.11	10	r.t.	71	95	53
2	0.5 / 0.28	10	r.t.	53	>95	55
3	0.25 / 0.25	10	r.t.	19	86	57
4	0.1 / 0.4	10	r.t.	13	>95	57
5	0 / 0.5	10	r.t.	13	>95	54
6	0.1 / 0.4	10	-24	87	73	66
7	0 / 0.2	10	-24	86	73	62
8	0.1 / 0.4	5	-24	92	79	68
9	0.1 / 0.4	20	-24	92	72	67
10	0.05 / 0.2	5	-24	92	56	63
11	0.2 / 0.8	5	-24	92	74	68
12	0.1 / 0.4	20	-38	6 d ^[d]	16	44

[a] Experimental conditions: To a solution of squaramide **15** in the corresponding mixture of MeCN/MeNO₂, aldehyde **14a** (0.1 mmol) was added at the temperature indicated in the table. After the reaction time, product **19aa** was isolated by column chromatography (from 9:1 to 7:3 Hex:EtOAc). [b] After isolation by column chromatography. [c] Determined by chiral HPLC analysis. [d] Days.

As seen in Table 3.2, variations in the MeCN/MeNO₂ ratio changed the reactivity and enantioselectivity of the process. In general, the best results were obtained at -24 °C when using MeCN/MeNO₂ mixtures with high proportions of MeNO₂ (Table 3.2, entries 6-11). At this point, diverse squaramide-based organocatalysts bearing different families of substituents were designed in order to improve the results of the Henry reaction (Figure 3.2). The squaramides synthesized contained hydrogen-bond donors and acceptors that could potentially create non-covalent interactions with the reagents. These organocatalysts were tested using diverse reaction conditions that led to good results in the previous studies (Table 3.3).

After all these screenings, the best results of enantioselectivity were obtained with catalyst **18**, which led to enantiomeric excesses up to 87% even when only 1% of catalyst load was employed (entries 16-25). Also, the yields obtained in these reactions were high, being in many cases >95%. The best reaction conditions were achieved when using 2% of catalyst **18** at -24 °C and using only MeNO₂ as the solvent (> 95% yield, 82% ee, Table 3.3, entry 25).



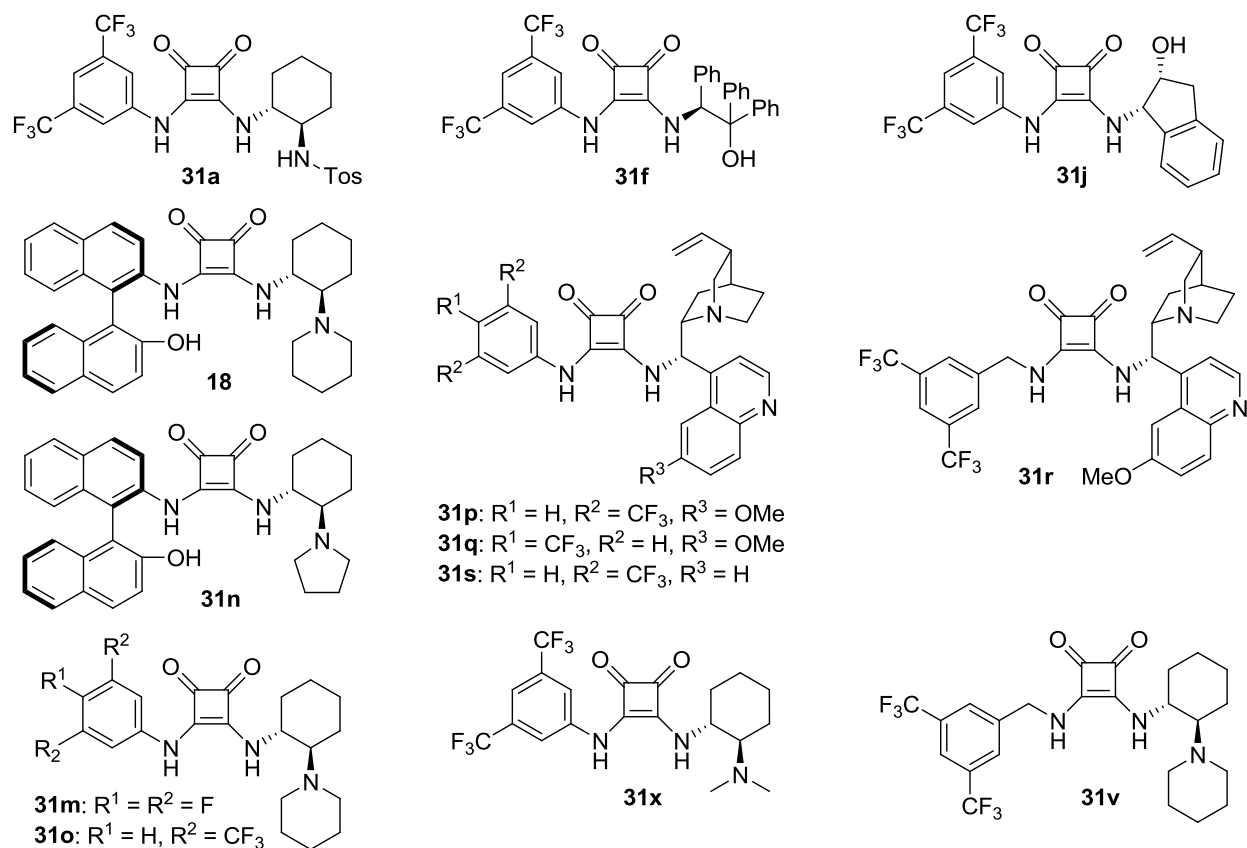


Figure 3.2. Squaramide-based organocatalysts tested in the Henry reaction.

Table 3.3. Screening of organocatalysts.

Entry ^[a]	Solvent (mL)	Squaramide (mol%)	T (°C)	t (h)	Yield (%) ^[b]	ee (%) ^[c]
1	MeCN (0.1)/MeNO ₂ (0.4)	31o (10)	-24	64	>95	62
2	MeCN (0.1)/MeNO ₂ (0.4)	31o (20)	-38	38	>95	66
3	MeCN (0.1)/MeNO ₂ (0.4)	31o (10)	-38	61	>95	68
4	MeCN (0.1)/MeNO ₂ (0.4)	31o (5)	-38	61	>95	70
5	MeCN (0.1)/MeNO ₂ (0.4)	31o (2.5)	-38	61	>95	70
6	MeCN (0.1)/MeNO ₂ (0.4)	31o (1)	-38	86	23	70
7	MeCN (0.1)/MeNO ₂ (0.4)	31m (10)	-24	86	54	59
8	MeCN (0.1)/MeNO ₂ (0.4)	31x (10)	-24	68	>95	64
9	MeCN (0.1)/MeNO ₂ (0.4)	31v (10)	-24	68	26	22
10	MeCN (0.1)/MeNO ₂ (0.4)	31s (10)	-24	62	>95	56
11	MeCN (0.1)/MeNO ₂ (0.4)	31s (20)	-38	62	52	48
12	MeCN (0.1)/MeNO ₂ (0.4)	31p (10)	-24	62	>95	53

13	CH ₂ Cl ₂ (0.5)/MeNO ₂ (0.054)	31p (20)	r.t.	15	>95	Rac.
14	MeCN (0.1)/MeNO ₂ (0.4)	31q (10)	-24	62	89	51
15	CH ₂ Cl ₂ (0.5)/MeNO ₂ (0.054)	31r (20)	r.t.	15	92	Rac.
16	MeCN (0.1)/MeNO ₂ (0.4)	18 (5)	r.t.	3	>95	60
17	MeCN (0.1)/MeNO ₂ (0.4)	18 (1)	-15	63	>95	79
18 ^[e]	MeCN (0.15)/MeNO ₂ (0.60)	18 (10)	-38	48	93	84
19 ^[e]	MeCN (0.15)/MeNO ₂ (0.60)	18 (5)	-38	48	84	87
20	MeCN (0.1)/MeNO ₂ (0.4)	18 (10)	-24	23	>95	84
21	MeCN (0.1)/MeNO ₂ (0.4)	18 (5)	-24	26	>95	85
22 ^[f]	MeCN (0.22)/MeNO ₂ (0.88)	18 (2.5)	-24	52	>95	84
23 ^[f]	MeCN (0.22)/MeNO ₂ (0.88)	18 (2)	-24	67	73	86
24 ^[g]	MeCN (0.55)/MeNO ₂ (2.2)	18 (1)	-24	72	55	86
25 ^[f]	MeNO ₂ (1.1)	18 (2)	-24	24	>95	83
26	MeCN (0.1)/MeNO ₂ (0.4)	31n (5)	-38	33	>95	68
27	CH ₂ Cl ₂ (0.5)/MeNO ₂ (0.054)	31a (20)	r.t.	48	n.r.	n.d. ^[c]
28	MeCN (0.2)/MeNO ₂ (0.8)	31a (10) ^[h]	-24	22	>95	6
29	CH ₂ Cl ₂ (0.5)/MeNO ₂ (0.054)	31j (20)	r.t.	48	n.r.	n.d. ^[c]
30	MeCN (0.2)/MeNO ₂ (0.8)	31j (10) ^[h]	-24	22	>95	28
31	CH ₂ Cl ₂ (0.5)/MeNO ₂ (0.054)	31f (20)	r.t.	48	n.r.	n.d. ^[c]
32	MeCN (0.2)/MeNO ₂ (0.8)	31f (10) ^[h]	-24	22	>95	20

[a] Reaction conditions: To a solution of the organocatalyst in the corresponding mixture of MeCN/MeNO₂, aldehyde **14a** (0.1 mmol) was added at the temperature indicated in the table. After the reaction time, product **19aa** was isolated by column chromatography (from 9:1 to 7:3 Hex:EtOAc). [b] After isolation by column chromatography. [c] Determined by chiral HPLC analysis. [d] n.d. = not determined. [e] Conditions for 0.15 mmol of aldehyde **14a**. [f] Reaction scale: 0.22 mmol of aldehyde **14a**. [g] Reaction scale: 0.55 mmol of aldehyde **14a**. [h] Et₃N (10 mol%) was used.

In order to test the efficiency of the process, aldehydes bearing different functional groups (**14a-o**) were used as initial reagents (Table 3.4). In all the cases, the Henry reactions led to the desired β -nitro alcohols **19** with good to excellent yields (up to >95%) and high enantioselectivities (up to 94% ee).

The results suggest that the enantioselectivity of the reactions did not depend on the electronic effects of the aldehydes. However, the reactivity of these processes is closely related with the electronic properties of the aldehydes used, since (1) the Henry reactions proceeded faster as the group in the aromatic ring of the aldehydes became more electron-withdrawing (Table 3.4, entries 1-5) and (2) reactions were slower when aldehydes with electron-donating groups were used (Table 3.4, entries 7 and 9). Additionally, good enantiomeric excesses were obtained when aliphatic aldehydes were used (Table 3.4, entry 15). The absolute configuration of products **19** (S) was determined by comparing their optical rotation values with previously reported values of the corresponding compounds. In all of the examples, the attack of the nitronate was directed to the same face of the aldehydes.

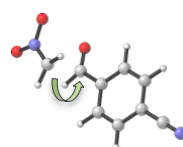
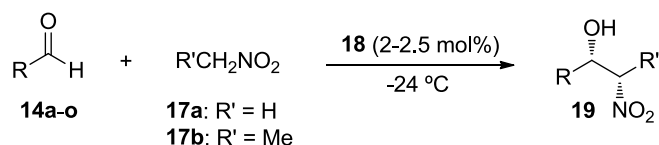


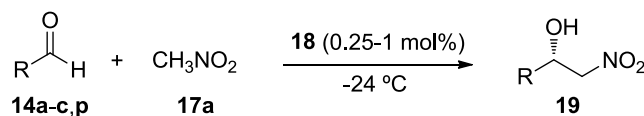
Table 3.4. Scope of the Henry reaction catalyzed by **18**.

Entry ^[a]	R	18 (mol%)	R'CH ₂ NO ₂	t (h)	Product	Yield (%) ^[b]	ee (%) ^[c]
1	4-NO ₂ C ₆ H ₄ (14a)	2	17a	24	19aa	>95	83
2	3-NO ₂ C ₆ H ₄ (14b)	2	17a	24	19ba	>95	94
3	4-CNC ₆ H ₄ (14c)	2	17a	71	19ca	96	82
4	4-ClC ₆ H ₄ (14d) ^[d]	2	17a	91	19da	81	86
5	4-BrC ₆ H ₄ (14e) ^[d]	2	17a	91	19ea	75	86
6	Ph (14f) ^[d]	2	17a	86	19fa	59	82
7	4-PhC ₆ H ₄ (14g)	2.5	17a	96	19ga	50	90
8	3-ClC ₆ H ₄ (14h) ^[d]	2	17a	86	19ha	62	90
9	4-MeC ₆ H ₄ (14i) ^[d]	2	17a	144	19ia	20	84
10	1-naphthyl (14j) ^[d]	2	17a	86	19ja	50	85
11	2-pyridyl (14k) ^[d]	2.5	17a	96	19ka	>95	80
12	3-pyridyl (14l) ^[d]	2	17a	92	19la	95	92
13	2-furyl (14m) ^[d]	2	17a	88	19ma	74	92
14	2-thiophenyl (14n) ^[d]	2	17a	92	19na	55	92
15	PhCH ₂ OCH ₂ (14o)	2	17a	92	19oa	66	76
16 ^[e]	4-NO ₂ C ₆ H ₄ (14a)	2	17b	88	19ab	75 ^[g]	72 ^[h]
17 ^[f]	3-NO ₂ C ₆ H ₄ (14b)	2	17b	91	19bb	74 ^[g]	88 ^[h]

[a] Experimental conditions: To a mixture of catalyst **18** (0.0044 or 0.0055 mmol) in MeNO₂ (1.1 mL), aldehyde **2a-o** (0.22 mmol) was added at -24 °C. After the reaction time, product **19** was isolated by column chromatography. [b] After isolation by column chromatography. [c] Determined by chiral HPLC analysis. [d] These aldehydes showed acid traces in their ¹H-NMR spectra and they were previously purified by column chromatography (very short column, eluted with CH₂Cl₂ or MeCN) or extraction (dissolving these aldehydes in CH₂Cl₂ and washing with a 0.3 M solution of NaOH). Then, the CH₂Cl₂ was evaporated under vacuum and the aldehydes were used within 2-5 min to avoid acid formation. [e] d.r. 1:1.3 *anti:syn*. [f] d.r. 1:1.4 *anti:syn*. [g] Sum of the yield of all the diastereoisomers. [h] Enantiomeric excess (ee) for the major pair of diastereoisomers.

It is worth noting that the presence of traces of acid in the aldehydes could inactivate the catalyst used since the catalyst loadings used are quite low. This occurs because these acids protonates the amine group of the catalyst and this group cannot deprotonate any nitromethane molecules, which is necessary to promote the Henry reaction. Aldehydes **14d-f,h-n** were previously treated in order to avoid such inactivation.

Motivated by the good yields obtained with 2 mol% of catalyst **18**, we decided to lower the catalyst loading for four representative aldehydes (**14a-c,p**). As seen in Table 3.5, we obtained good results in reasonable reaction times using catalyst loadings as low as 0.25 mol%. This is the lowest value used in an organocatalytic Henry reaction and one of the lowest amounts employed so far in organocatalysis.^[46]

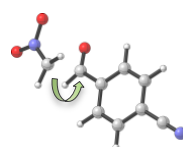
Table 3.5. Henry reactions catalyzed with 0.25-1 mol% of **18**.

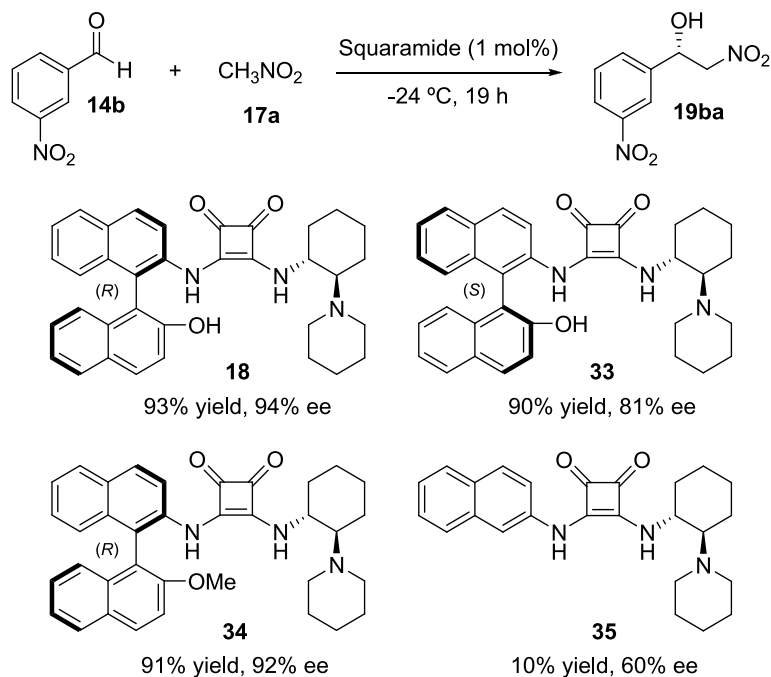
Entry ^[a]	R	18 (mol%)	t (h)	Product	Yield (%) ^[b]	ee (%) ^[c]
1	4-NO ₂ Ph (14a)	1	24	19aa	>95	82
2 ^[d]	4-NO ₂ Ph (14a)	0.5	76	19aa	>95	82
3 ^[e]	4-NO ₂ Ph (14a)	0.25	92	19aa	86	82
4	3-NO ₂ Ph (14b)	1	24	19ba	>95	94
5 ^[d]	3-NO ₂ Ph (14b)	0.5	76	19ba	>95	94
6 ^[e]	3-NO ₂ Ph (14b)	0.25	95	19ba	92	94
7 ^[f]	3-NO ₂ Ph (14b)	0.25	96	19ba	>95	94
8	4-CNPh (14c)	1	95	19ca	94	82
9 ^[d]	4-CNPh (14c)	0.5	91	19ca	>95	82
10 ^[e]	4-CNPh (14c)	0.25	92	19ca	59	82
11 ^[d]	F ₅ C ₅ (14p)	0.5	45	19pa	>95	86
12 ^[e]	F ₅ C ₅ (14p)	0.25	120	19pa	>95	86

^[a] Experimental conditions: To a mixture of catalyst **18** in MeNO₂ (1.1 mL), aldehyde **14a-c,p** (0.22 mmol) was further added at -24 °C. After the reaction time, product **19** was isolated by column chromatography (from 9:1 to 7:3 Hex:EtOAc). ^[b] After isolation by column chromatography. ^[c] Determined by chiral HPLC analysis. ^[d] Reaction scale: 0.44 mmol of aldehyde. ^[e] Reaction scale: 0.88 mmol of aldehyde. ^[f] Reaction scale: 1g of product.

In all of the examples, the products were obtained with the same enantiomeric excess, although the reaction times became longer as the amount of catalyst used was lower. Additionally, the reaction catalyzed with 0.25 mol% of squaramide **18** was successfully scaled up to obtain 1 gram of product **19ba** (Table 3.5, entry 7).

In order to determine which functional groups of catalyst **18** were playing significant roles in the catalysis, different squaramides derived from this compound were designed (Scheme 3.4). First, catalyst **33**, which has the opposite configuration (*S*) on the binaphthyl moiety compared to catalyst **18** (*R*), was synthesized. When this new catalyst (**33**) was used to promote the Henry reaction, product **19ba** was obtained with the same absolute configuration observed when **18** was employed. However, **19ba** was produced with a lower enantiomeric excess value compared to the corresponding product generated with catalyst **18** (81% vs 94% ee). This suggests that (1) the absolute configuration directly depends on the 2-(1-piperidinyl)cyclohexylamine moiety and (2) the difference in the enantiomeric excess of the products observed suggests that the orientation of the binaphthyl group of the catalysts affects the energy of the different reaction pathways.





Scheme 3.4. Additional squaramide-based organocatalysts tested.

Moreover, when catalyst **34** (with a OMe group instead of a OH group) was employed, the Henry reaction of **14b** showed the same yield and enantiomeric excess as those obtained with catalyst **18** (Scheme 3.4). This suggests that the OR (R = H or Me) group does not significantly participate in the reaction mechanism. Finally, when the reaction was performed with catalyst **35** (with a naphthyl group instead of the binaphthyl group of **18**), the reactivity and the enantioselectivity of the process became considerably lower (10% yield, 60% ee). These results show that the second naphthyl group of the binaphthyl structure of catalyst **18** plays a major role in the reaction mechanism.

In order to study how multifunctional catalyst **18** interacts with the substrates during the Henry reaction, diverse computational calculations were performed to determine the most favorable transition state for this reaction. These mechanistic studies will be described in detail in chapters 4 and 5.

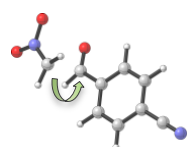
3.4 Conclusions

In conclusion, a new class of trifunctional squaramide catalyst (**18**) was developed to catalyze the Henry reaction. This catalyst creates different non-covalent interactions with the substrates through three different groups, which significantly improves the reactivity and the stereoselectivity of the process. In this Henry reaction, only 0.25 mol% of catalyst loading was required for various aldehydes, which is one of the lowest amounts used in organocatalysis.

Moreover, we observed that (1) the OH group of catalyst **18** did not affect the outcomes of the reaction and (2) the second naphthyl group of the binaphthyl moiety of this catalyst is significantly involved in the reaction mechanism. In fact, when a catalyst that does not contain this group (**36**) was employed, the yield and enantioselectivity of the reaction dropped dramatically in comparison with the results obtained when using catalyst **18**.

3.5 References

- [38] Henry, L. C. *R. Hebd. Séances Acad. Sci.* **1895**, 120, 1265.
- [39] Luzzio, F. A. *Tetrahedron* **2001**, 57, 915.
- [40] a) Ono, N. (Ed.) *The Nitro Group in Organic Synthesis*. Wiley-VCH, New York, **2001**; b) Bergmeier, S. C. *Tetrahedron* **2000**, 56, 2561.
- [41] Chinchilla, R.; Nájera, C.; Sánchez-Agulló, P. *Tetrahedron Asymmetry* **1994**, 5, 1393.
- [42] Álvarez-Casao, Y.; Marqués-López, E.; Herrera, R. P. *Symmetry* **2011**, 3, 220.
- [43] a) Boruwa, J.; Gogoi, N.; Saikia, P. P.; Barua, N. C. *Tetrahedron Asymmetry* **2006**, 17, 3315; b) Palomo, C.; Oiarbide, M.; Mielgo, A. *Angew. Chem. Int. Ed.* **2004**, 43, 5442; c) Palomo, C.; Oiarbide, M.; Laso, A. *Eur. J. Org. Chem.* **2007**, 2561.
- [44] a) Liu, F. *Chirality* **2013**, 25, 675; b) Kenny, R.; Liu, F. *Eur. J. Org. Chem.* **2015**, 5304.
- [45] Pihko, P. M. (Ed.) *Hydrogen Bonding in Organic Synthesis*. Wiley-VCH, Weinheim, **2009**.
- [46] Giacalone, F.; Gruttadauria, M.; Agrigento, P.; Noto, R. *Chem. Soc. Rev.* **2012**, 41, 2406.

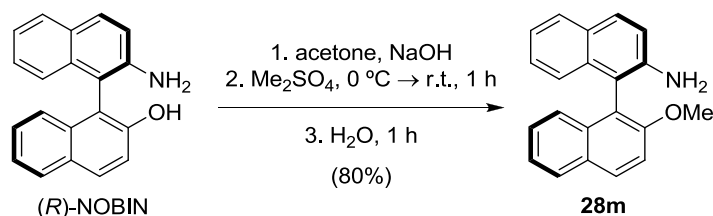


3.7 Supporting Information

General Experimental Methods

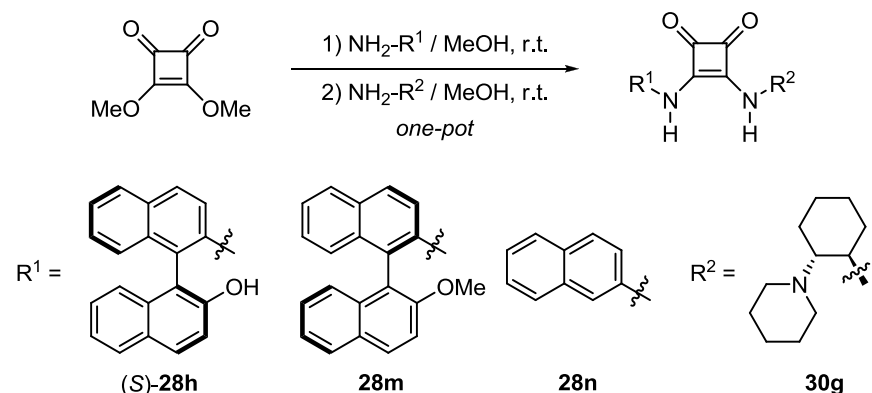
Purification of reaction products was carried out by filtration or flash chromatography using silica-gel (0.063-0.200 mm). Analytical thin layer chromatography was performed on 0.25 mm silica gel 60-F plates. ESI ionization method and mass analyzer type MicroTof-Q were used for the HRMS measurements. $^1\text{H-NMR}$ spectra were recorded at 300 and 400 MHz. ^{13}C APT-NMR spectra were recorded at 75 and 100 MHz. CDCl_3 , CD_3CN and DMSO-d_6 were used as the deuterated solvents. Chemical shifts were reported in the δ scale relative to residual CHCl_3 (7.26 ppm), MeCN (1.94 ppm) and DMSO (2.50 ppm) for $^1\text{H-NMR}$ and to the central line of CDCl_3 (77 ppm), CD_3CN (1.24 ppm) and DMSO-d_6 (39.43 ppm) for ^{13}C APT-NMR. $^1\text{H-NMR}$ and ^{13}C APT-NMR spectra of amine **28m** and squaramides **34-35** are included in the annex on the CD (Figures S3.1-S3.4). Additionally, HPLC chromatograms of compounds **19** are included in the annex (Figures S3.5-S3.40).

Synthesis of amine **28m**



To a stirred solution of (*R*)-NOBIN (0.2 mmol, 58 mg) in anhydrous acetone (0.85 mL), NaOH (0.6 mmol, 24 mg) was added. Then, the mixture was placed in an ice bath and Me_2SO_4 (0.3 mmol, 29 μL) was slowly added dropwise. When the addition of Me_2SO_4 was completed, the solution was allowed to stand at r.t. for 1 hour. Then, H_2O (0.3 mL) was added. After 1 hour, acetone was removed under vacuum and 0.3 mL of H_2O were added. The aqueous phase was extracted with EtOAc (3 x 1 mL). The combined organic phases were collected, dried over Na_2SO_4 , filtered and evaporated under vacuum. Amine **28m** was obtained by column chromatography (from 95:5 to 7:3 Hex:EtOAc) as a pale brown solid in 80% yield (47.9 mg). $[\alpha]_{\text{D}}^{24} = +115.5$ (*c* 0.17, THF). $^1\text{H-NMR}$ (300 MHz, CD_3CN) δ 8.07 (d, $J = 9.1\text{Hz}$, 1H), 7.94 (d, $J = 8.6\text{ Hz}$, 1H), 7.82-7.74 (m, 2H), 7.58 (d, $J = 9.1\text{ Hz}$, 1H), 7.38-7.03 (m, 6H), 6.84-6.75 (m, 1H), 3.93 (br s, 2H), 3.75 (s, 3H). ^{13}C APT-NMR (75 MHz, CD_3CN) δ 156.6 (1C), 144.5 (1C), 130.9 (1C), 130.7 (1C), 129.7 (1C), 129.2 (1C), 129.0 (1C), 128.8 (1C), 127.7 (1C), 127.2 (1C), 125.5 (1C), 124.8 (1C), 124.5 (1C), 122.6 (1C), 119.3 (1C), 115.4 (1C), 113.4 (1C), 57.1 (1C). (KBr film) (cm^{-1}) ν 3369, 3186, 3055, 2922, 2849, 1660, 1620, 1593, 1524, 1503, 1464, 1430, 1344, 1265, 1211, 1178, 1146, 1085, 1020, 865, 746, 730. MS (ESI+) 300.2 [$\text{M}+\text{H}$].

General procedure of the synthesis of squaramides **33-35**

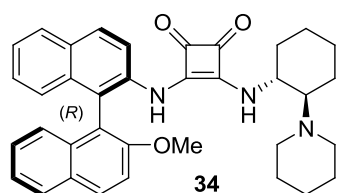


To a mixture of 3,4-dimethoxy-3-cyclobutene-1,2-dione (0.2 mmol) in MeOH (0.5-1 mL) the aromatic amine ($\text{NH}_2\text{-R}^1$) (0.2 mmol) was firstly added at room temperature. After the corresponding reaction time (t_1), the aliphatic amine ($\text{NH}_2\text{-R}^2$) (0.2 mmol) was then added dissolved in MeOH (1-2.5 mL). After the corresponding reaction time (t_2), the product was purified by filtration, washing with MeOH at $-25\text{ }^\circ\text{C}$, or by column chromatography. Pure compounds were obtained as stable solids.

3-((S)-2'-hydroxy-1,1'-binaphthyl-2-ylamino)-4-((1R,2R)-2-(piperidin-1-yl)cyclohexylamino)cyclobut-3-ene-1,2-dione (33**)**

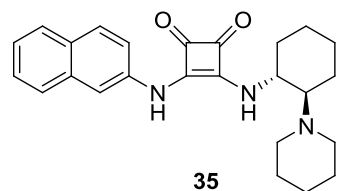
Following the general procedure, using 0.75 mL MeOH / 72 h and 1.25 mL MeOH / 3 h for the first and second step, respectively, **33** was obtained by filtration as a pale yellow solid in 58% yield (63.3 mg). $[\alpha]_{\text{D}}^{29} = -41.0$ (c 0.19, DMSO). $^1\text{H-NMR}$ (400 MHz, $\text{DMSO-}d_6$) δ 9.58 (br s, 1H), 8.57 (br s, 1H), 8.11-7.83 (m, 4H), 7.74-7.58 (m, 1H), 7.56-7.43 (m, 1H), 7.43-7.33 (m, 2H), 7.26 (t, $J = 7.4$ Hz, 2H), 7.18 (t, $J = 7.6$ Hz, 1H), 6.95 (d, $J = 8.4$ Hz, 1H), 6.88 (d, $J = 8.0$ Hz, 1H), 3.90-3.72 (m, 1H), 2.29-2.05 (m, 3H), 1.96-1.50 (m, 5H), 1.48-0.98 (m, 11H). $^{13}\text{C APT-NMR}$ (100 MHz, $\text{DMSO-}d_6$) δ 184.6 (1C), 180.3 (1C), 169.6 (1C), 163.7 (1C), 153.4 (1C), 135.0 (1C), 133.6 (1C), 132.6 (1C), 130.6 (1C), 129.8 (1C), 128.2 (1C), 128.1 (1C), 127.9 (2C), 126.3 (2C), 125.1 (1C), 124.5 (1C), 123.7 (1C), 122.6 (1C), 122.5 (1C), 118.6 (1C), 113.5 (1C), 68.2 (1C), 54.0 (1C), 49.2 (2C), 34.0 (1C), 26.2 (2C), 24.7 (1C), 24.4 (2C), 23.5 (2C). IR (KBr film) (cm^{-1}) ν 3249, 2924, 2853, 1794, 1655, 1594, 1524, 1506, 1465, 1448, 1434, 1377, 1339, 1270, 811, 751, 451. HRMS (ESI+) calcd $\text{C}_{35}\text{H}_{36}\text{N}_3\text{O}_3$ 546.2757; found 546.1961 [M+H].

3-((*R*)-2'-methoxy-1,1'-binaphthyl-2-ylamino)-4-((1*R*,2*R*)-2-(piperidin-1-yl)cyclohexylamino)cyclobut-3-ene-1,2-dione (**34**)



Following the general procedure in a 0.15 mmol scale, using 1 mL MeOH / 71 h and 1 mL MeOH / 14 h for the first and second step, respectively, compound **34** was obtained by column chromatography (from 6:4 Hex:EtOAc to 9:1 EtOAc:MeOH) as a pale yellow solid in 31% yield (26.0 mg). $[\alpha]_D^{28} = -54.8$ (*c* 0.26, MeCN). $^1\text{H-NMR}$ (300 MHz, CD_3CN) δ 8.13 (d, $J = 9.1$ Hz, 1H), 8.04 (d, $J = 8.9$ Hz, 1H), 8.00-7.93 (m, 2H), 7.89 (d, $J = 8.9$ Hz, 1H), 7.60 (d, $J = 9.1$ Hz, 1H), 7.44-7.19 (m, 5H), 7.04-6.94 (m, 2H), 6.11 (br s, 1H), 3.76 (s, 3H), 3.75-3.50 (m, 1H), 2.56-2.40 (m, 2H), 2.35-2.25 (m, 1H), 2.22-2.05 (m, 3H), 1.85-1.74 (m, 1H), 1.74-1.66 (m, 1H), 1.66-1.55 (m, 1H), 1.40-1.02 (m, 10H). ^{13}C APT-NMR (75 MHz, CD_3CN) δ 185.8 (1C), 182.3 (1C), 170.6 (1C), 164.8 (1C), 156.6 (1C), 135.8 (1C), 134.5 (1C), 134.1 (1C), 131.9 (1C), 131.8 (1C), 130.4 (1C), 129.7 (1C), 129.2 (1C), 129.1 (1C), 128.0 (1C), 127.7 (1C), 126.1 (1C), 125.9 (1C), 125.1 (1C), 124.8 (1C), 122.3 (1C), 117.6 (2C), 114.9 (1C), 69.3 (1C), 57.0 (1C), 55.6 (1C), 50.3 (2C), 35.2 (1C), 27.2 (2C), 26.0 (1C), 25.4 (2C), 24.0 (1C). IR (KBr film) (cm^{-1}) ν 3253, 2930, 2854, 2780, 1792, 1678, 1593, 1545, 1504, 1463, 1427, 1339, 1270, 1259, 1086, 1055, 810, 748, 419. HRMS (ESI+) calcd $\text{C}_{36}\text{H}_{38}\text{N}_3\text{O}_3$ 560.2313; found 560.2242 [M+H].

3-(naphthalen-2-ylamino)-4-((1*R*,2*R*)-2-(piperidin-1-yl)cyclohexylamino)cyclobut-3-ene-1,2-dione (**35**)



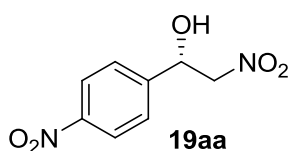
Following the general procedure, using 0.5 mL MeOH / 22 h and 2.5 mL MeOH / 8 h for the first and second step, respectively, compound **35** was obtained by filtration as a pale yellow solid in 81% yield (65.4mg). $[\alpha]_D^{29} = -47.4$ (*c* 0.20, DMSO). $^1\text{H-NMR}$ (300 MHz, $\text{DMSO-}d_6$) δ 9.89 (br s, 1H), 8.00-7.75 (m, 4H), 7.65 (d, $J = 8.3$ Hz, 1H), 7.51 (br s, 1H), 7.48 (t, $J = 7.3$ Hz, 1H), 7.38 (t, $J = 7.4$ Hz, 1H), 4.08-3.84 (m, 1H), 2.70-2.55 (m, 2H), 2.37-2.20 (m, 3H), 2.15-2.02 (m, 1H), 1.90-1.80 (m, 1H), 1.80-1.60 (m, 2H), 1.50-1.05 (m, 10H). ^{13}C APT-NMR (75 MHz, $\text{DMSO-}d_6$) δ 184.2 (1C), 180.2 (1C), 169.8 (1C), 162.9 (1C), 136.9 (1C), 133.7 (1C), 129.3 (1C), 129.2 (1C), 127.7 (1C), 127.0 (1C), 126.8 (1C), 124.4 (1C), 119.0 (1C), 113.5 (1C), 68.4 (1C), 54.4 (1C), 49.4 (2C), 34.1 (1C), 26.4 (2C), 24.8 (1C), 24.6 (1C), 24.5 (1C), 23.4 (1C). IR (KBr film) (cm^{-1}) ν 3178, 2924, 2853, 1791, 1657, 1634, 1605, 1588, 1567, 1512, 1453, 1380, 1272, 1138, 872, 740, 470. HRMS (ESI+) calcd $\text{C}_{25}\text{H}_{30}\text{N}_3\text{O}_2$ 404.2338; found 404.2180 [M+H].

Representative procedure of the Henry reaction of aldehydes **14** catalyzed by **18**

To a mixture of catalyst **18** (0.0044 mmol unless otherwise stated in Tables 3.4 and 3.5) and aldehyde **14a-p** (0.22 mmol), MeNO_2 (**17a**) or EtNO_2 (**17b**) (1.1 mL) was added in a test tube at -24 °C. After the corresponding reaction time, adducts **19** were isolated by flash

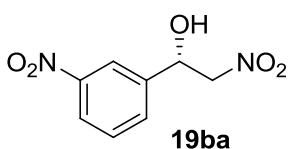
chromatography (from 9:1 to 7:3 Hex:EtOAc unless otherwise specified). Yields and enantiomeric excesses are reported in Tables 3.4 and 3.5. If acid traces were observed in the aldehydes by NMR, these aldehydes were previously purified by column chromatography (very short column, eluted with CH₂Cl₂ or MeCN) or extraction (dissolving these aldehydes in CH₂Cl₂ and washing them with a 0.3 M solution of NaOH). Then, the CH₂Cl₂ was evaporated in vacuum and the aldehydes were used within 2-5 minutes to avoid acid formation.

(S)-2-Nitro-1-(4-nitrophenyl)ethanol (19aa)^[S1]



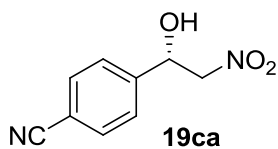
Following the general procedure, compound **19aa** was obtained after 24 h of reaction as a dark green oil in >95% yield. The ee of the product was determined to be 83% by HPLC using a Daicel Chiralpak IA column (Hex:PrOH = 80:20, flow rate 1 mL min⁻¹, λ = 230.3 nm): τ_{major} = 15.6 min; τ_{minor} = 12.1 min. [α]_D²⁸ = +23.2 (C 1.30, CHCl₃, 82% ee) {lit.,^[S1] [α]_D²⁴ = -30.4 (C 0.53, CHCl₃) for (*R*)-**19aa**, 88% ee}.

(S)-2-Nitro-1-(3-nitrophenyl)ethanol (19ba)^[S2]



Following the general procedure, compound **19ba** was obtained after 24 h of reaction as a dark green solid in >95% yield. The ee of the product was determined to be 94% by HPLC using a Daicel Chiralpak IB column (Hex:PrOH = 80:20, flow rate 1 mL min⁻¹, λ = 281.7 nm): τ_{major} = 10.5 min; τ_{minor} = 9.9 min. [α]_D²³ = +27.2 (C 0.33, CHCl₃, 94% ee) {lit.,^[S2] [α]_D²⁶ = -27.4 (C 0.87, CH₂Cl₂) for (*R*)-**19ba**, 96% ee}.

(S)-4-(1-Hydroxy-2-nitroethyl)benzonitrile (19ca)^[S3]



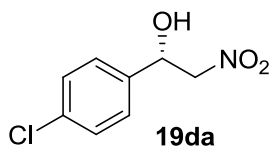
Following the general procedure, compound **19ca** was isolated by flash chromatography after 71 h of reaction as a pale brown solid in >95% yield. The ee of the product was determined to be 82% by HPLC using a Daicel Chiralpak IB column (Hex:PrOH = 90:10, flow rate 1 mL min⁻¹, λ = 243.5 nm): τ_{major} = 27.6 min; τ_{minor} = 25.3 min. [α]_D²⁴ = +36.3 (C 0.74, CHCl₃, 81% ee) {lit.,^[S4] [α]_D²⁰ = -32.8 (C 0.50, CH₂Cl₂) for (*R*)-**19ca**, 90% ee}.

[S1] Steurer, M.; Bolm, C. *J. Org. Chem.* **2010**, *75*, 3301.

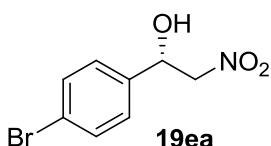
[S2] Kitagaki, S.; Ueda, T.; Mukai, C. *Chem. Commun.* **2013**, *49*, 4030.

[S3] Bray, C. V.-L.; Jiang, F.; Wu, X.-F.; Sortais, J.-B.; Darcel, C. *Tetrahedron Lett.* **2010**, *51*, 4555.

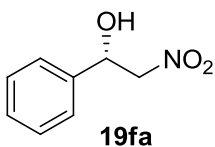
[S4] Constable, E. C.; Zhang, G.; Housecroft, C. E.; Neuburger, M.; Schaffner, S.; Woggon, W.-D.; Zampese, J. A. *New J. Chem.* **2009**, *33*, 2166.

(S)-1-(4-Chlorophenyl)-2-nitroethanol (19da)^[S1]

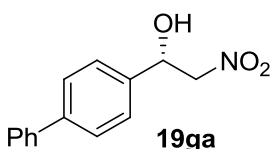
Following the general procedure and purifying the aldehyde by column chromatography (eluted with CH₂Cl₂), compound **19da** was obtained after 91 h of reaction as a dark brown oil in 81% yield. The ee of the product was determined to be 86% by HPLC using a Daicel Chiralpak IB column (Hex:PrOH = 90:10, flow rate 1 mL min⁻¹, λ = 230.1 nm): T_{major} = 12.6 min; T_{minor} = 11.1 min. [α]_D²³ = +27.2 (C 0.31, CHCl₃, 86% ee) {lit.,^[S1] [α]_D²² = -38.8 (C 0.55, CHCl₃) for (*R*)-**19da**, 90% ee}.

(S)-1-(4-Bromophenyl)-2-nitroethanol (19ea)^[S5]

Following the general procedure and purifying the aldehyde by column chromatography (eluted with CH₂Cl₂), compound **19ea** was obtained after 91 h of reaction as a dark brown oil in 75% yield. The ee of the product was determined to be 86% by HPLC using a Daicel Chiralpak IA column (Hex:PrOH = 90:10, flow rate 1 mL min⁻¹, λ = 237.2 nm): T_{major} = 14.9 min; T_{minor} = 12.2 min. [α]_D²³ = +20.1 (C 0.27, CHCl₃, 86% ee) {lit.,^[S5] [α]_D²³ = -68.6 (C 1.40, CHCl₃) for (*R*)-**19ea**, 89% ee}.

(S)-2-Nitro-1-phenylethanol (19fa)^[S6]

Following the general procedure and purifying the aldehyde by basic washing, compound **19fa** was obtained after 86 h of reaction as a dark brown oil in 59% yield. The ee of the product was determined to be 82% by HPLC using a Daicel Chiralpak IB column (Hex:PrOH = 90:10, flow rate 1 mL min⁻¹, λ = 248.1 nm): T_{major} = 11.3 min; T_{minor} = 10.1 min. [α]_D²⁵ = +11.9 (C 1.1, CH₂Cl₂, 82% ee) {lit.,^[S6] [α]_D²¹ = -41.6 (C 1.03, CH₂Cl₂) for (*R*)-**19fa**, 94% ee}.

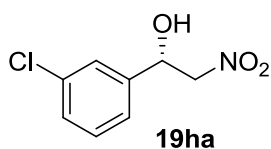
(S)-1-([1,1'-Biphenyl]-4-yl)-2-nitroethanol (19ga)^[S6]

Following the general procedure, compound **19ga** was isolated by flash chromatography after 96 h of reaction as a yellow solid in 50% yield. The ee of the product was determined to be 90% by HPLC using a Daicel Chiralpak IB column (Hex:PrOH = 90:10, flow rate 1 mL min⁻¹, λ = 231.2 nm): T_{major} = 16.3 min; T_{minor} = 13.3 min. [α]_D²³ = +25.8 (C 0.47, CHCl₃, 88% ee) {lit.,^[S6] [α]_D²³ = -36.1 (C 1.35, CH₂Cl₂) for (*R*)-**19ga**, 91% ee}.

[S5] Bulut, A.; Aslan, A.; Dogan, Ö. *J. Org. Chem.* **2008**, *73*, 7373.

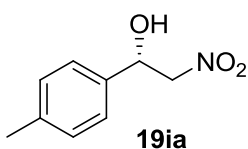
[S6] Evans, D. A.; Seidel, D.; Rueping, M.; Lam, H. W.; Shaw, J. T.; Downey, C. W. *J. Am. Chem. Soc.* **2003**, *125*, 12692.

(S)-1-(3-Chlorophenyl)-2-nitroethanol (19ha)^[S7]



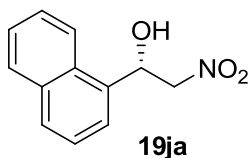
Following the general procedure and purifying the aldehyde by basic washing, compound **19ha** was obtained after 86 h of reaction as a dark brown oil in 62% yield. The ee of the product was determined to be 90% by HPLC using a Daicel Chiralpak IB column (Hex:ⁱPrOH = 90:10, flow rate 1 mL min⁻¹, λ = 226.2 nm): τ_{major} = 11.8 min; τ_{minor} = 10.3 min. [α]_D²⁴ = +24.8 (C 1.4, CHCl₃, 90% ee) {lit.,^[S7] [α]_D²⁷ = +31.17 (C 1.0, CHCl₃) for 95% ee}.

(S)-2-Nitro-1-*p*-tolylethanol (19ia)^[S8]



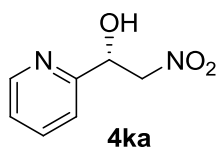
Following the general procedure and purifying the aldehyde by column chromatography (eluted with CH₂Cl₂), compound **19ia** was obtained after 6 days of reaction as a dark brown oil in 20% yield. The ee of the product was determined to be 84% by HPLC using a Daicel Chiralpak IB column (Hex:ⁱPrOH = 95:5, flow rate 1 mL min⁻¹, λ = 220 nm): τ_{major} = 19.8 min; τ_{minor} = 17.0 min. [α]_D¹⁸ = +26.8 (C 0.25, CHCl₃, 84% ee) {lit.,^[S8] [α]_D²⁰ = +34.1 (C = 1.90, CHCl₃) for (S)-**19ia**, 84% ee}.

(S)-1-(Naphthalen-1-yl)-2-nitroethanol (19ja)^[S1]



Following the general procedure and purifying the aldehyde by basic washing, compound **19ja** was obtained after 86 h of reaction as a dark brown oil in 50% yield. The ee of the product was determined to be 85% by HPLC using a Daicel Chiralpak IB column (Hex:ⁱPrOH = 90:10, flow rate 1 mL min⁻¹, λ = 254.0 nm): τ_{major} = 14.5 min; τ_{minor} = 11.6 min. [α]_D²⁷ = +19.1 (C 0.85, CHCl₃, 85% ee) {lit.,^[S1] [α]_D²¹ = +24.5 (C 0.53, CHCl₃, for (S)-**19ja**, 88% ee}.

(S)-2-Nitro-1-(pyridin-2-yl)ethanol (19ka)^[S9]

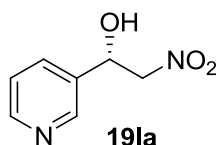


Following the general procedure and purifying the aldehyde by column chromatography (eluted with MeCN), compound **19ka** was isolated by flash chromatography (from 8:2 to 1:1 Hex:EtOAc) after 96 h of reaction as a dark brown oil in >95% yield. The ee of the product was determined to be 80% by HPLC using a Daicel Chiralpak IA column (Hex:ⁱPrOH = 90:10, flow rate 1 mL min⁻¹, λ = 218.4 nm): τ_{major} = 12.1 min; τ_{minor} = 15.3 min. [α]_D²⁴ = +49.8 (C 0.16, CHCl₃, 80% ee).

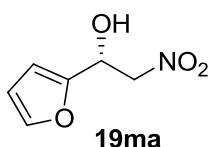
[S7] Soltani, O.; Ariger, M. A.; Vázquez-Villa, H.; Carreira, E. M. *Org. Lett.* **2010**, *12*, 2893.

[S8] Zheng, B.; Wang, M.; Li, Z.; Bian, Q.; Mao, J.; Li, S.; Liu, S.; Wang, M.; Zhong, J.; Guo, H. *Tetrahedron Asymmetry* **2011**, *22*, 1156.

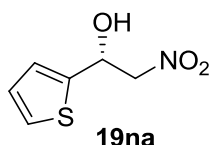
[S9] Kanagaraj, K.; Sureh, P.; Pitchumani, K. *Org. Lett.* **2010**, *12*, 4070.

(S)-2-Nitro-1-(pyridin-3-yl)ethanol (19la)^[S10]

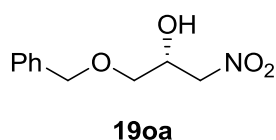
Following the general procedure and purifying the aldehyde by column chromatography (eluted with MeCN), compound **19la** was isolated by flash chromatography (from 7:3 to 2:8 Hex:EtOAc) after 92 h of reaction as a dark brown oil in 95% yield. The ee of the product was determined to be 92% by HPLC using a Daicel Chiralpak IA column (Hex:PrOH = 90:10, flow rate 1 mL min⁻¹, λ = 240.2 nm): T_{major} = 24.3 min; T_{minor} = 28.3 min. [α]_D²⁹ = +35.1 (C 0.23, MeCN, 92% ee).

(R)-1-(Furan-2-yl)-2-nitroethanol (19ma)^[S11]

Following the general procedure and purifying the aldehyde by column chromatography (eluted with CH₂Cl₂), compound **19ma** was obtained after 88 h of reaction as a dark brown oil in 74% yield. The ee of the product was determined to be 92% by HPLC using a Daicel Chiralpak IA column (Hex:PrOH = 90:10, flow rate 1 mL min⁻¹, λ = 224.8 nm): T_{major} = 10.9 min; T_{minor} = 10.2 min. [α]_D²⁹ = +36.3 (C 0.16, CHCl₃, 92% ee) {lit.,^[S3] [α]_D²³ = -36.7 (C 2.72, CHCl₃) for (S)-**19ma**, 85% ee}.

(R)-2-Nitro-1-(thiophen-2-yl)ethanol (19na)^[S11]

Following the general procedure and purifying the aldehyde by column chromatography (eluted with CH₂Cl₂), compound **19na** was obtained after 92 h of reaction as a dark brown oil in 55% yield. The ee of the product was determined to be 92% by HPLC using a Daicel Chiralpak IB column (Hex:PrOH = 90:10, flow rate 1 mL min⁻¹, λ = 246.6 nm): T_{major} = 12.0 min; T_{minor} = 11.4 min. [α]_D²⁹ = +35.9 (C 0.08, CHCl₃, 90% ee) {lit.,^[S5] [α]_D²³ = -26.4 (C 3.11, CHCl₃) for (S)-**19na**, 86% ee}.

(R)-1-(Benzyloxy)-3-nitropropan-2-ol (19oa)^[S12]

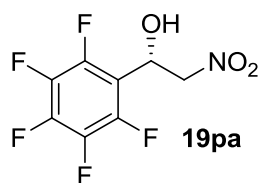
Following the general procedure, compound **19oa** was isolated by flash chromatography after 92 h of reaction as a dark brown oil in 66% yield. The ee of the product was determined to be 76% by HPLC using a Daicel Chiralpak IB column (Hex:PrOH = 95:5, flow rate 1 mL min⁻¹, λ = 227.7 nm): T_{major} = 22.6 min; T_{minor} = 25.0 min. [α]_D²⁴ = +7.8 (C 0.25, CHCl₃, 76% ee) {lit.,^[S13] [α]_D = +1.5 (C 0.9, CH₂Cl₂) for (R)-**19oa**, 80% ee}.

[S10] Marcelli, T.; van der Haas, R. N. S.; van Maarseveen, J. H.; Hiemstra, H. *Angew. Chem. Int. Ed.* **2006**, *45*, 929.

[S11] Kanagaraj, K.; Suresh, P.; Pitchumani, K. *Org. Lett.* **2010**, *12*, 4070.

[S12] Borah, J. C.; Gogoi, S.; Boruwa, J.; Barua, N. C. *Synth. Commun.* **2005**, *35*, 873.

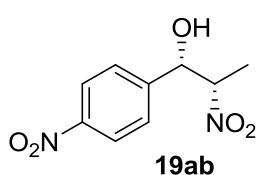
(S)-2-Nitro-1-(perfluorophenyl)ethanol (19pa)^[S13]



90% ee).

Following the general procedure, compound **19pa** was isolated by flash chromatography (from 95:5 to 9:1 Hex:EtOAc) after 120 h of reaction as a yellow oil in >95% yield. The ee of the product was determined to be 86% by HPLC using a Daicel Chiralpak IA column (Hex:ⁱPrOH = 95:5, flow rate 1 mL min⁻¹, λ = 232.8 nm): τ_{major} = 10.9 min; τ_{minor} = 12.4 min. [α]_D²⁸ = +2.8 (C 1.1, CHCl₃, 86% ee) {lit.,^[S13] [α]_D = +8.9 (C 0.8, CH₂Cl₂) for (S)-**19pa**,

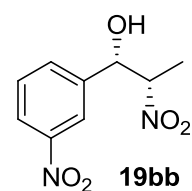
2-Nitro-1-(4-nitrophenyl)propan-1-ol (19ab)^[S11,S14]



min.

Following the general procedure, compound **19ab** was isolated by flash chromatography (from 95:5 to 9:1 Hex:EtOAc) after 88 h of reaction as a dark green solid in 75% yield.^[S11,S14] The diastereomeric ratio (*anti:syn*, 1:1.3) was determined by ¹H-NMR. The ee of the major product was determined to be 72% (*syn* isomer) by HPLC using a Daicel Chiralpak IA column (Hex:ⁱPrOH = 90:10, flow rate 1 mL min⁻¹, λ = 242.0 nm): τ_{major} = 29.9 min; τ_{minor} = 25.9

2-Nitro-1-(3-nitrophenyl)propan-1-ol (19bb)^[S11,S14]



Following the general procedure, compound **19bb** was isolated by flash chromatography (from 95:5 to 9:1 Hex:EtOAc) after 91 h of reaction as a dark green solid in 74% yield. The diastereomeric ratio (*anti:syn*, 1:1.4) was determined by ¹H-NMR.^[S11,S14] The ee of the major product was determined to be 87% (*syn* isomer) by HPLC using a Daicel Chiralpak IB column (Hex:ⁱPrOH = 95 : 5, flow rate 1 mL min⁻¹, λ = 238.4 nm): τ_{major} = 35.6 min; τ_{minor} = 31.5 min.

[S13] Bandini, M.; Piccinelli, F.; Tommasi, S.; Umami-Ronchi, A.; Ventrici, C. *Chem. Commun.* **2007**, 616.

[S14] Boobalan, R.; Lee, G.-H.; Chen, C. *Adv. Synth. Catal.* **2012**, 354, 2511.

4

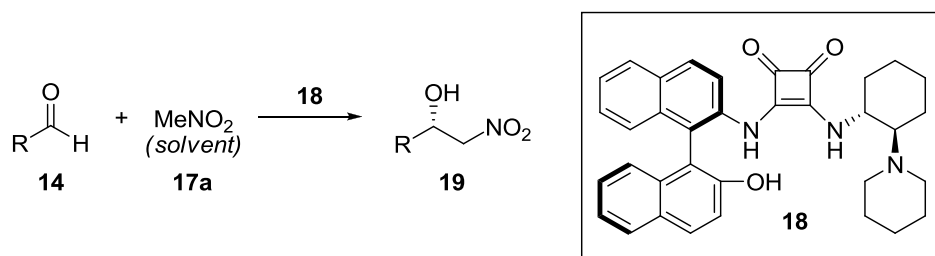
OPTIMIZING ACCURACY AND COMPUTATIONAL COST IN THEORETICAL SQUARAMIDE CATALYSIS: THE HENRY REACTION

4.1 Introduction

After millions of years of evolution, nature has shown us that the development of highly effective biocatalysts is related to the increase in the complexity of the catalytic systems. Currently, scientists are able to obtain a great number of chiral products that some decades ago were impossible to synthesize. One of the main factors that has made this possible is the emergence of novel complex catalytic systems that bind more efficiently and selectively to the substrates employed in the reactions.

In asymmetric organocatalysis, the non-covalent interactions created in the catalyst-substrate aggregates are typically crucial for promoting the chemical transformations.^[47] As the catalytic systems become more complex, they contain more non-covalent interactions and the study of reaction mechanisms is more challenging. In this area, squaramides are a good example of complex catalysts that lead to outstanding results through the creation of a significant number of non-covalent interactions with the substrates.^[48]

In this investigation, we studied the Henry reaction catalyzed by trifunctional squaramide **18** (Scheme 4.1). This reaction represents a clear example of a complex and effective catalytic system in which a great number of non-covalent interactions are formed, including hydrogen bonds, π -oxygen, π -hydrogen and other kinds of weak interactions.^[49] Furthermore, the catalyst-substrate complexes formed during the reaction mechanism are relatively large, containing around 100 atoms. This represents a challenge when choosing an appropriate computational approach to study the mechanism since the computation times might become prohibitively long with many approaches.



Scheme 4.1. Henry reaction catalyzed by squaramide **18**.

As detailed in the previous chapter, catalyst **18** creates non-covalent interactions with the substrates mainly through three different groups: an amino, a squaramido and a naphthyl group. All these interactions make the catalytic system very efficient to promote the process. In fact, the Henry reactions are performed with a catalyst loading of only 0.25 mol%, which is currently the lowest amount used for this reaction in organocatalysis.

Squaramide catalysis is a research field that has been scarcely developed in computational chemistry and there are not many studies that have tackled this issue up to date.^[50] Moreover, the accuracy of different combinations of basis sets and functionals has never been compared to experimental results. In this area, there are different factors that make the study of the mechanisms challenging, such as the large amount of atoms that the catalyst-substrate complexes contain. Many times, relatively large basis sets are used to obtain reliable results in computational Organocatalysis; however, sometimes the amount of calculation time required is prohibitive for studying considerably large systems. Another challenge is that squaramide catalysts show complex structures with functional groups that can adopt multiple conformations.^[48b,51]

4.2 Objectives

The main goal of this research was to find a suitable computational approach to study the Henry reaction catalyzed by squaramide **18**. It is highly desirable to find computational approaches that provide accurate results while requiring the least amount of computation time as possible in organocatalysis. This investigation could be crucial for the development of computational squaramide catalysis, an area in which researchers normally deal with catalyst-substrate aggregates that contain large amounts of atoms and complex structures.

In this study, different methods and basis sets will be tested in order to find the computational approach with the best compromise of accuracy and computation time. Additionally, the changes in the results when ultrafine grids and diverse corrections are included will be evaluated.

4.3 Results and Discussion

Initially, in order to gather useful information about this reaction for the calculations, diverse kinetic, kinetic isotope effect (KIE) and ¹H-NMR experiments were performed. Also, we studied the outcomes of the reactions when different catalysts and additives were used. As the model aldehyde, we used 4-cyanobenzaldehyde (**14c**) because it is already available, easy to handle and the amount of its acid form is neglectable. Moreover, the same temperature was employed in all the experiments (30.9 °C, measured with a glycol solution in DMSO-*d*₆).

¹H-NMR experiments to study the interactions created between the catalyst and substrates.

First, we investigated how the different substrates of the reaction and the catalyst interacted with each other with NMR spectroscopy. CD_3CN was used as the solvent for the $^1\text{H-NMR}$ experiments instead of CD_3NO_2 because when we used CD_3NO_2 the reaction started right after the addition of aldehyde **14c**. In CD_3CN , the conformations that the molecules adopt are different than those observed in CD_3NO_2 ; however, the results obtained when using CD_3CN could bring a useful vision of the interactions formed in the catalyst-reagent complexes. In the $^1\text{H-NMR}$ experiments, the concentration of the catalyst was maintained constant and the shifts in its ^1H signals were measured after the addition of different amounts of MeNO_2 (**17a**) and aldehyde **14c**.

The catalyst's ^1H signals showed only small shifts when **14c** was added, even when large amounts of this aldehyde were used (Figure 4.1). This suggests that **14c** interacts very weakly with catalyst **18** and, with this information, we cannot determine the exact parts involved in the interactions.

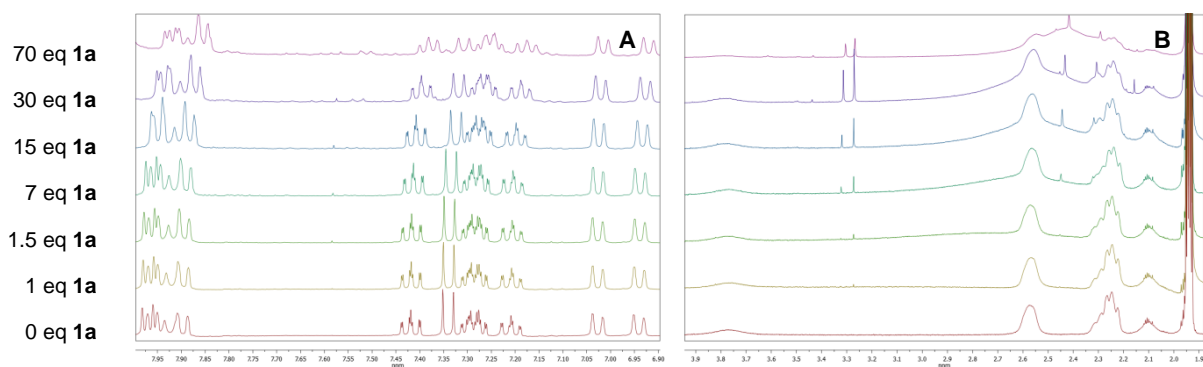


Figure 4.1. $^1\text{H-NMR}$ spectra of squaramide **18** (0.01 mmol) in CD_3CN (0.5 mL) after the addition of different amounts of **14c** (0-70 eq). (A) Aromatic region (from 7.95 to 6.90 ppm). (B) Aliphatic region (from 3.95 to 1.85 ppm).

On the contrary, the squaramide's peaks moved significantly when one equivalent of MeNO_2 was added (Figure 4.2). After this point, they did not shift further after subsequent MeNO_2 additions. This indicates that squaramide **18** deprotonates MeNO_2 forming complex $[\mathbf{18-H}^+][\text{CH}_2\text{NO}_2^-]$, which is the main species in solution when one or more equivalents of MeNO_2 are added. Therefore, when squaramide **18** is dissolved in MeNO_2 , the main species in solution is probably complex $[\mathbf{18-H}^+][\text{CH}_2\text{NO}_2^-]$.

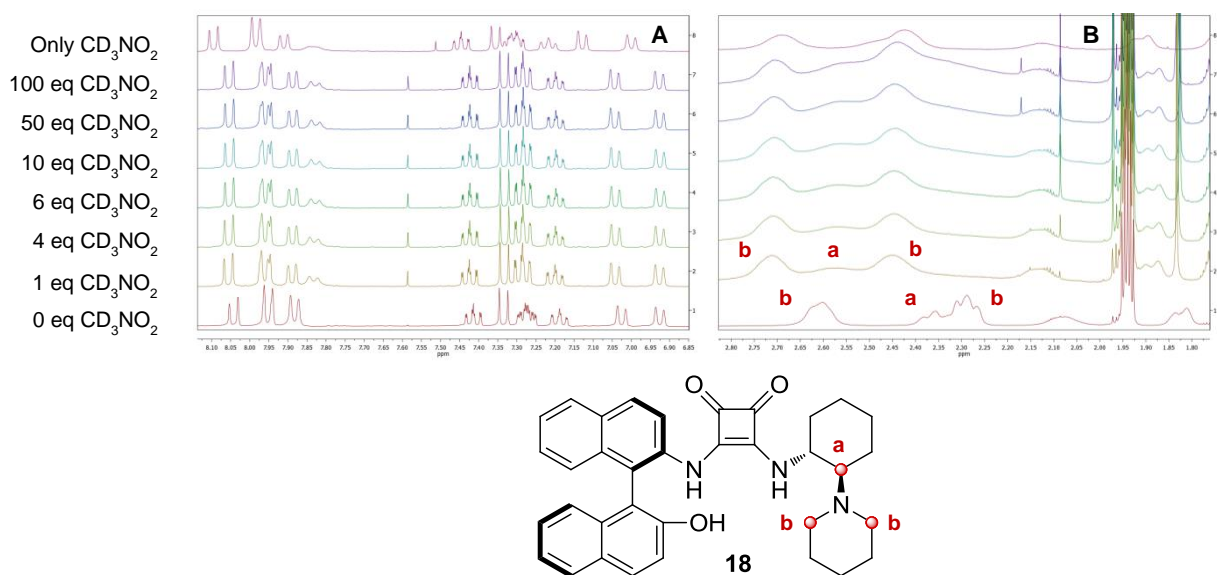


Figure 4.2. ¹H-NMR spectra of squaramide **18** (0.01 mmol) in CD₃CN (0.5 mL) after the addition of different equivalents of CD₃NO₂ at 30.9 °C (0 eq-only CD₃NO₂). (A) Aromatic region (from 8.10 to 6.85 ppm). (B) Aliphatic region (from 2.80 to 1.75 ppm).

Retro-Henry and other side reactions.

Additionally, different tests were performed in order to determine whether or not the retro-Henry or other side reactions took place under the reaction conditions. The term retro-Henry reaction will refer to the process that transforms the products (**19**) into the initial reagents (**14** and **17**).

First, the Henry reaction with **14c** was carried out at -24 °C and the corresponding product **19ca** was obtained with 80% ee. Then, the same experiment was performed at 30.9 °C and product **19ca** showed an enantiomeric excess of 54%. In order to determine whether or not the retro-Henry reaction proceeded, the product **19ca** with 80% ee was dissolved in a solution of MeNO₂ containing catalyst **18** at 30.9 °C and the ee of this product **19ca** was measured at different times (Table 4.1). This experiment suggested that the retro-Henry reaction proceeded at this temperature, since the initial enantiomeric excess of the product changed from 80% to 58% ee over two days.

Table 4.1. Variations in the enantiomeric excess values of product **19ca** with 80% ee when it is dissolved in a solution of MeNO₂ containing squaramide **18** at 30.9 °C.

T (°C) ^[a]	t (h)	ee of 19ca (%) ^[b]
30.9	0	80 (initial)
	24	68
	48	58

[a] Reaction conditions: Product **19ca** with 80% ee (0.2 mmol, 0.2 M) was added to a solution of squaramide **18** (0.002 mmol, 0.002 M) dissolved in MeNO₂ (1 mL) at 30.9 °C. Then, after the corresponding time, an aliquot was extracted and the product was isolated by column chromatography. [b] Determined by chiral HPLC analysis using a Daicel Chiralpak IB column.

This experiment indicates that the retro-Henry reaction observed in these conditions is much slower than the Henry reaction. In fact, Henry reactions are normally completed within a few hours at 30.9 °C, while the variations in the enantiomeric excess of product **19ca** produced by the retro-Henry reaction required much longer times (48 hours for a variation from 80% to 58% ee). In addition, it is worth to mention that the enantiomeric excess of product **19ca** does not vary in the Henry reaction over one day at 30.9 °C (Table 4.2). This suggests that other side reactions are not affecting significantly the enantiomeric excess of the product during the course of the Henry reaction.

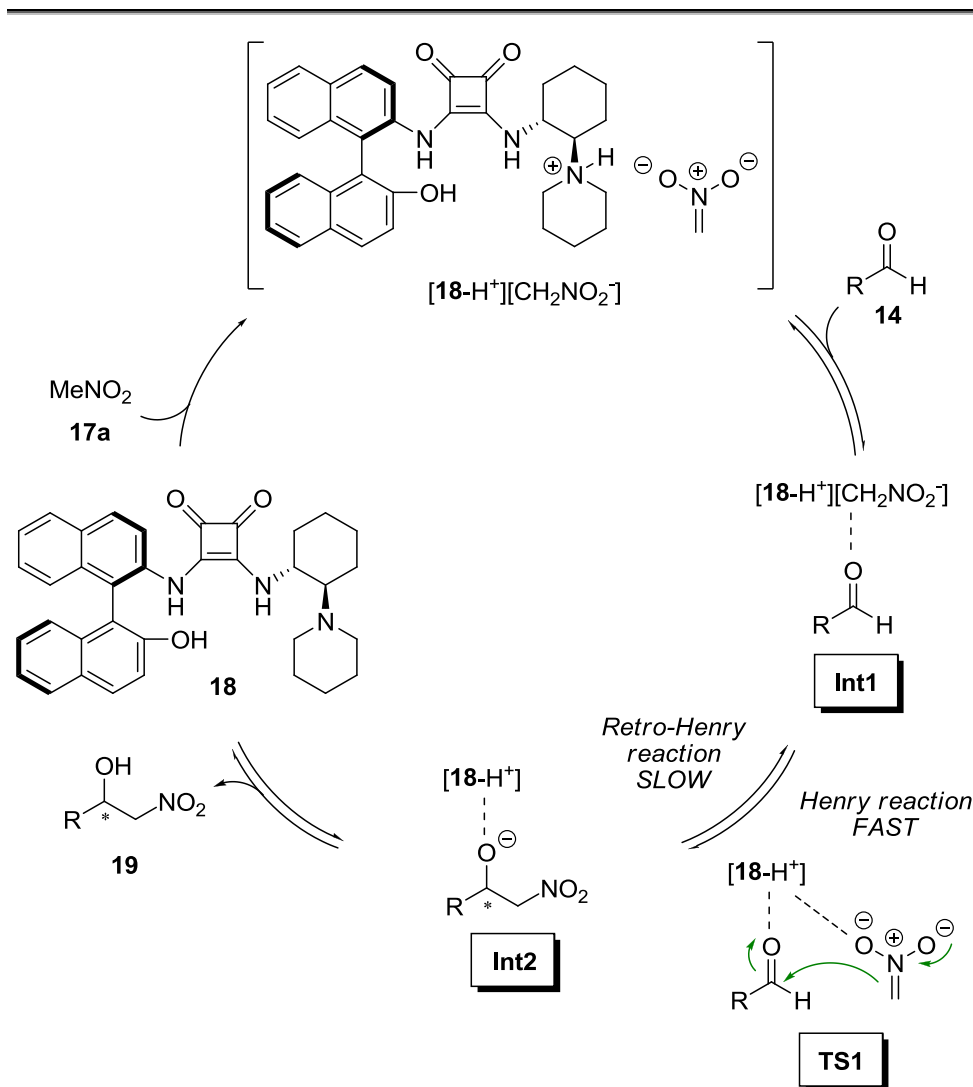
Table 4.2. Variations in the enantiomeric excess of **19ca** over time at 30.9 °C in the Henry reaction.

Entry ^[a]	t (h)	ee (%) ^[b]
1	1.5	54
2	3	53
3	4	52
4	24	52

[a] Reaction conditions: Aldehyde **14c** (0.2 mmol) was added to a solution of squaramide **18** (0.002 mmol) dissolved in MeNO₂ (1 mL) at 30.9 °C. Then, after the corresponding reaction time, an aliquot was extracted and the product was isolated by column chromatography. [b] Determined by chiral HPLC analysis.

In previous studies, the mechanism observed in the Henry reaction^[52,53] consisted in an initial deprotonation of MeNO₂ followed by the attack of the forming nitronate to an aldehyde. The results of our initial experimental study are in line with the traditional mechanism, suggesting that the different reaction pathways forming the global mechanism contain the reaction steps depicted in Scheme 4.2. In these pathways, the Henry reaction starts with the MeNO₂ deprotonation carried out by squaramide **18** followed by the coordination through non-covalent interactions of aldehyde **14** to complex [**18**-H⁺][CH₂NO₂⁻] (**Int1**). After this, the nitronate attacks to the aldehyde (**TS1**) to form an alcoxy intermediate (**Int2**), which is transformed to the product through a protonation process. In Scheme 4.2, the term “Henry reaction” refers to all the

steps from **Int1** to the final step where product **19** separates from the catalyst. Similarly, the term “retro-Henry reaction” refers to the same steps of the Henry reaction but in the opposite direction of the reaction.



Scheme 4.2. Catalytic cycle created in the individual reaction pathways of the Henry reaction studied.

Orders of reaction of the Henry reaction.

The determination of the orders of reaction of the different components could be crucial in mechanistic studies, since these orders give useful information about the amount of molecules of each type involved in the reaction mechanism. We calculated the orders of reaction of the reagents and the catalyst with NMR spectroscopy. First, the changes in aldehyde concentration (C) and $\ln(C)$ over time were measured at different temperatures and using diverse catalyst loadings (Figure 4.3). The results of these experiments determined that the order of reaction of aldehyde **14c** was 1.

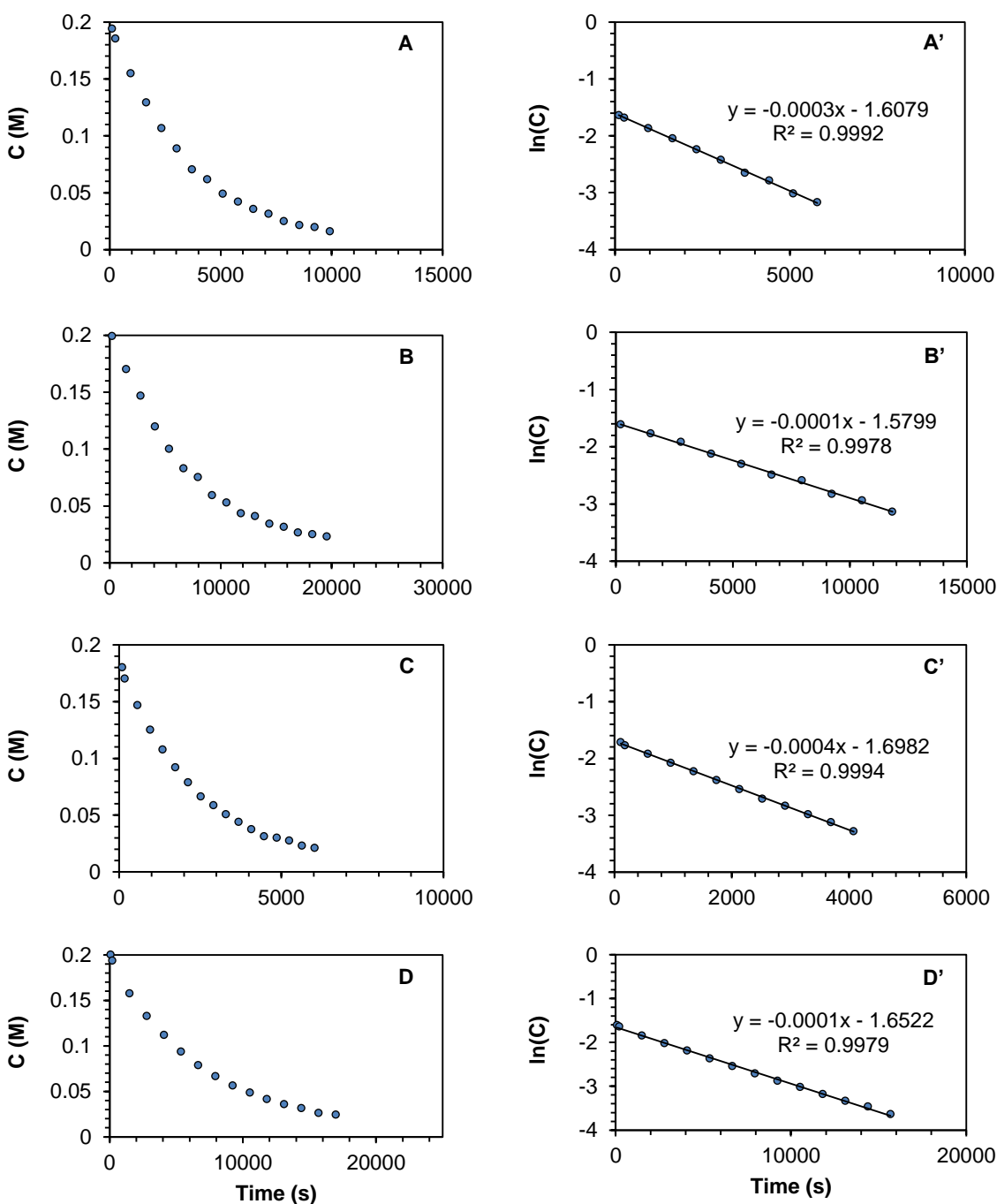


Figure 4.3. (A-D) Concentration (C) and (A'-D') ln(C) of aldehyde **14c** vs time. (A-A') 30.9 °C and 2.5 mol% of catalyst **18**. (B-B') 30.9 °C and 1 mol% of catalyst **18**. (C-C') 45.1 °C and 2.5 mol% of catalyst **18**. (D-D') 45.1 °C and 1 mol% of catalyst **18**.

Then, the order of reaction of catalyst **18** was calculated using the method of initial rates with the previous ¹H-NMR experiments.^[54] The results suggested that the order of reaction of squaramide **18** was 1 at different temperatures (Table 4.3).

Table 4.3. Initial reaction rates calculated using different conditions.

T (°C)	Catalyst loading (mol%)	Initial rate (M s ⁻¹)	Order of reaction
30.9	2.5	0.00005603	1
	1	0.00002255	
45.1	2.5	0.00012809	1
	1	0.00005247	

The determination of the order of reaction of MeNO₂ was more challenging and it could not be determined with NMR spectroscopy for various reasons: (1) MeNO₂ is the solvent of the reaction and its concentration does not vary during the course of the reaction; and (2) using other solvents or modifying the concentration of MeNO₂ in the reactions might cause important errors in the determination of this order of reaction, since these changes trigger variations in the aggregation and conformation of the molecules involved in the reaction pathways (Figure 4.4).

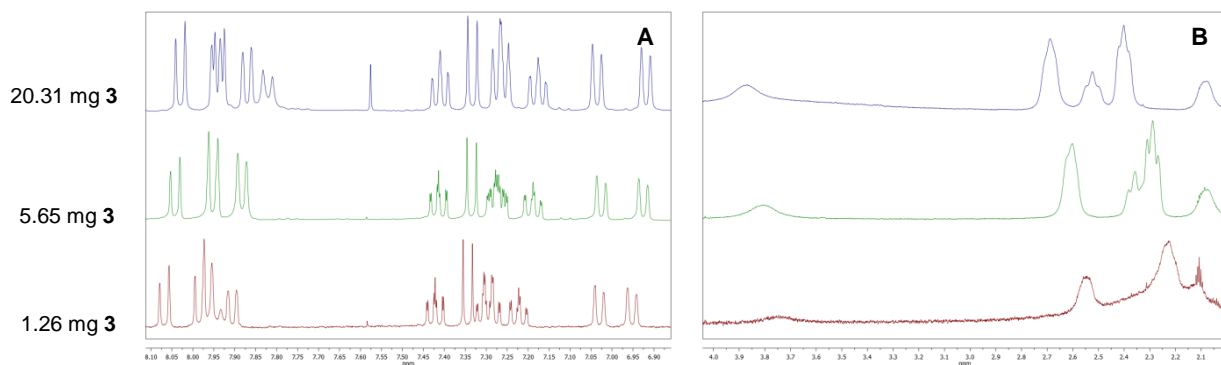


Figure 4.4. ¹H-NMR spectra of squaramide **18** in CD₃CN (0.5 mL) at different concentrations. (A) Aromatic region (from 8.12 to 6.87 ppm). (B) Aliphatic region (from 4.05 to 2.00 ppm).

In this study, we will explicitly represent the molecule of MeNO₂ that is involved in the Henry reaction. The solvation effects that the other MeNO₂ molecules cause during the reaction will be calculated with the solvation model based on density (SMD).^[55]

Kinetic isotope effect (KIE).

Additionally, KIE experiments were carried out using CD₃NO₂ in order to determine the rate-limiting reaction step. This step is very important since the outcomes of the reactions strongly depend on it. Inverse secondary KIE effects were observed in the Henry reaction catalyzed by squaramide **18** (Table 4.4). This type of effect has been previously observed in Henry reactions where the C atom of the nitronate molecule that performs the attack changes its hybridization from sp² to sp³.^[56] Therefore, these results suggest that the nitronate attack on the aldehyde (**TS1**) is the rate-limiting reaction step.

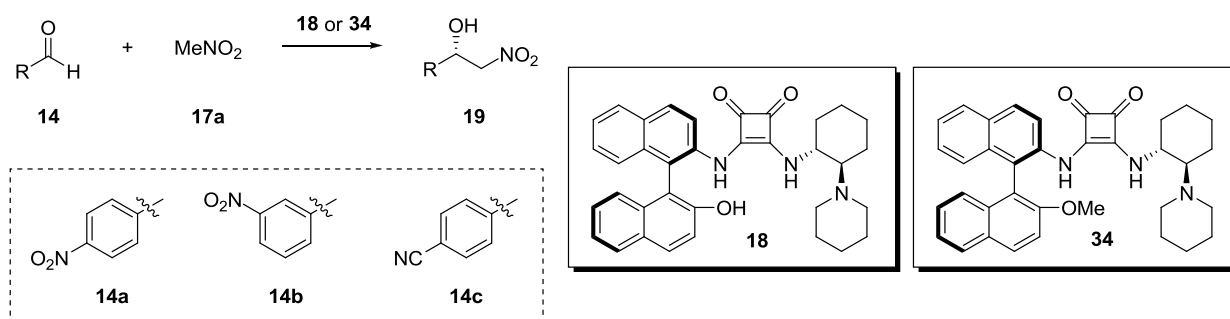
Table 4.4. KIE and reaction rate measurements of the Henry reaction at different temperatures.

T (°C)	K_H (s ⁻¹) ^[a]	K_D (s ⁻¹) ^[a]	KIE
30.9 °C	0.0002578	0.0004795	0.54 ^[b]
25.5 °C	0.0002430	0.0003726	0.65 ^[c]

[a] Rate constants K_H were calculated following the *General Method for Measuring the Order of Reaction of Aldehyde 14c* using 2.5 mol% of catalyst detailed in the Supporting Information of this chapter. Rate constants K_D were calculated following the same method but using only CD₃NO₂ as the solvent. [b] The KIE value is not exact, since the solvent used for determining K_H contained 5% of CD₃NO₂. [c] This value was obtained using a mixture CH₃NO₂:CD₃NO₂ (1:9).

Role of the OH group of squaramide **18**.

In previous experiments, we observed that the OH group of squaramide **18** did not significantly affect the outcomes of the reactions.^[49] Additional experiments were carried out in order to verify that the OH group is not involved in the reaction mechanism. For this, we compared the results obtained with catalyst **18** and those observed with catalyst **34**, which does not contain the OH group (Table 4.5). The results obtained with these two catalysts were quite similar, showing variations of only 2-8% yield and 2-5% ee. The small changes in the results suggest that the OH group does not affect the reaction mechanism in a great extent.

Table 4.5. Henry reactions using catalysts **18** or **34** with diverse aldehydes and temperatures.

Entry ^[a]	Catalyst	Aldehyde	T (°C)	t (h)	Yield (%)	ee (%) ^[b]
1	18	14a	-24	20	70	82
2	34	14a	-24	20	63	77
3	18	14b	-24	17	91	94
4	34	14b	-24	17	93	92
5	18	14c	-24	19	56	78
6	34	14c	-24	19	48	74
7	18	14c	30.9	14	>95	54
8	34	14c	30.9	14	90	54

[a] Reaction conditions: Aldehyde **14** (0.2 mmol, 0.2 M) was added to a solution of squaramide **18** or **34** (0.002 mmol, 0.002 M) dissolved in MeNO₂ (1 mL) at the temperature indicated in the table. Then, after the corresponding reaction time, the products were isolated by column chromatography. [b] Determined by chiral HPLC analysis.

Role of water in the Henry reaction.

Diverse experiments were performed in order to determine whether or not water molecules coming from the solvent were involved in the mechanism. The addition of a considerable amount of water did not affect the results of the reactions (Table 4.6), which suggests that water molecules do not play an important role in the mechanism.

Table 4.6. Henry reactions using aldehydes **14b** and **14c** with different amounts of water.

$$\text{R}-\text{CHO} + \text{MeNO}_2 \xrightarrow[-24\text{ }^\circ\text{C}]{\text{18 (1 mol\%)}} \text{R}-\text{CH}(\text{OH})-\text{CH}_2\text{NO}_2$$

14b-c **17a** **19**

Entry ^[a]	Additive	Aldehyde	t (h)	Yield (%)	ee (%) ^[b]
1	-	14b	17	91	94
2	11 μL H_2O ^[c]	14b	17	87	95
3	-	14c	19	55	80
4	11 μL H_2O ^[c]	14c	19	47	82

[a] Reaction conditions: Aldehyde **14** (0.2 mmol, 0.2 M) was added to a solution of squaramide **18** (0.002 mmol, 0.002 M) dissolved in anhydrous MeNO_2 (1 mL) at $-24\text{ }^\circ\text{C}$. Then, after the corresponding reaction time, the products were isolated by column chromatography. [b] Determined by chiral HPLC analysis. [c] Addition of larger amounts of H_2O resulted in heterogeneous reactions that led to the same results compared to those obtained when adding 11 μL H_2O .

Summary of the experimental study.

The results obtained in these initial experiments were useful to generate the catalyst-substrate complexes for the computational calculations. These experiments suggested that: (1) squaramide **18** deprotonates MeNO_2 in solution and interacts weakly with the aldehydes used; (2) the reaction pathways follow the steps depicted in Scheme 4.2; (3) the order of reaction of the catalyst and the aldehyde is 1; (4) the nitronate attack on the aldehydes (**TS1**) is the rate-limiting reaction step; (5) the OH group of the catalyst does not affect significantly the outcomes of the reactions; and (6) water molecules from the solvent are not involved in the mechanism.

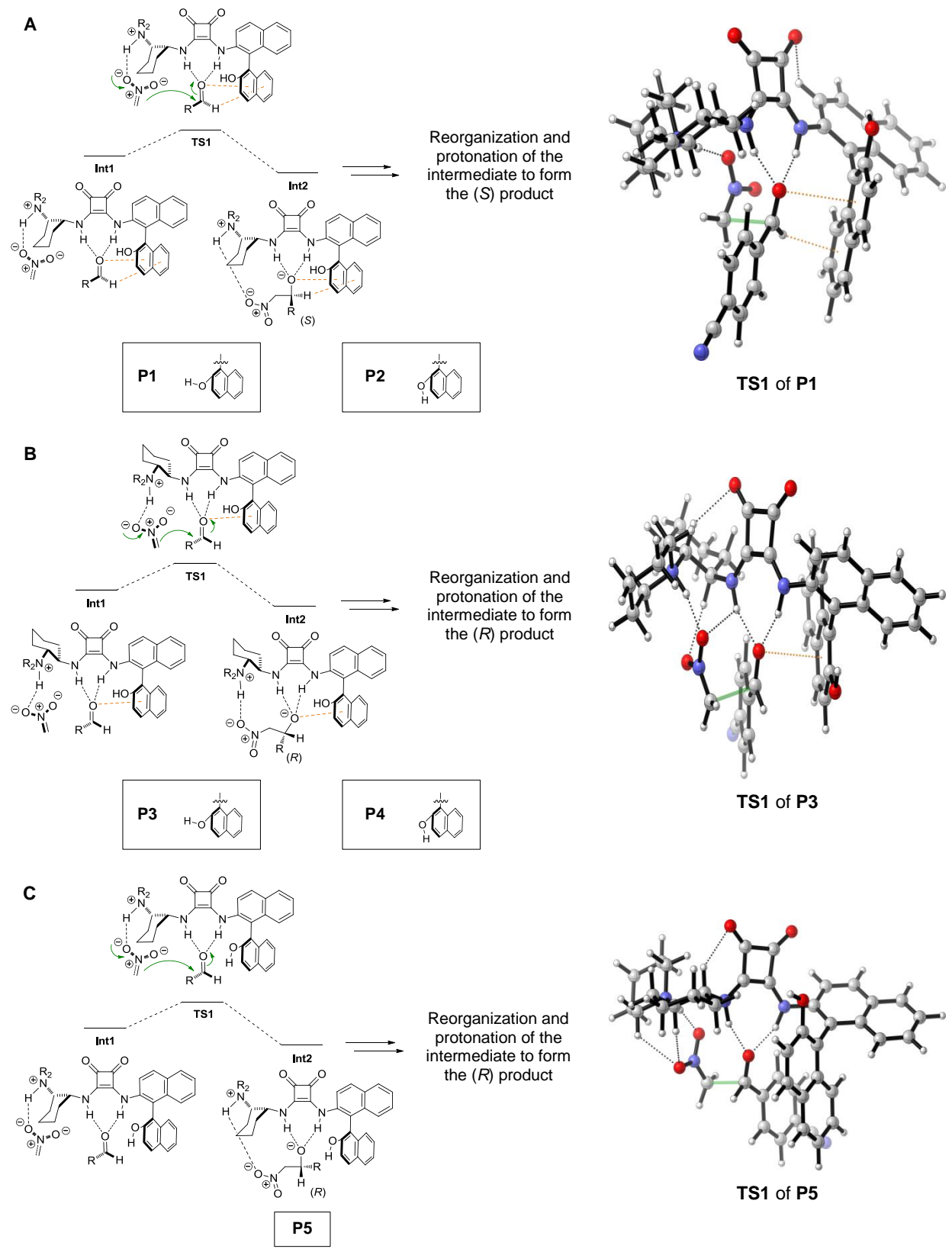
Computational study of the mechanism.

After the preliminary experimental study, we analyzed the reaction mechanism using computational chemistry. We focused on the nitronate attack on the aldehyde since it is the rate-limiting step of the reaction and determines the stereoselectivity of the process. First, a wide variety of **Int1** systems were designed in which the three initial components of the reaction

(protonated squaramide **18**, deprotonated nitromethane and aldehyde **14c**) interacted through non-covalent interactions and adopted different conformations and spatial dispositions. Overall, more than 50 catalyst-substrate complexes were generated using B3LYP/6-31G(d)^[57,58] (see Figure S4.1 in the annex on the CD for more information). These systems contained relatively complex non-covalent interaction networks that included hydrogen bonds, π -stacking and electrostatic interactions, among others.

From all the systems generated, we selected the substrate-catalyst complexes that could lead to the attack of the nitronate on the aldehyde with the characteristics observed in the preliminary experimental studies. Consequently, the substrate-catalyst complexes that were discarded either: (1) did not have any pathway that connected them to any product of the Henry reaction; or (2) led to Henry reactions in which the OH group of the catalyst was an important part of the mechanism.

In total, seven pathways were found using the B3LYP/6-31G(d) and ω B97X-D/6-31G(d)^[59] computational approaches (Figure 4.5). Within these pathways, pathways **P1**, **P3** and **P6** are analogous to pathways **P2**, **P4** and **P7**, respectively, with the only difference being the direction of the OH group in the naphthyl moiety of the catalyst. The position of this group affects differently the energy of each pathway and, therefore, it was an important factor for the study at this point. As stated above, we focused on the rate limiting step (**TS1**) because this is the stereo-determining step of the reactions.



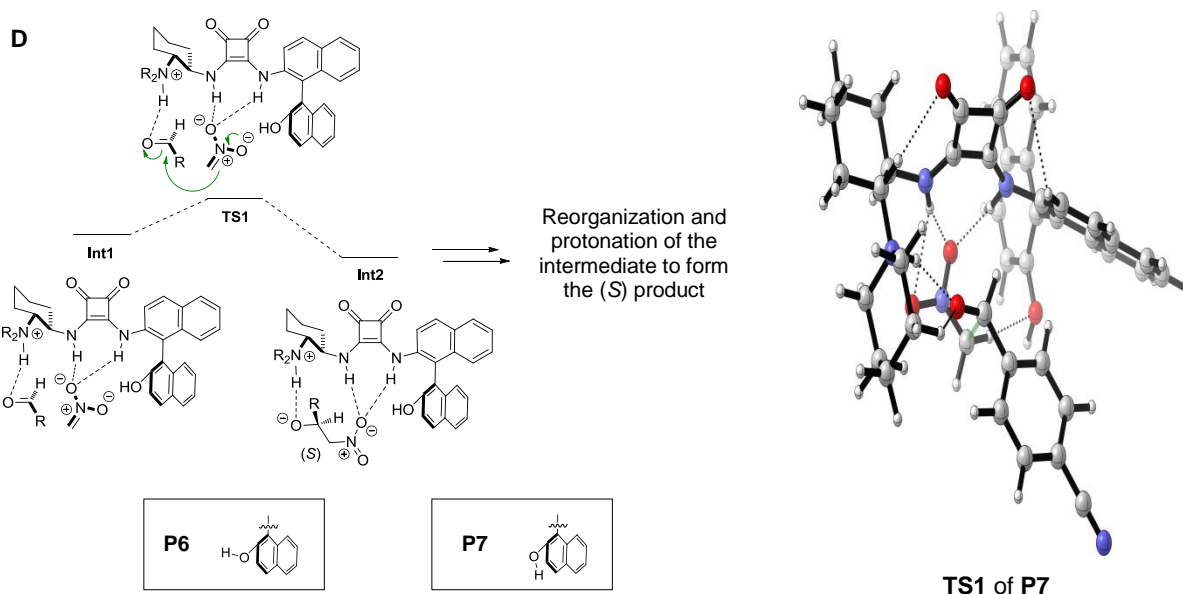


Figure 4.5. Reaction pathways **P1-P7**, along with a tridimensional representation of their **TS1** steps at the ω B97X-D/6-31G(d)(SMD=MeNO₂) level of theory. Black dotted lines represent hydrogen bonds, orange dotted lines represent π -interactions and the semi-transparent green bonds represent the attack of the nitronate on aldehyde **14c**. Calculations were carried out using Gaussian 09.^[60]

The results observed using the two approaches varied in a great extent. First, B3LYP did not calculate the absolute configuration of product **19ca** observed in the experiments (Table 4.7). This was to be expected as this functional has previously shown low accuracy when it is used to study systems with non-covalent interactions.^[61] Contrarily, functional ω B97X-D showed good outcomes, leading to the correct enantiomer with a precise value of enantiomeric excess at 30.9 °C (51% ee [calculated] vs 54% ee [experimental]).

Table 4.7. Relative Gibbs free energy (G) in kcal/mol of the **TS1** steps of pathways **P1-P7** using aldehyde **14c**, nitromethane (**17a**) and catalyst **18** along with their probability at 30.9 °C.

B3LYP/6-31G(d)(SMD=MeNO ₂)			ω B97X-D/6-31G(d)(SMD=MeNO ₂)		
Pathway	Relative G of TS1 (kcal/mol)	Probability (%) ^[a]	Pathway	Relative G of TS1 (kcal/mol)	Probability (%) ^[a]
P1	-1.02	7.9 (S)	P1	-4.13	71.8 (S)
P2	-0.55	3.6 (S)	P2	-2.21	3.0 (S)
P3	-2.34	70.3 (R)	P3	-3.40	21.5 (R)
P4	-1.29	12.4 (R)	P4	-1.92	1.9 (R)
P5	-0.32	2.5 (R)	P5	-1.48	0.9 (R)
P6	-0.13	1.8 (S)	P6	0.00	<0.1 (S)
P7	0.00	1.4 (S)	P7	-1.49	0.9 (S)

Calculated ee (using all the pathways) = -71%
Experimental ee = 54%

Calculated ee (using all the pathways) = 51%
Calculated ee (using only **P1** and **P3**) = 54%
Experimental ee = 54%

[a] Probabilities were calculated using Maxwell-Boltzmann statistics (see the *Computational Calculation of $\Delta\Delta G^\ddagger$* section in the Supporting Information of this chapter for more information).

In the results obtained with the ω B97X-D functional, the **TS1** steps of **P1** and **P3** significantly contributed more than the others. These two steps represented the 93.3% (71.8% **P1(TS1)** and 21.5% **P3(TS1)**) of the total Boltzmann population (Table 4.7). Additionally, the enantiomeric excess calculated using only the **TS1** of **P1** and **P3** was very similar to the excess obtained when using the seven **TS1**. This was also observed in the determination of the enantiomeric excesses of others aldehydes and, therefore, only the **TS1** of **P1** and **P3** were considered in subsequent calculations. This approximation saves precious time, since it reduces the amount of data of the studies and leads to enantiomeric excess values that are almost identical to those obtained using the seven pathways.

Then, the accuracy of different computational approaches for calculating enantiomeric excesses in Henry reactions that used diverse aldehydes were compared. Including different substrates in this study is quite useful to find a reliable and versatile computational approach, since we can collect more information about how accurate the methods are when different functional groups are included. Moreover, this study would help to create a considerable amount of data that will be useful to determine the methods that show the smallest error margins and that require the smallest amount of computation time. As stated above, the enantiomeric excesses were calculated using the difference of G between the **TS1** of pathways **P1** and **P3** ($\Delta\Delta G^\ddagger$) in different Henry reactions and the results were compared to the corresponding experimental values.

This study included diverse *para* substituted aldehydes, which contained various functional groups and atoms from different rows in the periodic table, such as Cl and Br. Additionally, in order to broaden the scope of this computational screening, aldehydes with substituents in the *meta* position and heterocycles were also used. In these examples, the aromatic substituent (or heteroatom) can be oriented in two directions, creating two systems that have different G. To account for this, four pathways (**P1(A)**, **P1(B)**, **P3(A)** and **P3(B)**) were generated in these calculations (Figure 4.6).

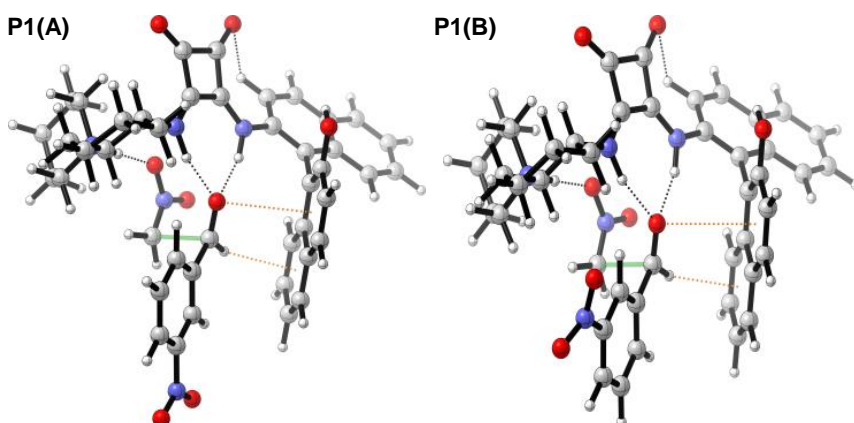


Figure 4.6. Example of the two **TS1** steps of **P1** formed with the different positions that the aromatic NO_2 substituent adopts when using aldehyde **14b** (3- NO_2).

In total, the accuracy of four different functionals, B3LYP, ω B97X-D, M06-2X^[62] and B3LYP-D3(BJ),^[63] was tested using the 6-31G(d) basis set. Additionally, we studied the precision of “single-point strategies”, in which single point energy calculations were performed employing geometries optimized at a lower level of theory, using the G correction from the approach used in the optimization process. In this type of system, it is important to evaluate different DFT methods to calculate G since each functional could lead to completely different results.^[64] In fact, the reaction coordinates of the pathways and the calculated enantiomeric excesses are totally different if B3LYP is used instead of ω B97X-D (Figure 4.7 and Table 4.7).

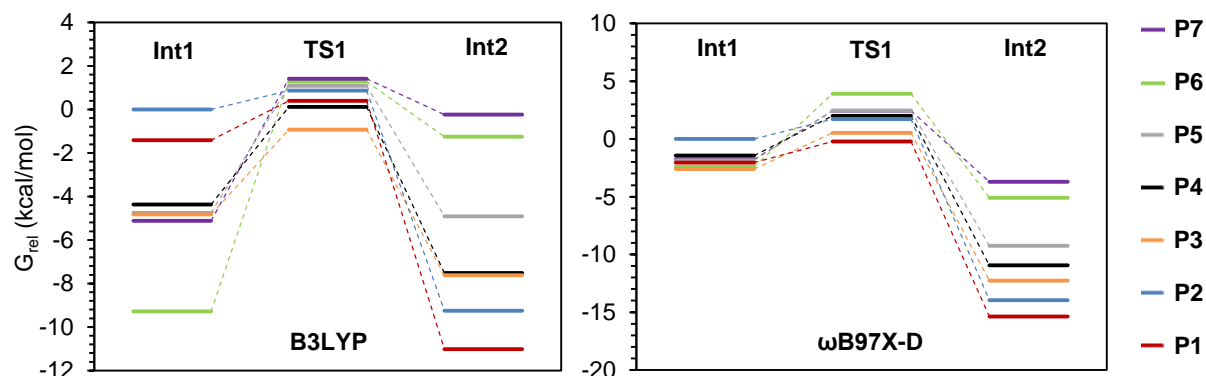



Figure 4.7. Relative G (in kcal/mol) of the reaction steps **Int1**, **TS1** and **Int2** of the different reaction pathways using aldehyde **14c**, nitromethane (**17a**) and catalyst **18** at 30.9 °C and obtained at the B3LYP/6-31G(d)(SMD=MeNO₂) (left) and ω B97X-D/6-31G(d)(SMD=MeNO₂) (right) levels of theory. See the Supporting Information of this chapter for all the G values (Tables S4.1-2).

As expected, the results were quite different in the computational screening of aldehydes depending on the functional employed. First, the B3LYP functional did not lead to accurate results. This functional calculated the wrong absolute configuration of the products in four out of five aldehydes studied (**14c-d,f-g**) and could not obtain the **TS1** of **14a** (Table 4.8).

Also, M06-2X was not a precise method for this reaction, since it obtained the wrong enantioselectivity in five out of six reactions (**14a,c-d,f-g**). Probably, the combinations of the M06-2X functional with larger basis sets would lead to better results since, when single-point strategies were used with M06-2X, the correct absolute configurations were observed Table 4.9, entries 1-3).^[66]

Table 4.8. Performance of different functionals for calculating the enantiomeric excess of the Henry reaction using different aldehydes. $\Delta\Delta G^\ddagger$ and errors are shown in kcal/mol and in all the cases the 6-31G(d) basis set was used with the SMD (using MeNO₂ as the solvent).


Aldehyde	B3LYP		ω B97X-D		M06-2X		B3LYP-D3 ^[a]		Experimental	
	$\Delta\Delta G^\ddagger$ ^[b]	Error	$\Delta\Delta G^\ddagger$ ^[b]	Error	$\Delta\Delta G^\ddagger$ ^[b]	Error	$\Delta\Delta G^\ddagger$ ^[b]	Error	$\Delta\Delta G^\ddagger$ ^[b]	ee (%)
14a	No P1	-	-1.34	-0.56	1.95	2.73	No P1	-	-0.78	57±1
14c	1.32	2.05	-0.73	0.00	0.77	1.50	No P1	-	-0.73	54±1.5
14d	0.79	1.58	0.43	1.22	0.68	1.47	0.37	1.16	-0.79	57.5±1.5
14e	-0.45	0.30	0.02	0.77	-0.50	0.25	n.d.	-	-0.75	55
14f	0.11	0.84	-1.17	-0.44	0.34	1.07	-1.27	-0.54	-0.73	54±2
14g	0.49	1.37	-3.13	-2.25	0.75	1.63	-1.93	-1.05	-0.88	62
14b	n.d.	-	-0.35	0.72	n.d.	-	n.d.	-	-1.07	71±1
14h	n.d.	-	-1.00	-0.12	n.d.	-	n.d.	-	-0.88	62
14m	n.d.	-	-0.53	0.52	n.d.	-	-0.36	0.69	-1.05	70±0

[a] In many cases, two imaginary frequencies existed in the **TS1** calculations using B3LYP-D3, one corresponding to the transition state and one extra imaginary frequency. As an approximation, the additional imaginary frequencies were inverted into frequencies with positive values in the G calculations of these **TS1** as seen previously.^[65] [b] $\Delta\Delta G^\ddagger$ is the difference of G between the **TS1** of pathways **P1** and **P3** ($\Delta\Delta G^\ddagger = \Delta G^{(\text{TS1}, \text{P1})} - \Delta G^{(\text{TS1}, \text{P3})}$). Positive $\Delta\Delta G^\ddagger$ values are represented in red and correspond to calculations that led to the opposite absolute configuration of the product compared to experimental results.

Table 4.9. $\Delta\Delta G^\ddagger$ and errors (in kcal/mol) of the Henry reaction with 4-cyanobenzaldehyde (**14c**) using single point energy calculations with geometries obtained at the B3LYP/6-31G(d), M06-2x/6-31G(d) and ω B97X-D/6-31G(d) levels of theory.

Entry	Approach ^[a]	$\Delta\Delta G^\ddagger$	Error
1	M06-2X/6-311++G(d,p)(UF grid)//B3LYP/6-31G(d)	-2.32	-1.59
2	M06-2X/6-311++G(d,p)(UF grid)// ω B97X-D/6-31G(d)	-2.92	-2.19
3	M06-2X/6-311++G(d,p)(UF grid)//M06-2X/6-31G(d)	-2.03	-1.30
4	ω B97X-D/6-311++G(d,p)(UF grid)//B3LYP/6-31G(d)	-4.30	-3.57
5	ω B97X-D/6-311++G(d,p)(UF grid)// ω B97X-D/6-31G(d)	-3.96	-3.23
6	Experimental	-0.73	0.00

[a] Single point energy calculations are performed using geometries optimized at a lower level of theory. The G corrections are calculated with the approach employed in the optimization process.

The B3LYP-D3 method did not lead to accurate results either. Even though it showed good precision in several examples (**14f,g,m**), the **TS1** of **P1** could not be found in various reactions (**14a,c**), even when larger Pople's basis sets, such as 6-311G(d),^[67] and basis sets from a different type, such as Def2-SVP^[68] and cc-pVDZ,^[69] were used (Figure 4.8).

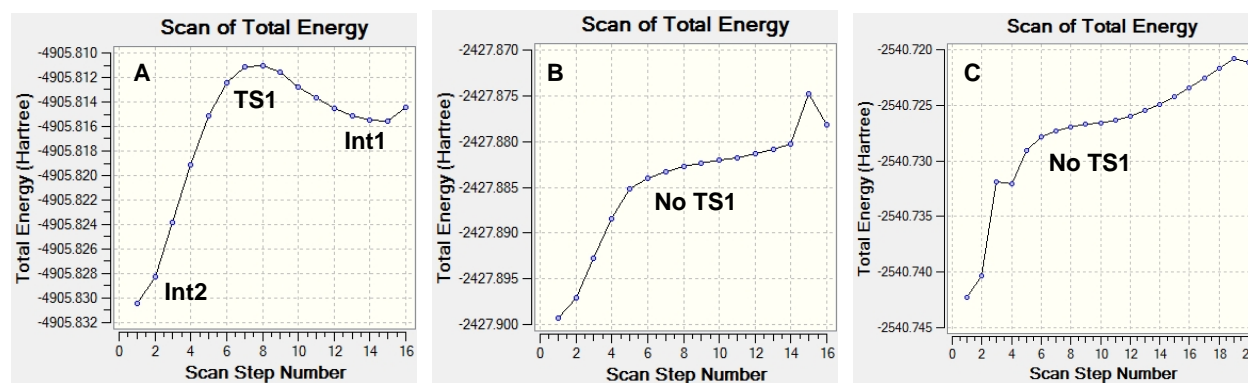
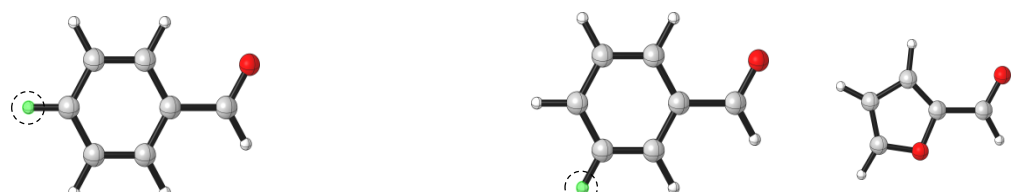


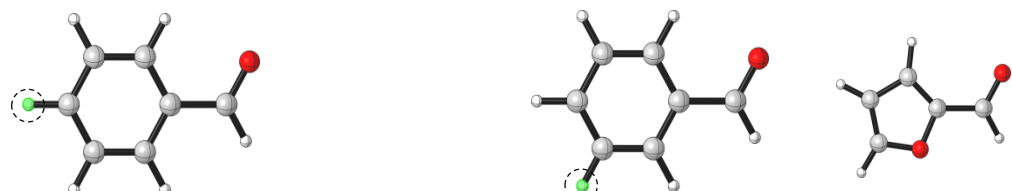
Figure 4.8. Relaxed potential energy surface scans using the C-C bond formed in **P1** as the changing coordinate. (A) Typical curve obtained for the Henry reactions with ω B97X-D/6-31G(d). (B) Curve obtained using **14c** with B3LYP-D3(BJ)/6-31G(d). (C) Curve obtained using **14c** with B3LYP-D3(BJ)/6-311G(d).

In sharp contrast, ω B97X-D performs quite well considering that 6-31G(d) is a relatively small basis set. All the **TS1** steps were found with this functional and the correct enantioselectivities were calculated in seven out of nine reactions (**14a-c,f-h,m**). Furthermore, the error margins were lower than 1 kcal/mol in six of these examples (**14a-c,f,h,m**), which is typically considered to be within “chemical accuracy” in computational chemistry.

Even though the ω B97X-D/6-31G(d) approach led to good outcomes in most of the cases, this combination did not calculate the correct absolute configuration in two cases (**14d-e**). In order to obtain more accurate results, we applied different variations to the calculations performed with the ω B97X-D/6-31G approach, such as the introduction of ultrafine (UF) grids, hindered rotor^[70] and counterpoise (CP) corrections^[71], and Truhlar’s and Grimme’s quasiharmonic approximations (QHAs, also called quasi-RRHOs).^[72] The results indicated that a significant improvement in the accuracy is achieved when the calculations include UF grids and QHAs. Compared to the initial ω B97X-D/6-31G approach, in the calculations performed with UF grids and QHAs (1) lower $\Delta\Delta G^\ddagger$ mean absolute errors (MAEs) were observed; (2) the correct absolute configurations were obtained more often; and (3) $\Delta\Delta G^\ddagger$ with error margins below 1 kcal/mol were more frequently calculated (Table 4.10, entries 1-6). It is worth noting that the precision of the calculations was similar when using Truhlar’s and Grimme’s QHAs.

Table 4.10. Study of the accuracy of the different functional-basis set combinations for calculating the enantioselectivity of diverse Henry reactions between aldehydes **14a-h,m** and MeNO₂ (**17a**) using **18** as the catalyst. All the methods include the SMD using MeNO₂ as the solvent.


Entry	Computational approach	Correct absolute configuration ^[a]									$\Delta\Delta G^\ddagger$ error within ± 1 kcal/mol ^[a,b]									$\Delta\Delta G^\ddagger$ MAE (kcal/mol) ^[b]	
		a	c	d	e	f	g	b	h	m	a	c	d	e	f	g	b	h	m		
1	ω B97X-D/6-31G(d)	✓	✓	○	○	✓	✓	✓	✓	✓	✓	✓	✓	○	○	✓	○	✓	✓	✓	0.73
2	ω B97X-D/6-31G(d) - QHA Truhlar	✓	✓	○	✓	✓	✓	✓	✓	✓	✓	✓	✓	○	✓	✓	✓	✓	✓	✓	0.42
3	ω B97X-D/6-31G(d) - QHA Grimme	✓	✓	○	✓	✓	✓	✓	✓	✓	✓	✓	✓	○	✓	✓	○	✓	✓	✓	0.53
4	ω B97X-D/6-31G(d) - UF grid	○	✓	○	✓	✓	✓	✓	✓	✓	○	✓	○	✓	✓	✓	✓	✓	✓	✓	0.40
5	ω B97X-D/6-31G(d) - UF grid - QHA Truhlar	○	✓	✓	✓	✓	✓	✓	✓	✓	○	✓	✓	✓	✓	✓	✓	✓	✓	✓	0.43
6	ω B97X-D/6-31G(d) - UF grid - QHA Grimme	○	✓	✓	✓	✓	✓	✓	✓	✓	○	✓	✓	✓	✓	✓	✓	✓	✓	✓	0.44
7	ω B97X-D/6-311G(d)	✓	✓	✓	✓	✓	✓	✓	✓	✓	○	✓	○	○	○	○	✓	✓	✓	1.06	
8	ω B97X-D/6-311G(d) - QHA Truhlar	✓	✓	✓	✓	✓	✓	✓	✓	✓	✓	✓	✓	✓	✓	○	✓	✓	✓	0.67	
9	ω B97X-D/6-311G(d) - QHA Grimme	✓	✓	✓	✓	✓	✓	✓	✓	✓	✓	✓	○	✓	○	○	✓	✓	✓	0.82	
10	ω B97X-D/6-311G(d) - UF grid	✓	✓	✓	✓	✓	✓	✓	✓	✓	✓	✓	✓	○	✓	✓	○	✓	○	0.64	
11	ω B97X-D/6-311G(d) - UF grid - QHA Truhlar	✓	✓	✓	✓	✓	✓	✓	✓	✓	✓	✓	✓	✓	✓	○	✓	✓	✓	0.44	
12	ω B97X-D/6-311G(d) - UF grid - QHA Grimme	✓	✓	✓	✓	✓	✓	✓	✓	✓	✓	✓	✓	✓	✓	✓	✓	✓	✓	0.48	



Entry	Computational approach	Correct absolute configuration ^[a]									$\Delta\Delta G^\ddagger$ error within ± 1 kcal/mol ^[a,b]									$\Delta\Delta G^\ddagger$ MAE (kcal/mol) ^[b]
		a	c	d	e	f	g	b	h	m	a	c	d	e	f	g	b	h	m	
13	ω B97X-D/6-311G(d,p)																			1.06
14	ω B97X-D/6-311G(d,p) - QHA Truhlar																			0.70
15	ω B97X-D/6-311G(d,p) - QHA Grimme																			0.83
16	ω B97X-D/6-311G(d,p) - UF grid																			0.77
17	ω B97X-D/6-311G(d,p) - UF grid - QHA Truhlar																			0.57
18	ω B97X-D/6-311G(d,p) - UF grid - QHA Grimme																			0.63

[a] Each circle (“☑” or “○”) corresponds to a substrate shown in the representations above the table, following the order in which they are displayed. “☑” = positive result in a specific substrate; “○” = negative result in a specific substrate. [b] Compared to experimental $\Delta\Delta G^\ddagger$ values and only valid when the correct absolute configuration is calculated. See the Supporting Information of this chapter for all the $\Delta\Delta G^\ddagger$ and error values (Figures S4.3-7).

Contrarily, the accuracy of the calculations did not improve when counterpoise and hindered rotor corrections were applied to the initial ω B97X-D/6-31G approach (Tables 4.11-12).

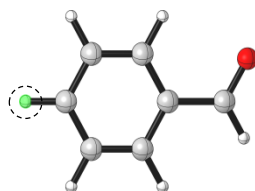
Table 4.11. $\Delta\Delta G^\ddagger$ and errors (in kcal/mol) of the Henry reactions using ω B97X-D/6-31G(d)(UF grid) with hindered rotor corrections (HR).

Aldehyde	ω B97X-D UF Grid		ω B97X-D UF grid HR		Experimental	
	$\Delta\Delta G^\ddagger$	Error	$\Delta\Delta G^\ddagger$	Error	$\Delta\Delta G^\ddagger$	ee (%)
14c	-0.86	-0.13	-0.93	-0.20	-0.73	54±1.5
14g	-1.14	-0.26	-1.13	-0.25	-0.88	62

Then, we defined a more ambitious objective: to find a computational approach that led to the correct absolute configuration of the products with $\Delta\Delta G^\ddagger$ errors in the calculated enantioselectivities within 1 kcal/mol in the majority of the nine reactions. In order to achieve this goal, different basis sets were employed in combination with the ω B97X-D functional, including double zeta (Def2SVP, 6-31G(d,p), 6-31+G(d),^[73] 6-31++G(d,p)) and triple zeta (6-311G(d), 6-311G(d,p), 6-311++G(d,p), 6-311+G(d), TZVP^[74] and Def2TZVP) basis sets. These new

combinations were tested using 4-chlorobenzaldehyde (**14d**) (Table 4.13), since the majority of the computational approaches evaluated before led to the product with the wrong absolute configuration.

Table 4.12. $\Delta\Delta G^\ddagger$ and errors (in kcal/mol) of the Henry reactions using ω B97X-D/6-31G(d)(UF grid) with counterpoise corrections (CP).



14a 4-NO₂ **14c** 4-CN **14d** 4-Cl **14e** 4-Br **14f** 4-H **14g** 4-Ph

Aldehyde	ω B97X-D - UF Grid		ω B97X-D - UF Grid - CP2 ^[a]		ω B97X-D - UF Grid - CP3 ^[b]		Experimental	
	$\Delta\Delta G^\ddagger$	Error	$\Delta\Delta G^\ddagger$	Error	$\Delta\Delta G^\ddagger$	Error	$\Delta\Delta G^\ddagger$	ee (%)
14a	0.18	0.96	n.d.	n.d.	0.01	0.79	-0.78	57±1
14c	-0.86	-0.13	-0.47	0.26	-1.00	-0.27	-0.73	54±1.5
14d	0.15	0.94	0.51	1.30	0.04	0.83	-0.79	57.5±1.5
14e	-0.67	0.08	-0.34	0.41	-0.77	-0.02	-0.75	55
14f	-0.97	-0.24	-0.51	0.22	-1.05	-0.32	-0.73	54±2
14g	-1.14	-0.26	-1.00	-0.12	-1.29	-0.41	-0.88	62

[a] CP2 = counterpoise correction using two fragments: (**14** + **17a**) and (**18**). [b] CP3 = counterpoise correction using three fragments (**14**), (**17a**) and (**18**).

Table 4.13. $\Delta\Delta G^\ddagger$ and errors of the Henry reaction with 4-chlorobenzaldehyde (**14d**) using ω B97X-D with different basis sets.

Entry	Basis set	$\Delta\Delta G^\ddagger$ (kcal/mol)	Error
1	6-31G(d,p)	0.49	1.28
2	6-31+G(d)	-2.22	-1.43
3	6-311G(d)	-2.17	-1.38
4	6-311G(d,p)	-1.20	-0.41
5	6-311+G(d)	-1.75	-0.96
6	6-311++G(d,p)	n.d. ^[a]	-
7	Def2SVP	0.68	1.47
8	TZVP	-3.17	-2.38
9	Def2TZVP	n.d. ^[a]	-
10	Experimental	-0.79	0.00

[a] The relatively long computational times required for the studies that employed these basis sets made their use unpractical compared to the times required when using other basis sets.

The Def2SVP and 6-31G(d,p) basis sets were discarded because they obtained the product with the undesired absolute configuration (Table 4.13, entries 1 and 7). On the other hand, the 6-31G basis set with diffuse functions (6-31+G(d)) and the triple zeta basis sets calculated the correct enantioselectivity of the product (Table 4.13, entries 2-5 and 8). The 6-

311++G(d,p) and Def2TZVP basis sets were discarded due to their long computation times, which were considerably higher than the times required for the other basis sets (Table 4.13, entries 6 and 9).

From all the basis sets that showed good results in the reaction with 4-chlorobenzaldehyde (**14d**) (triple zeta basis sets and double zeta basis sets with diffuse functions), we continued the investigation using Pople's 6-311G(d) and 6-311G(d,p) basis sets since these two basis sets showed much shorter computational times than the others. The 6-311G(d) basis set led to the correct absolute configuration in all of the products, showing MAEs that were similar to those obtained with the ω B97X-D/6-31G(d)-based approaches (Table 4.10, entries 7-12). Despite 6-311G(d,p) is a basis set larger than 6-311G(d), the calculations carried out with the 6-311G(d,p) basis set were less precise and needed more computation time than those performed with the 6-311G(d) basis set (Table 4.10, entries 13-18).

When using the 6-311G(d) and 6-311G(d,p) basis sets, the introduction of UF grids and QHAs improved the results. This also happened when UF grids and QHAs were applied to the ω B97X-D/6-31G(d) approach, which indicates that these modifications contribute significantly to achieving more precise results in the majority of the cases. This is especially important in the case of QHAs, since these corrections are rarely used in organocatalysis even though the systems studied in this area normally have many low-lying vibrational modes that are potential sources of error in the calculations.^[75]

From all the combinations tested in the computational screening of substrates, method ω B97X-D/6-311G(d) with QHAs and UF grid showed the most precise results (Table 4.10, entries 11-12). Using this approach, the results obtained in most of the nine reactions were within an absolute error margin of only 1 kcal/mol. These are very good results and show that this computational method could be very precise in systems that are relatively large (around 100 atoms) and include complex non-covalent interaction networks created between the different reaction components. Additionally, the 6-311G(d) basis sets requires less calculation time than larger triple-zeta basis sets used in other organocatalytic studies, such as the TZV and Def2TZV basis set families.

4.4 Conclusions

This study represents the first investigation where the precision and computational times of different computational approaches have been evaluated in squaramide catalysis. Different combinations of functionals and basis sets were tested in order to find an accurate method that required the least possible amount of calculation time. We tested the different combinations in Henry reactions catalyzed by squaramide **18**. These processes are quite difficult to analyze, since complex catalytic systems containing about 100 atoms and a significant number of non-covalent interactions are created.

First, we performed some experiments to gather information about the catalyst-substrate complexes formed during the reaction. The results suggested that: (1) catalyst **18** and aldehyde

14c interact through weak non-covalent interactions; (2) the amino group of squaramide **18** deprotonates a molecule of MeNO₂ (**17a**) in the reaction media; (3) retro-Henry reactions could proceed in the reaction conditions but they are significantly slower than their corresponding Henry reactions; (4) the orders of reaction of **18** and **14c** are both 1; (5) the rate-limiting reaction step is the nitronate attack on aldehydes **14** (**TS1** step); and (6) neither the OH group of catalyst **18** or water molecules are involved in the reaction mechanism.

At the beginning of the computational study, many different catalyst-substrate complexes were generated in order to investigate all the possible modes of interaction between the catalyst and the substrates. Moreover, from all the systems created, we discarded the catalyst-substrate complexes that either did not lead to Henry reaction products **19** or had the OH group of the catalyst involved significantly in the mechanism. In total, we found seven valid reaction pathways, **P1** to **P7**. Out of these pathways, **P1** and **P3** contained the most favorable **TS1** steps. The enantiomeric excess values calculated using only the G of the **TS1** of these two pathways were very similar to those values obtained using the seven pathways; therefore, only the **TS1** of **P1** and **P3** were taken into account to calculate the $\Delta\Delta G^\ddagger$ of the different reactions.

The accuracy of the different combinations of functionals and basis sets were evaluated using a screening of nine aldehydes with diverse functional groups. In this study, we calculated the enantiomeric excesses of the nine products and compared them with their corresponding experimental values. The calculations using the 6-31G(d) basis sets indicated that the choice of the functional has a great impact on the results. First, the B3LYP and M06-2X functionals did not lead to precise outcomes, since they led to products with the wrong absolute configuration in most of the aldehydes. Also, B3LYP-D3 was not a good method to study this reaction either, since the **TS1** of pathway **P1** could not be found in some reactions, even when larger Pople's basis sets were used. In contrast, ω B97X-D achieved significantly good results considering that 6-31G(d) is a relatively small basis set.

In addition, the ω B97X-D/6-31G(d) approach was combined with UF grids and QHAs in order to obtain more precise and versatile results. Also, different double-zeta and triple-zeta basis sets were used with the ω B97X-D functional. In this study, the ω B97X-D/6-311G(d) combination used with QHAs and UF grids showed the best results, leading to accurate calculated $\Delta\Delta G^\ddagger$ values with error margins lower than 1 kcal/mol in most of the nine aldehydes employed in the screening. It is worth to mention that the outcomes became considerably more reliable when QHAs (either Truhlar's or Grimme's QHA) were included, which stresses the importance of using QHAs in organocatalysis.

4.5 References

[47] a) Berkessel, A.; Gröger, H. (Eds.) *Asymmetric Organocatalysis*. Wiley-VCH: Weinheim, **2005**; b) Dalko, P. I. (Ed.) *Enantioselective Organocatalysis: Reaction and Experimental Procedures*. Wiley & Sons: New York, **2007**; c) Dalko, P. (Ed.) *Comprehensive Enantioselective Organocatalysis*. Wiley-VCH: Weinheim, **2013**.

[48] For the pioneering example of squaramide catalysis, see: a) Malerich, J. P.; Hagihara, K.; Rawal, V. H. *J. Am. Chem. Soc.* **2008**, *130*, 14416. For some reviews, see: b) Storer, R. I.; Aciro, C.; Jones, L. H. *Chem. Soc. Rev.* **2011**, *40*, 2330; c) Alemán, J.; Parra, A.; Jiang, H.; Jørgensen, K. A. *Chem. Eur. J.* **2011**, *17*, 6890; d) Tsakos, M.; Kokotos, C. G. *Tetrahedron* **2013**, *69*, 10199; e) Alegre-Requena, J. V. *Synlett* **2014**, *25*, 298; f) Chauhan, P.; Mahajan, S.; Kaya, U.; Hack, D.; Enders, D. *Adv. Synth. Catal.* **2015**, *357*, 253.

[49] Alegre-Requena, J. V.; Marqués-López, E.; Herrera, R. P. *Adv. Synth. Catal.* **2016**, *358*, 1801.

[50] a) Lu, T.; Wheeler, S. E. *Chem. Eur. J.* **2013**, *19*, 15141; b) Martínez, J. I.; Villar, L.; Uria, U.; Carrillo, L.; Reyes, E.; Vicario, J. L. *Adv. Synth. Catal.* **2014**, *356*, 3627; c) Kótai, B.; Kardos, G.; Hamza, A.; Farkas, V.; Pápai, I.; Soós, T. *Chem. Eur. J.* **2014**, *20*, 5631; d) Yang, C.; Wang, J.; Liu, Y.; Ni, X.; Li, X.; Cheng, J.-P. *Chem. Eur. J.* **2017**, *23*, 5488; e) Guo, J.; Wong, M. W. *J. Org. Chem.* **2017**, *82*, 4362; f) Grayson, M. N. *J. Org. Chem.* **2017**, *82*, 4396; g) Li, Y.; He, C. Q.; Gao, F.-X.; Li, Z.; Xue, X.-S.; Li, X.; Houk, K. N.; Cheng, J.-P. *Org. Lett.* **2017**, *19*, 1926.

[51] For a relevant example in which rotamers of squaramides were studied, see: Rotger, M. C.; Piña, M. N.; Frontera, A.; Martorell, G.; Ballester, P.; Deyà, P. M.; Costa, A. *J. Org. Chem.* **2004**, *69*, 2302.

[52] Henry, L. *Compt. Rend. Hebd. Séances Acad. Sci.* **1895**, *120*, 1265.

[53] a) Palomo, C.; Oiarbide, M.; Mielgo, A. *Angew. Chem. Int. Ed.* **2004**, *43*, 5442; b) Palomo, C.; Oiarbide, M.; Laso, A. *Eur. J. Org. Chem.* **2007**, 2561; c) Alvarez-Casao, Y.; Marqués-López, E.; Herrera, R. P. *Symmetry* **2011**, *3*, 220.

[54] Espenson, J. H. (Ed.) *Chemical Kinetics and Reaction Mechanisms*. McGraw-Hill: New York, **1981**.

[55] Marenich, A. V.; Cramer, C. J.; Truhlar, D. G. *J. Phys. Chem. B* **2009**, *113*, 6378.

[56] For an example involving nitronates, see: Kurtz, K. A.; Fitzpatrick, P. F. *J. Am. Chem. Soc.* **1997**, *119*, 1155.

[57] a) Becke, A. D. *J. Chem. Phys.* **1993**, *98*, 5648; b) Lee, C.; Yang, W.; Parr, R. G. *Phys. Rev. B* **1988**, *37*, 785; c) Vosko, S. H.; Wilk, L.; Nusair, M. *Can. J. Phys.* **1980**, *58*, 1200; d) Stephens, P. J.; Devlin, F. J.; Chabalowski, C. F.; Frisch, M. J. *J. Phys. Chem.* **1994**, *98*, 11623.

[58] a) Hehre, W. J.; Ditchfield, R.; Pople, J. A. *J. Chem. Phys.* **1972**, *56*, 2257; b) Hariharan, P. C.; Pople, J. A. *Theoret. Chim. Acta* **1973**, *28*, 213; c) Francl, M. M.; Pietro, W. J.; Hehre, W. J.; Binkley, J. S.; Gordon, M. S.; DeFrees, D. J.; Pople, J. A. *J. Chem. Phys.* **1982**, *77*, 3654; d) Rassolov, V. A.; Ratner, M. A.; Pople, J. A.; Redfern, P. C.; Curtiss, L. A. *J. Comp. Chem.* **2001**, *22*, 976.

[59] For references about the ω B97X-D functional, see: a) Becke, A. D. *J. Chem. Phys.* **1997**, *107*, 8554; b) Chai, J.-D.; Head-Gordon, M. *Phys. Chem. Chem. Phys.* **2008**, *10*, 6615.

[60] Frisch, M. J.; Trucks, G. W.; Schlegel, H. B.; Scuseria, G. E.; Robb, M. A.; Cheeseman, J. R.; Scalmani, G.; Barone, V.; Mennucci, B.; Petersson, G. A.; Nakatsuji, H.; Caricato, M.; Li, X.; Hratchian, H. P.; Izmaylov, A. F.; Bloino, J.; Zheng, G.; Sonnenberg, J. L.; Hada, M.; Ehara, M.; Toyota, K.; Fukuda, R.; Hasegawa, J.; Ishida, M.; Nakajima, T.; Honda, Y.; Kitao, O.; Nakai, H.; Vreven, T.; Montgomery, J. A., Jr.; Peralta, J. E.; Ogliaro, F.; Bearpark, M.; Heyd, J. J.; Brothers, E.; Kudin, K. N.; Staroverov, V. N.; Kobayashi, R.; Normand, J.; Raghavachari, K.; Rendell, A.; Burant, J. C.; Iyengar, S. S.; Tomasi, J.; Cossi, M.; Rega, N.; Millam, J. M.; Klene, M.; Knox, J. E.; Cross, J. B.; Bakken, V.; Adamo, C.; Jaramillo, J.; Gomperts, R.; Stratmann, R. E.; Yazyev, O.; Austin, A. J.; Cammi, R.; Pomelli, C.; Ochterski, J. W.; Martin, R. L.; Morokuma, K.; Zakrzewski, V. G.; Voth, G. A.; Salvador, P.; Dannenberg, J. J.; Dapprich, S.; Daniels, A. D.; Farkas, O.; Foresman, J. B.; Ortiz, J. V.; Cioslowski, J.; Fox, D. J. *Gaussian 09, Revision D.01*. Gaussian, Inc., Wallingford CT, 2016.

[61] a) Hobza, P.; Šponer, J.; Reschel, T. *J. Comp. Chem.* **1995**, *16*, 1315; b) Tsuzuki, S.; Lüthi, H. P. *J. Chem. Phys.* **2001**, *114*, 3949; c) Johnson, E. R.; Wolkow, R. A.; DiLabio, G. A. *Chem. Phys. Lett.* **2004**, *394*, 334.

[62] Zhao, Y.; Truhlar, D. G. *Theor. Chem. Acc.* **2008**, *120*, 215.

[63] a) Grimme, S.; Antony, J.; Ehrlich, S.; Krieg, H. *J. Chem. Phys.* **2010**, *132*, 154104; b) Grimme, S.; Ehrlich, S.; Goerigk, I. *J. Comput. Chem.* **2011**, *32*, 1456.

[64] a) Krishnan, R.; Binkley, J. S.; Seeger, R.; Pople, J. A. *J. Chem. Phys.* **1980**, *72*, 650; b) McLean, A. D.; Chandler, G. S. *J. Chem. Phys.* **1980**, *72*, 5639; c) Curtiss, L. A.; McGrath, M. P.; Blaudeau, J.-P.; Davis, N. E.; Binning, R. C.; Radom, L. *J. Chem. Phys.* **1995**, *103*, 6104.

[65] Sure, R.; Grimme, S. *J. Chem. Theory Comput.* **2015**, *11*, 3785.

[66] For an extensive study where single-point corrections on smaller basis-set optimizations show accurate results, see: Simón, L.; Goodman, J. M. *Org. Biomol. Chem.* **2011**, *9*, 689.

[67] a) Krishnan, R.; Binkley, J. S.; Seeger, R.; Pople, J. A. *J. Chem. Phys.* **1980**, *72*, 650; b) McLean, A. D.; Chandler, G. S. *J. Chem. Phys.* **1980**, *72*, 5639; c) Curtiss, L. A.; McGrath, M. P.; Blaudeau, J.-P.; Davis, N. E.; Binning, R. C.; Radom, L. *J. Chem. Phys.* **1995**, *103*, 6104.

[68] Weigend, F.; Ahlrichs, R. *Phys. Chem. Chem. Phys.* **2005**, *7*, 3297.

[69] a) Dunning Jr., T. H. *J. Chem. Phys.* **1989**, *90*, 1007; b) Woon, D. E.; Dunning Jr., T. H. *J. Chem. Phys.* **1993**, *98*, 1358.

[70] a) McClurg, R. B.; Flagan, R. C.; Goddard, W. A. *J. Chem. Phys.* **1997**, *106*, 6675; b) Ayala, P. Y.; Schlegel, H. B. *J. Chem. Phys.* **1998**, *108*, 2314; c) McClurg, R. B. *J. Chem. Phys.* **1999**, *111*, 7163.

[71] Boys, S. F.; Bernardi, F. *Mol. Phys.* **1970**, *19*, 553.

[72] For the script employed to apply the QHAs: a) *GoodVibes*, v1.0.1. Funes-Ardoiz, I.; Paton, R. S. 2016. <http://doi.org/10.5281/zenodo.60811>. For the QHAs theoretical basis: b) Ribeiro, R.

F.; Marenich, A. V.; Cramer, C. J.; Truhlar, D. G. *J. Phys. Chem. B* **2011**, *115*, 14556; c) Grimme, S. *Chem. Eur. J.* **2012**, *18*, 9955.

[73] Clark, T.; Chandrasekhar, J.; Spitznagel, G. W.; Schleyer, P. von R. *J. Comput. Chem.* **1983**, *4*, 294.

[74] a) Schäfer, A.; Horn, H.; Ahlrichs, R. *J. Chem. Phys.* **1992**, *97*, 2571; b) Schäfer, A.; Huber, C.; Ahlrichs, R. *J. Chem. Phys.* **1994**, *100*, 5829.

[75] For previous examples where QHAs were applied in organocatalysis, see: a) Wheeler, S. E.; Seguin, T. J.; Guan, Y.; Doney, A. C. *Acc. Chem. Res.* **2016**, *49*, 1061; b) Simón, L.; Paton, R. S. *J. Org. Chem.* **2017**, *82*, 3855; c) Grayson, M. N. *J. Org. Chem.* **2017**, *82*, 4396.

4.7 Supporting Information

General Experimental Methods

Purification of reaction products was carried out by filtration or flash chromatography using silica-gel (0.063-0.200 mm). Analytical thin layer chromatography was performed on 0.25 mm silica gel 60-F plates. $^1\text{H-NMR}$ spectra were recorded at 300 MHz. CD_3CN and CD_3NO_2 were used as the deuterated solvents. Chemical shifts were reported in the δ scale relative to residual MeCN (1.94 ppm) and CH_3NO_2 (4.33 ppm) for $^1\text{H-NMR}$. The different modes of interaction between catalyst **18** and substrates **14c** and **17a** found at the beginning of the computational study are represented in the annex on the CD (Figure S4.1). Furthermore, the molecular coordinates of the most relevant reaction steps are included in the annex (see sections S4.2-3 of the annex).

General Method for Measuring the Order of Reaction of Aldehyde 14c

The amount of aldehyde in solution was calculated by integrating the $^1\text{H-NMR}$ signal of the hydrogen of the aldehyde group (13.0 ppm) at different reaction times and comparing the integration values with the initial value that corresponds to a concentration of 0.2 M. In these experiments, the NMR tubes were placed at a constant temperature inside the NMR device until the reactions finished. There were no other significant side reactions besides the Henry reaction during the course of the reactions. Then, all the changes in the $^1\text{H-NMR}$ signal at 13.0 ppm corresponded to the conversion of aldehyde **14c** into the corresponding product of the Henry reaction. The rate constants K are the slopes in the $\ln(C)$ vs time plots.

2.5 mol% of catalyst: Catalyst **18** (0.0025 mmol) was dissolved in 0.5 mL of a $\text{CH}_3\text{NO}_2:\text{CD}_3\text{NO}_2$ (95:5) mixture inside a NMR tube. The solution stayed at 30.9 °C for 10 minutes inside the NMR device. Temperature was measured using a solution of 80% glycol in $\text{DMSO-}d_6$ (provided by Bruker). Then, the tube was taken out of the NMR device and aldehyde **14c** (0.1 mmol) was quickly added in one portion, mixed vigorously and introduced into the NMR device to start the measurements.

1 mol% of catalyst: catalyst **18** (0.0025 mmol) was dissolved in 1.25 mL of a mixture $\text{CH}_3\text{NO}_2:\text{CD}_3\text{NO}_2$ (95:5) inside a vial. Then, 0.5 mL of this solution were poured into a NMR tube and the process followed the same steps explained above.

General Method for Measuring the Order of Reaction of catalyst 18

Four experiments were performed, two of them at 30.9 °C and the other two at 45.1 °C, in which we varied the initial concentration of squaramide **18** while the initial concentration of MeNO_2 and aldehyde **14c** was the same in all the experiments. Then, we measured the initial reaction rates of these reactions using the first two points of the C vs time graphs and employed the method of initial rates to determine the order of reaction of squaramide **18**:

$$\frac{(\text{Initial rate})_1}{(\text{Initial rate})_2} = \frac{[\text{Squaramide}]_1^\alpha}{[\text{Squaramide}]_2^\alpha} \quad (1)$$

where α is the order of reaction of this squaramide. In this equation, [Squaramide] is the initial concentration of catalyst **18** and we assumed that the amount of squaramides interacting with the substrates is similar at the two concentrations employed.

Representative procedure of the Henry reaction of aldehydes 14 catalyzed by 18

To a mixture of catalyst **18** (0.004 mmol) and aldehyde **14a-p** (0.2 mmol), MeNO₂ (**17a**) (1 mL) was added in a test tube at 30.9 °C. After the initial aldehyde was consumed (determined using TLC, normally after 1-3 h of reaction), adducts **19** were isolated by flash chromatography (see the *Representative procedure of the Henry reaction of aldehydes 14 catalyzed by 18* section in the Supporting Information of Chapter 3 for more information). Enantiomeric excesses are reported in Table 4.8. If acid traces were observed in the aldehydes by NMR, these aldehydes were previously purified by column chromatography or extraction as detailed in the Supporting Information of Chapter 3.

Computational Methods

Diverse combinations of density functional theory (DFT) methods and basis sets were used to optimize the geometries of the stationary points (the functionals and basis sets employed are detailed in each case). Vibrational frequency calculations were carried out in order to (1) confirm that the stationary points were either energy minima or transition states and (2) calculate the thermal corrections to Gibbs free energies at 304.05 K (30.9 °C). Also, intrinsic reaction coordinate (IRC) calculations^[S15] were performed to verify that the transition states (**TS1**) of the different pathways connected to their corresponding **Int1** and **Int2**. Solvent effects (solvent = nitromethane) were included employing the integral equation formalism variant of the polarizable continuum model (IEF-PCM)^[S16] using the SMD.^[55] All the calculations were performed using Gaussian 09^[60] installed in the Trueno cluster facility of SGAI-CSIC. The Ultrafine grid was used as implemented in Gaussian 09 [Integral(Grid=UltraFineGrid)]. Graphical representations of the structures were created using CYLView^[S17] and POV-Ray.^[S18]

Quasi-harmonic approximations (QHAs) were calculated from Gaussian frequency calculations using the script created by Dr. Robert Paton and Ignacio Funes-Ardoiz.^[72a] Two QHA versions were used: one developed by Truhlar and col.^[72b] and the other by Grimme.^[72c] In both cases, the frequency cut-off was 100 cm⁻¹.

[S15] Fukui, K. *Acc. Chem. Res.* **1981**, *14*, 363.

[S16] Tomasi, J.; Mennucci, B.; Cancès, E. *J. Mol. Struct. (Theochem)* **1999**, *464*, 211.

[S17] *CYLview*, v1.0b. C. Y. Legault, Université de Sherbrooke, 2009.

[S18] *POV-Ray*, v3.6. Persistence of Vision Pty. Ltd., 2004.

We carried out a thorough initial study in order to define the possible pathways that lead to Henry reactions catalyzed by squaramide **18**. In this study, we generated a great amount of systems in which **18** and substrates **14c** and **17a** were interacting, adopting different conformations and positions in each system. Although more than 50 potential pathways were found (see Figure S4.1 in the annex on the CD), many of them did not lead to the Henry reaction and, therefore, were discarded. There were other pathways where the OH group played a significant role in the reaction mechanism. These pathways were discarded based on previous experimental results, since these experiments suggested that the OH group of the catalyst was not affecting the outcome of the reactions. These initial studies led to seven pathways (**P1-P7**) that conduced to Henry reactions.

Computational Calculation of $\Delta\Delta G^\ddagger$

$\Delta\Delta G^\ddagger$ is defined as the difference in Gibbs free energy of the **TS1** in **P1** and **P3** at 30.9 °C ($\Delta\Delta G^\ddagger = \Delta G^{(\text{TS1,P1})} - \Delta G^{(\text{TS1,P3})}$) and is related to the enantiomeric excesses of the reactions with Maxwell-Boltzmann distributions, following the formula:^[S19]

$$ee (\%) = \frac{1 - e^{-\frac{-\Delta\Delta G^\ddagger}{RT}}}{1 + e^{-\frac{-\Delta\Delta G^\ddagger}{RT}}} \times 100 \quad (2)$$

where R is the molar gas constant and T = 304.05 K. To calculate the enantiomeric excesses in reactions with more than two pathways, we employed the following formula:^[S20]

$$p_i = \frac{e^{-\frac{-\Delta G_i}{RT}}}{\sum_i \left(e^{-\frac{-\Delta G_i}{RT}} \right)} \times 100 \quad (3)$$

where p_i is the probability of a certain **TS1** and ΔG_i is the relative Gibbs free energy of the corresponding **TS1**. The enantioselectivity of a reaction is the difference between the sum of probabilities of the **TS1** that lead to the (S) enantiomer and the sum of probabilities of the **TS1** that lead to the (R) enantiomer.

The errors represented in the tables below correspond to the difference between the calculated $\Delta\Delta G^\ddagger$ values and the experimental $\Delta\Delta G^\ddagger$ values measured at the same temperature [Error = $\Delta\Delta G^\ddagger(\text{calculated}) - \Delta\Delta G^\ddagger(\text{experimental})$]. In reactions including **P1(A)**, **P1(B)**, **P3(A)** and **P3(B)** (3-NO₂, 3-Cl and Furyl), the experimental values were calculated as in the previous case, assuming that there were only two pathways. This is an approach that is employed to compare the experimental $\Delta\Delta G^\ddagger$ values with their analogous calculated values. In these examples, the enantiomeric excesses were calculated using the four **TS1** and the values were converted into $\Delta\Delta G^\ddagger$ following the same method employed to calculate the experimental $\Delta\Delta G^\ddagger$ values: as a difference in G of two pathways. This allowed us to do a better comparison of the errors of the

[S19] Sunoj, R. B. *Acc. Chem. Res.* **2016**, *49*, 1019.

[S20] Kótai, B.; Kardos, G.; Hamza, A.; Farkas, V.; Pápai, I.; Soós, T. *Chem. Eur. J.* **2014**, *20*, 5631.

calculated values with their corresponding experimental values. For example, in the reaction of aldehyde 3-NO₂ using ω B97X-D/6-31G(d), the calculated enantiomeric excess from equation 3 was 27.9% using the probabilities of **P1(A)**, **P1(B)**, **P3(A)** and **P3(B)**. This value of enantiomeric excess corresponds to a $\Delta\Delta G^\ddagger$ of -0.35 kcal/mol using equation 2 when assuming that there are only two pathways. Additionally, the $\Delta\Delta G^\ddagger$ is also calculated using the latter method for the experimental enantiomeric excess and both calculated and experimental $\Delta\Delta G^\ddagger$ values can be compared.

G of the Int1, TS1 and Int2 steps calculated with B3LYP/6-31G(d) and ω B97X-D/6-31G(d)

Table S4.1. G of the **Int1**, **TS1** and **Int2** steps of pathways **P1-P7** calculated with B3LYP/6-31G(d) (solvent = MeNO₂).

Pathway	Reaction Step	ΔG_{rel} (kcal/mol)
P1 (S)	Int1	-1.41
	TS1	0.39
	Int2	-11.01
P2 (S)	Int1	0.00
	TS1	0.86
	Int2	-9.25
P3 (R)	Int1	-4.82
	TS1	-0.93
	Int2	-7.62
P4 (R)	Int1	-4.37
	TS1	0.12
	Int2	-7.52
P5 (R)	Int1	-4.75
	TS1	1.09
	Int2	-4.92
P6 (S)	Int1	-9.28
	TS1	1.27
	Int2	-1.25
P7 (S)	Int1	-5.12
	TS1	1.41
	Int2	-0.24

Table S4.2. G of the **Int1**, **TS1** and **Int2** steps of pathways **P1-P7** calculated with ω B97X-D/6-31G(d) (solvent = MeNO₂).

Pathway	Reaction Step	ΔG_{rel} (kcal/mol)
P1 (S)	Int1	-2.03
	TS1	-0.21
	Int2	-15.36
P2 (S)	Int1	0.00
	TS1	1.71
	Int2	-13.95
P3 (R)	Int1	-2.61
	TS1	0.52
	Int2	-12.26
P4 (R)	Int1	-1.43
	TS1	2.00
	Int2	-10.95
P5 (R)	Int1	-1.87
	TS1	2.45
	Int2	-9.26
P6 (S)	Int1	-2.41
	TS1	3.92
	Int2	-5.10
P7 (S)	Int1	-1.76
	TS1	2.43
	Int2	-3.72

 $\Delta\Delta G^\ddagger$ values of Table 4.10**Table S4.3.** $\Delta\Delta G^\ddagger$ and errors (in kcal/mol) of the Henry reactions using ω B97X-D/6-31G(d) and ω B97X-D/6-31G(d) with UF grids.

Aldehyde	ω B97X-D/6-31G(d)		ω B97X-D/6-31G(d) - UF Grid		Experimental	
	$\Delta\Delta G^\ddagger$	Error	$\Delta\Delta G^\ddagger$	Error	$\Delta\Delta G^\ddagger$	ee (%)
14^a	-1.34	-0.56	0.18	0.96	-0.78	57±1
14^c	-0.73	0.00	-0.86	-0.13	-0.73	54±1.5
14^d	0.43	1.22	0.15	0.94	-0.79	57.5±1.5
14^e	0.02	0.77	-0.67	0.08	-0.75	55
14^f	-1.17	-0.44	-0.97	-0.24	-0.73	54±2
14^g	-3.13	-2.25	-1.14	-0.26	-0.88	62
14^b	-0.35	0.72	-0.82	0.25	-1.07	71±1
14^h	-1.00	-0.12	-0.47	0.41	-0.88	62
14^m	-0.53	0.52	-0.70	0.35	-1.05	70±0

Table S4.4. $\Delta\Delta G^\ddagger$ and errors (in kcal/mol) of the Henry reactions using combinations of the ω B97X-D/6-31G(d) method with UF grids and QHAs.

Aldehyde	ω B97X-D - QHA Grimme		ω B97X-D - QHA Truhlar		ω B97X-D - UF grid - QHA Grimme		ω B97X-D - UF grid - QHA Truhlar		Experimental	
	$\Delta\Delta G^\ddagger$	Error	$\Delta\Delta G^\ddagger$	Error	$\Delta\Delta G^\ddagger$	Error	$\Delta\Delta G^\ddagger$	Error	$\Delta\Delta G^\ddagger$	ee (%)
14^a	-0.90	-0.12	-0.66	0.12	0.15	0.93	0.10	0.88	-0.78	57±1
14^c	-0.51	0.22	-0.35	0.38	-0.67	0.06	-0.58	0.15	-0.73	54±1.5
14^d	0.25	1.04	0.14	0.93	-0.35	0.44	-0.72	0.07	-0.79	57.5±1.5
14^e	-0.28	0.47	-0.55	0.20	-0.54	0.21	-0.54	0.21	-0.75	55
14^f	-1.12	-0.39	-1.06	-0.33	-1.06	-0.33	-1.11	-0.38	-0.73	54±2
14^g	-2.26	-1.38	-1.70	-0.82	-1.19	-0.31	-1.40	-0.52	-0.88	62
14^b	-0.50	0.57	-0.71	0.36	-0.33	0.74	-0.32	0.75	-1.07	71±1
14^h	-0.84	0.04	-0.84	0.04	-0.41	0.47	-0.44	0.44	-0.88	62
14^m	-0.50	0.55	-0.47	0.58	-0.60	0.45	-0.59	0.46	-1.05	70±0

Table S4.5. $\Delta\Delta G^\ddagger$ and errors (in kcal/mol) of the Henry reactions using ω B97X-D/6-311G(d) and ω B97X-D/6-311G(d,p) with UF grids.

Aldehyde	ω B97X-D/6- 311G(d)		ω B97X-D/6- 311G(d,p)		ω B97X-D/6- 311G(d) - UF grid		ω B97X-D/6- 311G(d,p) - UF grid		Experimental	
	$\Delta\Delta G^\ddagger$	Error	$\Delta\Delta G^\ddagger$	Error	$\Delta\Delta G^\ddagger$	Error	$\Delta\Delta G^\ddagger$	Error	$\Delta\Delta G^\ddagger$	ee (%)
14^a	-1.91	-1.13	-2.28	-1.50	-0.31	0.47	0.04	0.82	-0.78	57±1
14^c	-1.44	-0.71	-0.54	0.19	-0.54	0.19	-0.25	0.48	-0.73	54±1.5
14^d	-2.17	-1.38	-1.20	-0.41	-0.27	0.52	-0.85	-0.06	-0.79	57.5±1.5
14^e	-1.76	-1.01	-1.51	-0.76	-1.91	-1.16	-1.62	-0.87	-0.75	55
14^f	-2.21	-1.48	-3.34	-2.61	-1.48	-0.75	-2.29	-1.56	-0.73	54±2
14^g	-3.58	-2.70	-3.39	-2.51	-1.46	-0.58	-0.78	0.10	-0.88	62
14^b	-0.92	0.15	-0.88	0.19	-2.08	-1.01	-2.78	-1.71	-1.07	71±1
14^h	-1.92	-0.87	-1.52	-0.64	-0.84	0.04	-1.62	-0.74	-0.88	62
14^m	-0.98	0.07	-1.78	-0.73	-2.08	-1.03	-1.61	-0.56	-1.05	70±0

Table S4.6. $\Delta\Delta G^\ddagger$ and errors (in kcal/mol) of the Henry reactions using ω B97X-D/6-311G(d) and ω B97X-D/6-311G(d,p) with QHAs.

Aldehyde	ω B97X-D/6-311G(d) - QHA Grimme		ω B97X-D/6-311G(d) - QHA Truhlar		ω B97X-D/6-311G(d,p) - QHA Grimme		ω B97X-D/6-311G(d,p) - QHA Truhlar		Experimental	
	$\Delta\Delta G^\ddagger$	Error	$\Delta\Delta G^\ddagger$	Error	$\Delta\Delta G^\ddagger$	Error	$\Delta\Delta G^\ddagger$	Error	$\Delta\Delta G^\ddagger$	ee (%)
14a	-1.40	-0.62	-1.11	-0.33	-1.58	-0.80	-1.17	-0.39	-0.78	57 \pm 1
14c	-1.24	-0.51	-1.08	-0.35	-0.72	0.01	-0.73	0.00	-0.73	54 \pm 1.5
14d	-1.83	-1.04	-1.61	-0.82	-1.27	-0.48	-1.28	-0.49	-0.79	57.5 \pm 1.5
14e	-1.61	-0.86	-1.56	-0.81	-1.46	-0.71	-1.49	-0.74	-0.75	55
14f	-1.91	-1.18	-1.67	-0.94	-2.83	-2.10	-2.50	-1.77	-0.73	54 \pm 2
14g	-2.97	-2.09	-2.73	-1.85	-2.86	-1.98	-2.64	-1.76	-0.88	62
14b	-0.82	0.25	-0.78	0.29	-0.71	0.36	-0.71	0.36	-1.07	71 \pm 1
14h	-1.62	-0.74	-1.45	-0.57	-1.41	-0.53	-1.36	-0.48	-0.88	62
14m	-1.10	-0.05	-1.16	-0.11	-1.52	-0.47	-1.40	-0.35	-1.05	70 \pm 0

Table S4.7. $\Delta\Delta G^\ddagger$ and errors (in kcal/mol) of the Henry reactions using ω B97X-D/6-311G(d) and ω B97X-D/6-311G(d,p) with UF grids and QHAs.

Aldehyde	ω B97X-D/6-311G(d) - UF grid - QHA Grimme		ω B97X-D/6-311G(d) - UF grid - QHA Truhlar		ω B97X-D/6-311G(d,p) - UF grid - QHA Grimme		ω B97X-D/6-311G(d,p) - UF grid - QHA Truhlar		Experimental	
	$\Delta\Delta G^\ddagger$	Error	$\Delta\Delta G^\ddagger$	Error	$\Delta\Delta G^\ddagger$	Error	$\Delta\Delta G^\ddagger$	Error	$\Delta\Delta G^\ddagger$	ee (%)
14a	-0.47	0.31	-0.68	0.10	-0.30	0.48	-0.63	0.15	-0.78	57 \pm 1
14c	-0.65	0.08	-0.59	0.14	-0.60	0.13	-0.72	0.01	-0.73	54 \pm 1.5
14d	-0.72	0.07	-0.98	-0.19	-1.15	-0.36	-1.38	-0.59	-0.79	57.5 \pm 1.5
14e	-1.73	-0.98	-1.65	-0.90	-1.57	-0.82	-1.55	-0.80	-0.75	55
14f	-1.50	-0.77	-1.50	-0.77	-2.06	-1.33	-1.87	-1.14	-0.73	54 \pm 2
14g	-1.72	-0.84	-2.09	-1.21	-1.21	-0.33	-1.68	-0.80	-0.88	62
14b	-1.52	-0.45	-1.16	-0.09	-2.09	-1.02	-1.65	-0.58	-1.07	71 \pm 1
14h	-0.97	-0.09	-0.88	0.00	-1.51	-0.63	-1.39	-0.51	-0.88	62
14m	-1.79	-0.74	-1.61	-0.56	-1.59	-0.54	-1.61	-0.56	-1.05	70 \pm 0

5

“PUSH-PULL π +/ π -” (PP $\pi\pi$) SYSTEMS IN CATALYSIS

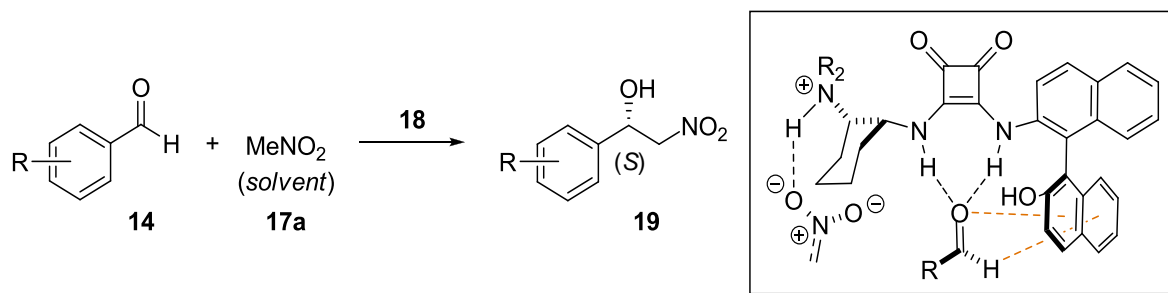
5.1 Introduction

In many organocatalytic studies, where normally a great amount of non-covalent interactions are formed, π -interactions have played a secondary role since stronger non-covalent interactions such as hydrogen bonds were the focus of these investigations. However, π -interactions are gaining importance due to the great number of examples where these interactions have played crucial roles. For example, π -interactions have been vital in diverse areas, molecular recognition,^[76] crystal engineering,^[77] and biochemistry.^[78] Furthermore, in many organocatalytic processes, these interactions have influenced the stereoselectivity and yield of the reactions in a great extent,^[79] which makes the creation of innovative and more efficient π systems highly desirable.

Within the structures that can form π -interactions, push-pull π surfaces are aromatic groups that are able of interacting at the same time with a cation and an anion or, as observed in this investigation, with a δ^+ atom and a δ^- atom. These three components (the aromatic group, the δ^+ atom and the δ^- atom) form an interacting system with two π -interactions that is denoted in this study as “push-pull π +/ π -” (PP $\pi\pi$) system. These systems are very rare and their properties remain practically unknown since PP $\pi\pi$ systems were not observed until 2014 and so far there are only a few studies about them.^[80] Until now, only some properties of PP $\pi\pi$ systems were determined, but no concrete applications for these systems had been discovered apart from spectral tuning. However, as detailed in this investigation, the use of PP $\pi\pi$ systems to catalysis has a lot of unexplored potential.

5.2 Objectives

The main goal of this research was to examine an unprecedented mode of activation in catalysis based on a π - δ^+ atom (π -H) and a π - δ^- atom (π -O) interaction. This system of interactions was found in the reaction pathway **P1** of the Henry reaction catalyzed by squaramide **18** studied in Chapter 4 (Scheme 5.1). The π -interactions are formed between the two rings of the catalyst's naphthyl group and one oxygen and one hydrogen atom of the aldehydes. More interestingly, this PP $\pi\pi$ system presents a unique design, where the δ^+ atom and the δ^- atom that form the π -interactions are not covalently linked to the π surface as seen in the existing examples.^[80]



Scheme 5.1. Henry reaction catalyzed by squaramide **18** along with a representation of the π -interactions (orange dotted lines) created in **P1**.

5.3 Results and Discussion

Computational study of π -interactions.

In the previous chapter, we disclosed all the possible pathways that we found in this Henry reaction using 4-cyanobenzaldehyde (**14c**) as the model aldehyde (Figure 5.1, **P1-P7**). These pathways followed the mechanism observed in previous Henry reactions (MeNO₂ deprotonation followed by the nitronate attack) and the rate-limiting reaction step is the nitronate attack on aldehydes **14** (**TS1**). This is also the step that determines the stereoselectivity of this Henry reaction.

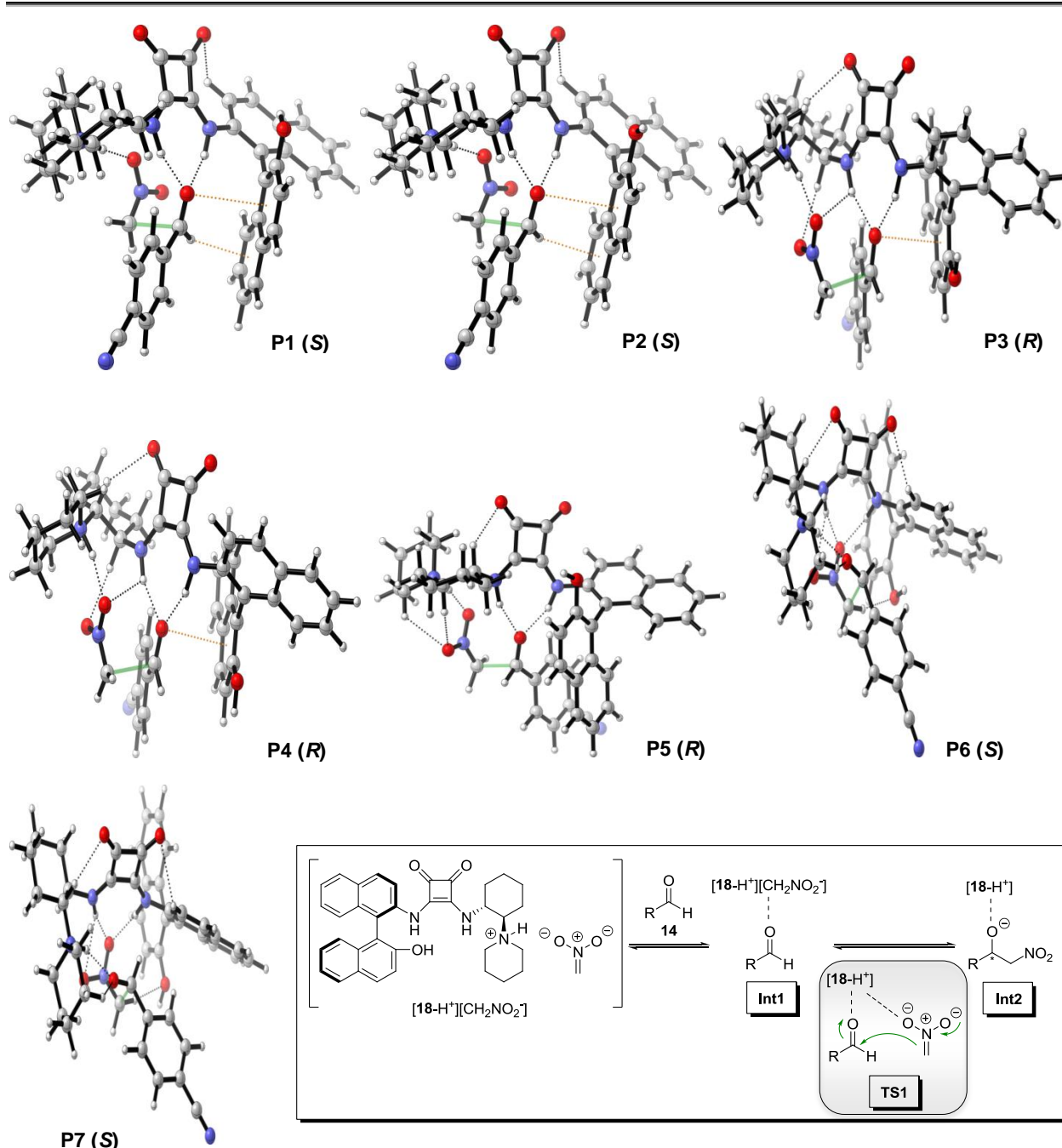
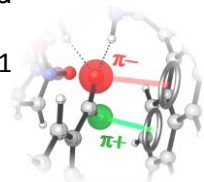


Figure 5.1. Reaction pathways **P1-P7** (with the absolute configuration of the product derived from each pathway), with tridimensional representations of their **TS1** steps using ω B97X-D/6-31G(d)(SMD=MeNO₂). Black dotted lines represent hydrogen bonds, orange dotted lines represent π -interactions and the semi-transparent green bonds represent the attack of the nitronate on aldehyde **14c**. For a more detailed representation of each reaction pathway, see Figure 4.5 in Chapter 4.

We observed something unusual when determining the non-covalent interactions formed in the different pathways of this Henry reaction. In the most favorable reaction pathways, **P1/P2** and **P3/P4**,^[81] the second naphthyl group of squaramide **18** interacted through π -interactions with the aldehyde. In **P3**, a π -oxygen (π -O) interaction is created between the oxygen atom and



the phenol ring of the lower naphthyl group (Figure 5.2, B). More interestingly, in **P1**, the hydrogen and the oxygen atoms of the aldehyde interacted with the catalyst's lower naphthyl group at the same time (Figure 5.2, A).

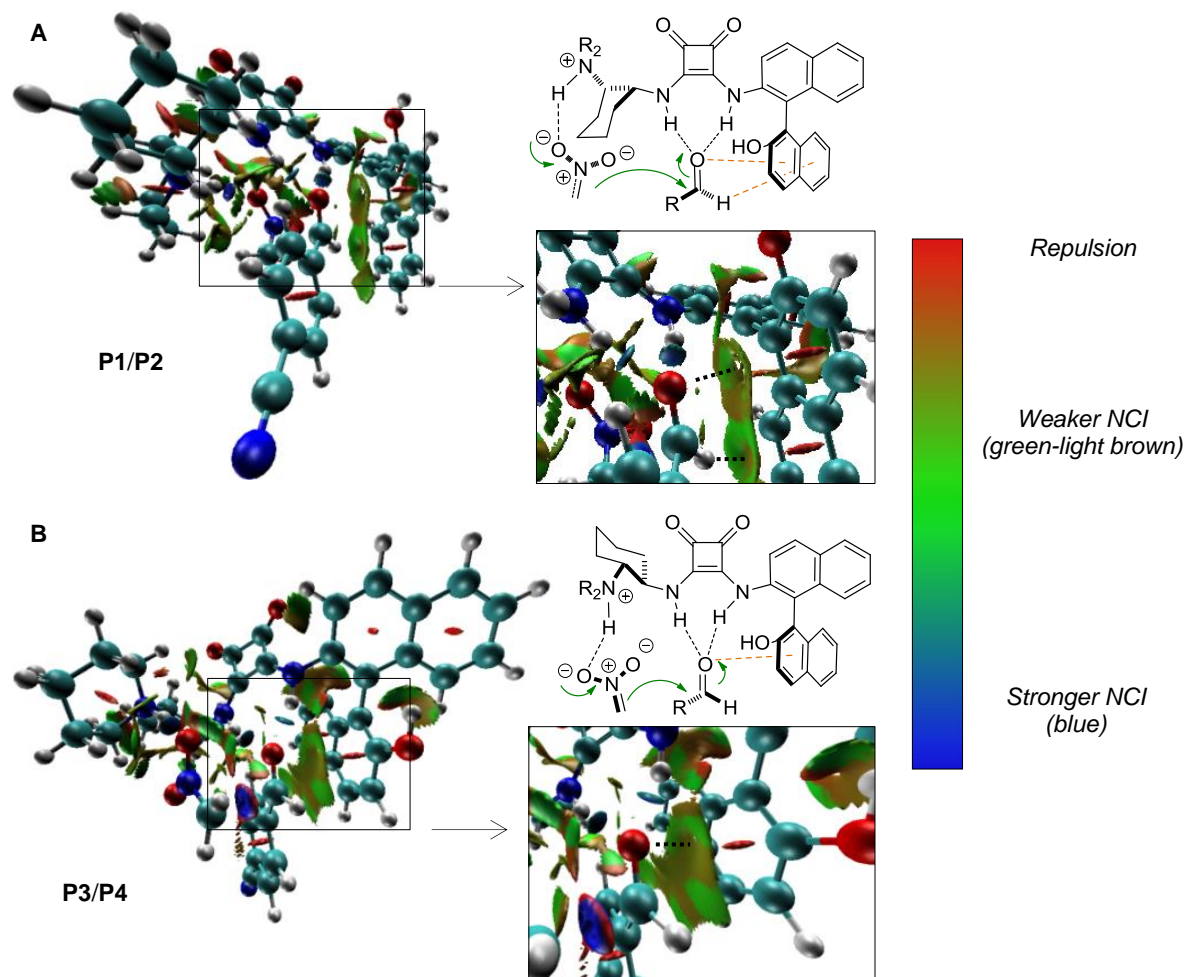


Figure 5.2. Non-covalent interactions that are created by aldehyde **14c** and catalyst **18** in **TS1** of **P1/P2** (A) and **P3/P4** (B) with enlarged representations of the regions with π -interactions using ω B97X-D/6-31G(d)(SMD=MeNO₂). Non-covalent interactions are equivalent in **P1** and **P2**, as well as in **P3** and **P4**.^[81] The grid data for $\text{sign}(\lambda_2)\rho$ and reduced density gradient (RDG) was generated with Multiwfn^[82] and the images were created using VMD.^[83] The black dotted lines inside the expanded images represent the π -oxygen and π -hydrogen interactions. NCI = non-covalent interactions.

The mode of interaction created in **P1** where the naphthyl group creates two π -interactions is particularly uncommon. These interactions can be divided into two main groups, π -hydrogen (π -H) and π -O interactions, and their properties vary during the course of the reaction due to the structural modifications that the initial aldehyde go through after the nitronate attack (Figure 5.3, A, B and C).

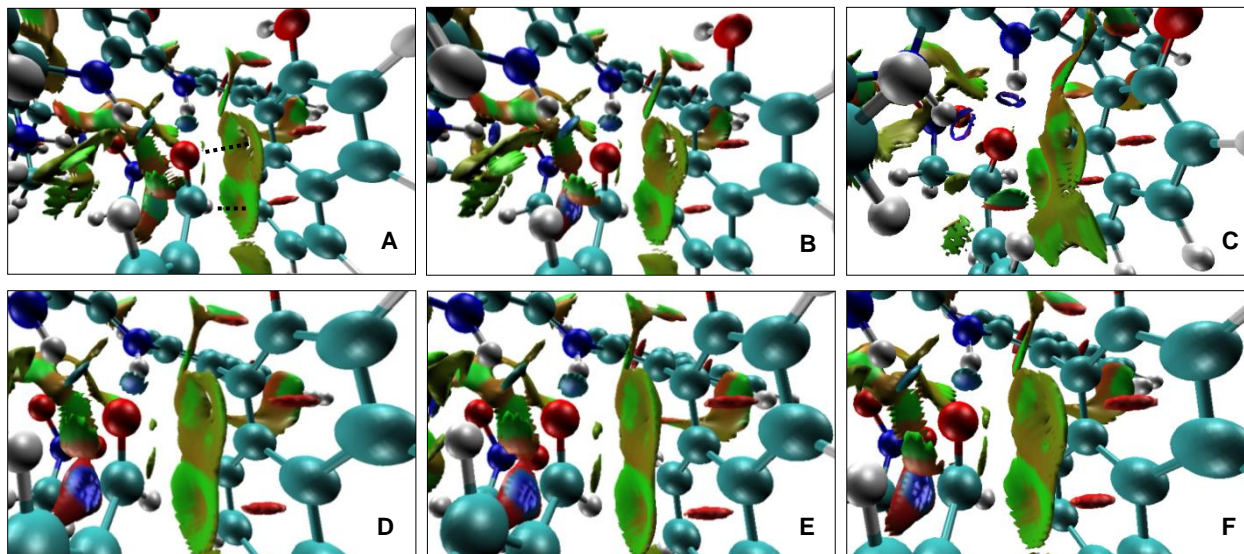
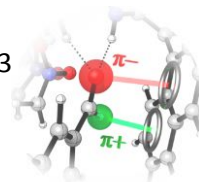


Figure 5.3. Top: Enlarged images of the regions with π -interactions created by catalyst **18** and aldehyde **14c** in **Int1**, **TS1** and **Int2** of **P1** (A, B, and C, respectively). These structures were optimized with the ω B97X-D/6-31G(d)(SMD=MeNO₂) approach. Bottom: π -interactions in **TS1** of **P1** obtained after single point energy calculations with diverse basis sets using the geometries obtained with ω B97X-D/6-31G(d)(SMD=MeNO₂). (D) ω B97X-D/6-311G(d)(SMD=MeNO₂). (E) ω B97X-D/6-311G++(d,p)(Ultrafine grid)(SMD=MeNO₂). (F) ω B97X-D/Def2QZVPP(SMD=MeNO₂).^[84] For reference, the π -oxygen and π -hydrogen interactions are represented with black dotted lines in image A.

In **Int1** of **P1**, the catalytic system contains one π -H (π --H-C=O) and one π -O lone pair (π -O=C-H) interaction. In **TS1**, the π -interactions created have properties similar to those observed in the interactions present in **Int1**. Finally, in **Int2**, the same interactions are observed but their properties are different than in the previous reaction steps. This is caused by the nitronate attack on the aldehyde, which triggers changes in the properties of the hydrogen and oxygen atoms involved in the π -interactions. These changes mainly occur because the sp^2 C atom of the aldehyde changes into a sp^3 C atom after the nitronate attack and the O atom becomes an anion. Therefore, the interactions observed in **Int2** are one π -H (π --H-C-O⁻) and one π -O anion (π --O-C-H) interaction. The creation of a π -anion in this system attracts special attention since this kind of interaction is quite rare in catalysis.^[85]

In order to verify that the π -H and π -O interactions are present in **P1**, we performed additional calculations with larger basis sets (Figure 5.3, D, E and F). In all the calculations, the results obtained were similar and suggested that these two interactions are generated between the second naphthyl group of catalyst **18** and aldehyde **14c**.

As stated above, PP π π systems include two π -interactions that show different polarities: one of the interactions involves a cation or a δ^+ atom while the other includes an anion or a δ^- atom. Using electrostatic potential (ESP) maps, we studied whether the H atom and O atom that form the π -interactions are δ^+ or δ^- with respect to the polarity of the aromatic rings (Figure 5.4, A and B). These maps were created using the ω B97X-D/6-311G++(d,p)(Ultrafine grid)(SMD=MeNO₂)/ ω B97X-D/6-31G(d)(SMD=MeNO₂) approach and the results are in line with



the definition of PP $\pi\pi$ systems, indicating that (1) the hydrogen atom has a higher ESP value (δ^+) than the components of the aromatic ring and (2) the oxygen atom displays a lower ESP value (δ^-). Also, an additional ESP map was generated using a different level of theory (ω B97X-D/6-31G(d)(SMD=MeNO₂)) and isodensity value and the conclusion obtained was the same as that found with the initial ESP map (Figure 5.4, C and D).

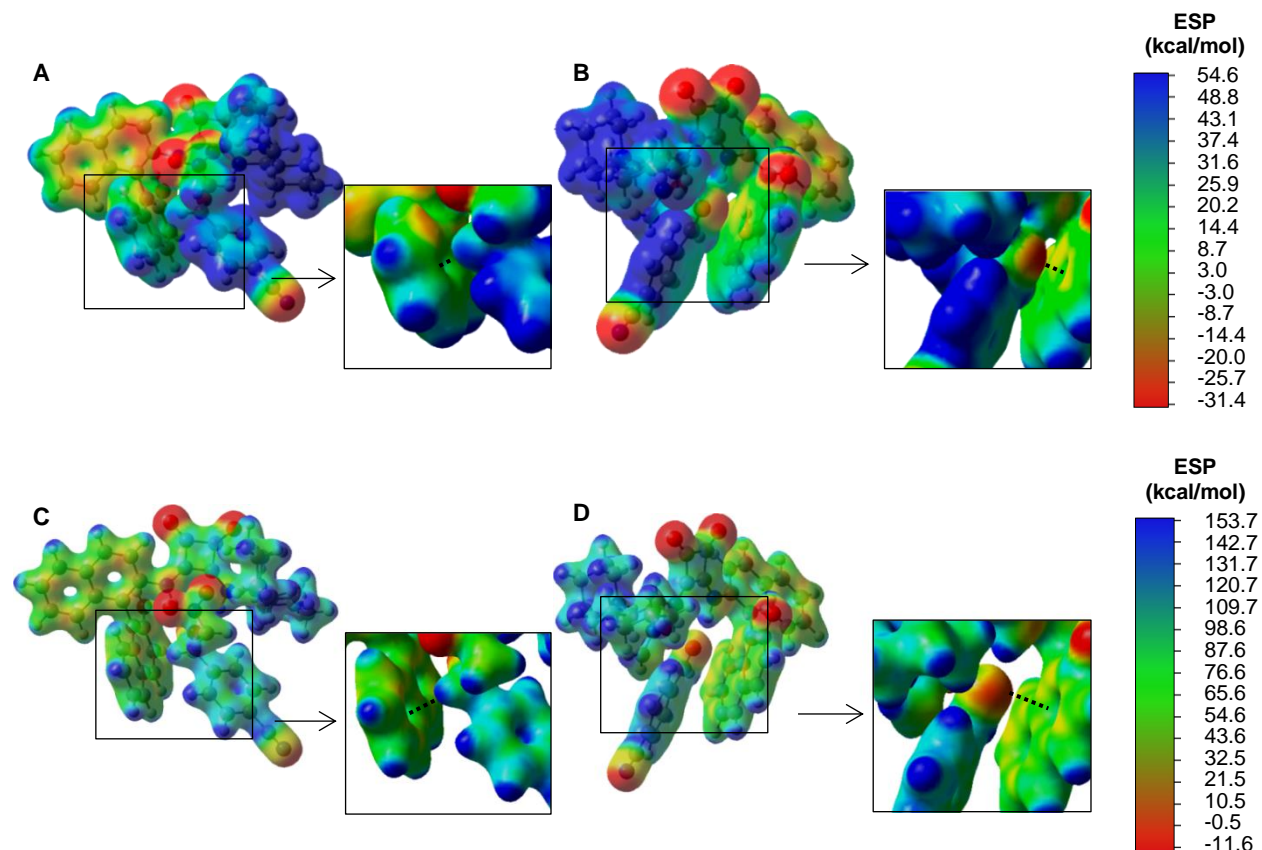


Figure 5.4. Electrostatic potential (ESP) surfaces of the **TS1** step of **P1** in the Henry reaction with aldehyde **14c** and catalyst **18** with enlarged images of the regions of the π -H interaction (A and C) and the π -O interaction (B and D). The ESP surfaces were generated with the ω B97X-D/6-311G++(d,p)(Ultrafine grid)(SMD=MeNO₂)// ω B97X-D/6-31G(d)(SMD=MeNO₂) (A-B) and the ω B97X-D/6-31G(d)(SMD=MeNO₂) (C-D) approaches. π -interactions are represented as black dotted lines. The isodensity values were 0.01 e/Bohr³ for A and B and 0.04 e/Bohr³ for C and D.

Interestingly, the naphthyl group that creates the π -interactions shows an ESP distribution that differs greatly from those previously observed in other PP $\pi\pi$ systems.^[80] In fact, each of these systems contains an aromatic surface with two regions that have significantly different ESP distributions. On the contrary, in the Henry reaction catalyzed by **18**, the ESP observed in the two rings of the naphthyl group included in the PP $\pi\pi$ system is quite similar (Figure 5.4). Another outstanding feature that makes this PP $\pi\pi$ system unique is that the H atom and the O atom involved in the π -interactions are not covalently linked to the aromatic surface. This might be useful to generate new systems with π surfaces that are compatible with a high number of structural variations.

The calculation of the energy of the PP $\pi\pi$ system is quite challenging, since the catalytic system contains a great number of non-covalent interactions. Previously, some authors have determined the energy of π -H interactions using the potential energy density at critical points of hydrogen bonds [$V(r_{CP})$]. This strategy was first proposed by Espinosa and col.,^[86] but it was designed to measure the strength of X-H...O (X = C, N, O) bonds and it has never been compared to experimental results for other interactions, such as π -hydrogen interactions. This casts doubt on whether or not this is a valid approach for calculating the strength of π -interactions. Moreover, other authors have determined the energy of π -H and π -cation/anion interactions using the electron densities in cage critical points (CCPs).^[87] However, as observed previously in some aromatic compounds,^[87a] the π -H and the π -O interactions created in **P1** did not generate any CCPs.^[88] Therefore, the energy of the PP $\pi\pi$ system could not be determined using any of the methods detailed above.

Inspired by a method created by Gadre and col.,^[89] we designed a simple strategy to calculate the energy of the PP $\pi\pi$ system during the reaction: the naphthyl group included in the PP $\pi\pi$ system was replaced with a H atom conserving the same geometry of **18** (complexes **P1-H**, Table 5.1). Maintaining the same geometry of **18** in **P1-H** is important for determining the energy of the PP $\pi\pi$ system since, if a geometry optimization process was carried out in **P1-H**, the structural reorganization of the catalyst-substrate complexes would cause that the energies of the non-covalent interactions become different than those observed in **P1**.

With this structural modification, the non-covalent interactions created in **P1-H** would be the same as those generated in **P1** except for the two π -interactions of the PP $\pi\pi$ system (Table 5.1, A and B). Consequently, the interaction energy generated by the two π -interactions of the PP $\pi\pi$ system results from the difference in the total interaction energies that the catalyst creates with the two reagents in **P1** and **P1-H**: $E(\text{PP}\pi\pi \text{ system}) = E_{\text{int}}(\mathbf{P1}) - E_{\text{int}}(\mathbf{P1-H})$.

In this strategy, we first examined whether or not the substitution of the lower naphthyl group for a H atom led to changes in the strength of different non-covalent interactions that exist in both **P1** and **P1-H**. This is very important because, if the energy of these non-covalent interactions changed, the energy created by the PP $\pi\pi$ system would not be the difference in the total interaction energies of **P1** and **P1-H**. In order to confirm that the energy of non-covalent interactions did not vary from **P1** to **P1-H**, the strength of the most important hydrogen bonds (interactions "a" to "d") was calculated in both systems in solution (Table 5.1). The results determined that the energies of these non-covalent interactions do not vary more than 0.04 kcal/mol from **P1** to **P1-H** even in interaction "a", which is created with a H atom from the aromatic ring that is modified.

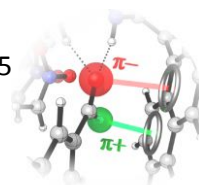
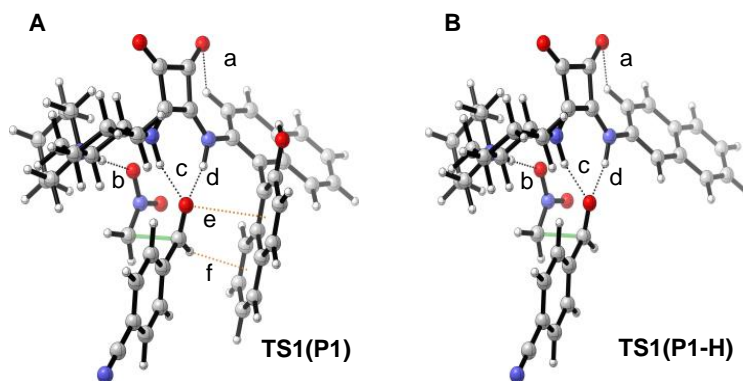


Table 5.1. Energies of the most relevant hydrogen bonds created in **P1** and **P1-H**.



H bond	Type	Step	Energy in P1 (kcal/mol) ^[a]	Energy in P1-H (kcal/mol) ^[a]
a	C-H--O	Int1	-2.40	-2.40
		TS1	-2.54	-2.55
		Int2	-2.67	-2.67
b	*N-H--O	Int1	-14.55	-14.55
		TS1	-12.16	-12.16
		Int2	-4.95	-4.95
c	N-H--O	Int1	-7.25	-7.24
		TS1	-8.40	-8.39
		Int2	-19.52	-19.50
d	N-H--O	Int1	-7.29	-7.30
		TS1	-8.11	-8.12
		Int2	-18.29	-18.33

[a] Energies calculated using the Espinosa's formula $E_{HB} = \frac{1}{2} V(r_{cp})$ and employing Multiwfn to calculate $V(r_{cp})$ from calculations performed at the ω B97X-D/Def2TZVPP(SMD=MeNO₂)/ ω B97X-D/6-31G(d)(SMD=MeNO₂) level. Negative values represent stabilizing interactions.

Additionally, we generated representations of the non-covalent interactions that exist in **P1-H** in order to verify that the H atom introduced was not creating any new interactions between catalyst and substrates. This is very important because, if new interactions were introduced, these would add energy to the total interaction energy of **P1-H** and would lead to erroneous energy values. As seen in Figure 5.5, no significant interactions were created in the region of the PP $\pi\pi$ system when the H atom replaces the naphthyl group of catalyst **18**.

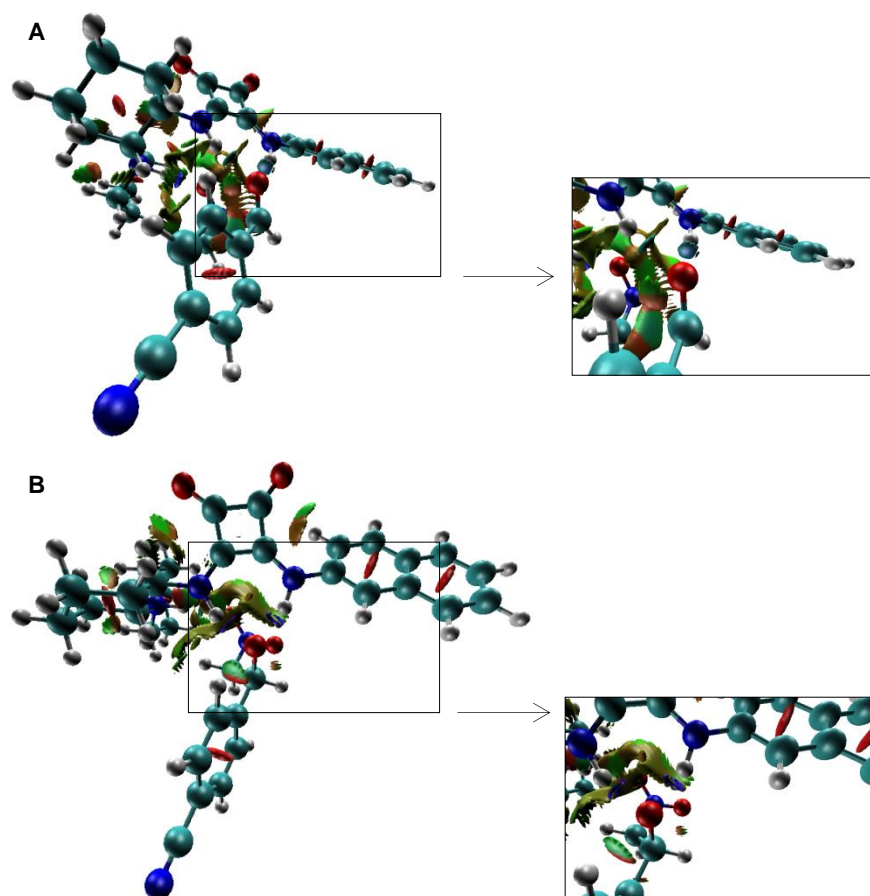


Figure 5.5. Non-covalent interactions created in **Int1** (A) and **Int2** (B) of **P1-H** with enlarged representations of the regions where aldehyde **14c** and catalyst **18** formed the PP $\pi\pi$ system in **P1**.

Furthermore, in order to study how solvent effects influence the energy of non-covalent interactions in the strategy employed, the energies of hydrogen bonds “a”, “b”, “c” and “d” were calculated in gas phase and in solution. The results did not differ more than 0.07 kcal/mol from gas phase to solution (Table 5.2), which indicates that the interaction energy of the PP $\pi\pi$ system calculated in gas phase would be very similar to that obtained in solution.

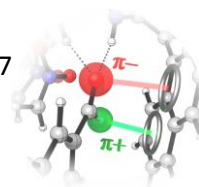
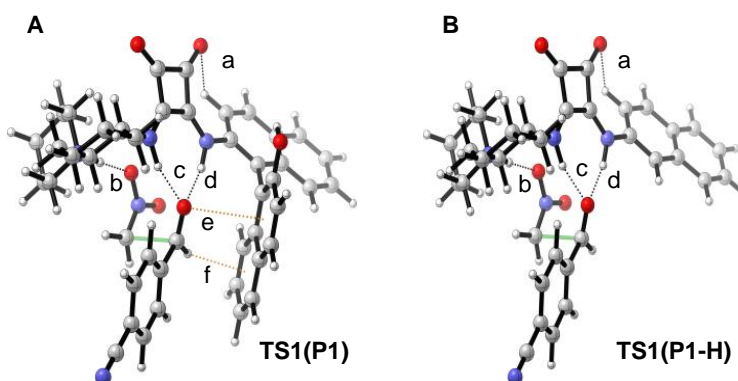


Table 5.2. Energies of the strongest hydrogen bonds of **Int1**, **TS1** and **Int2** of **P1** and **P1-H** obtained in gas phase and in solution.

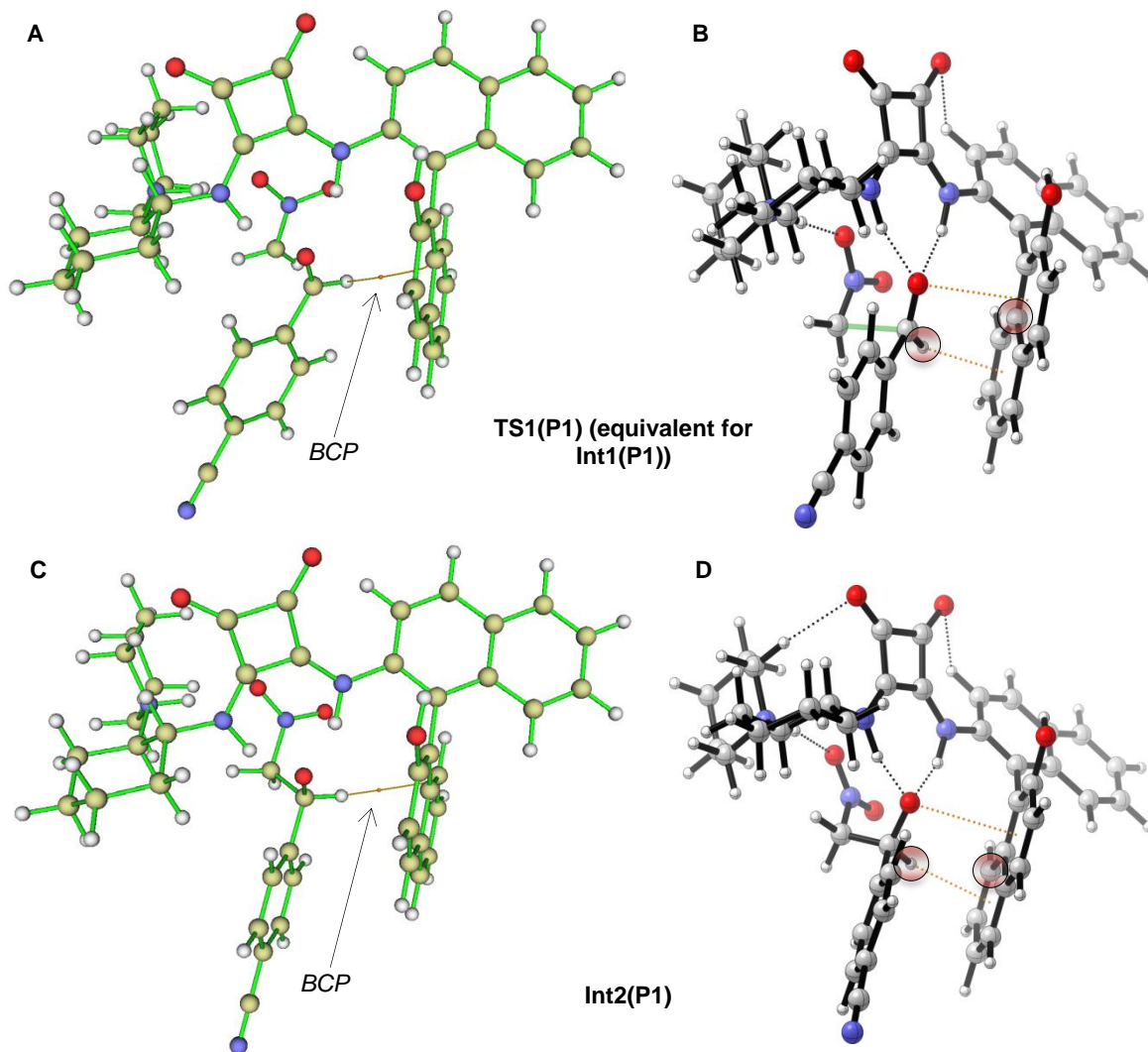


Step	System	H bond	Energy in gas-phase (kcal/mol) ^[a]	Energy in solution (kcal/mol) ^[a]
Int1	P1	a	-2.39	-2.40
		b	-14.57	-14.55
		c	-7.28	-7.25
		d	-7.28	-7.29
TS1	P1-H	a	-2.54	-2.55
		b	-12.17	-12.16
		c	-8.42	-8.39
		d	-8.14	-8.12
Int2	P1-H	a	-2.66	-2.67
		b	-4.96	-4.95
		c	-19.49	-19.50
		d	-18.26	-18.33

[a] Energies calculated using Espinosa's formula $E_{HB} = \frac{1}{2} V(r_{cp})$ and employing Multiwfn to calculate $V(r_{cp})$ from structures at the ω B97X-D/Def2QZVPP// ω B97X-D/6-31G(d)(SMD=MeNO₂) or the ω B97X-D/Def2QZVPP(SMD=MeNO₂)// ω B97X-D/6-31G(d)(SMD=MeNO₂) level.

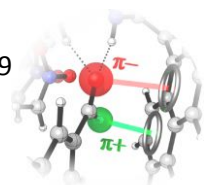
An additional test was performed in order to determine whether or not the energies of the π -interactions obtained in gas phase significantly differ from the values obtained in solution. In this test, the electron density (ρ) and its Laplacian ($\nabla^2\rho$) were calculated in bond critical points (BCPs) created by the hydrogen atom and one aromatic carbon atom that form the π -H interaction (Table 5.3). In BCPs generated by a H atom or a cation and one aromatic carbon of a π -interaction, the ρ and $\nabla^2\rho$ calculated have previously been related to the energy of diverse π -interactions.^[87a] Therefore, the ρ and $\nabla^2\rho$ were measured in the BCPs created in the π -H interaction in gas phase and in solution in order to verify that the energy of this interaction in gas phase does not varies considerably when the solvent is included in the calculations.

Table 5.3. Electron density (ρ) and its Laplacian ($\nabla^2\rho$) in atomic units at the bond critical point (BCP) connecting the hydrogen atom of the aldehyde and one aromatic carbon atom of the second naphthyl group of the catalyst. The BCPs are represented using Multiwfn in pictures A (for **Int1** and **TS1** of **P1**) and C (for **Int2** of **P1**) and the two carbon atoms connected through these BCPs are marked in pictures B (for **Int1** and **TS1** of **P1**) and D (for **Int2** of **P1**).



Step	Gas phase ^[a]		Solution ^[a]		Relative variation between gas phase and solution (%) ^[b]	
	ρ	$\nabla^2\rho$	ρ	$\nabla^2\rho$	ρ	$\nabla^2\rho$
Int1	0.008009	0.02831	0.007959	0.02843	0.6	-0.4
TS1	0.007994	0.02857	0.007987	0.02861	0.1	-0.2
Int2	0.008523	0.02755	0.008634	0.02777	-1.3	-0.8

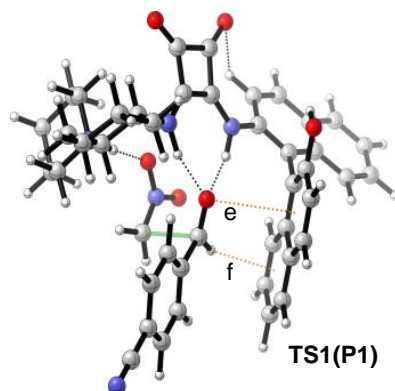
[a] Electron density (ρ) and its Laplacian ($\nabla^2\rho$) were calculated using Multiwfn from structures at the ω B97X-D/Def2QZVPP// ω B97X-D/6-31G(d)(SMD=MeNO₂) or the ω B97X-D/Def2QZVPP(SMD=MeNO₂)// ω B97X-D/6-31G(d)(SMD=MeNO₂) level. [b] Calculated with the formulas: $[\rho(\text{gas phase}) - \rho(\text{solution})] \times 100 / \rho(\text{gas phase})$ and $[\nabla^2\rho(\text{gas phase}) - \nabla^2\rho(\text{solution})] \times 100 / \nabla^2\rho(\text{gas phase})$.



The results calculated in gas phase did not vary more than 1.3% when the solvent was added in any reaction step (Table 5.3). This suggests that, in the approach using **P1** and **P1-H**, the energies of the π -interactions observed in gas phase are nearly identical to those obtained in solution, as it was determined in the previous study depicted in Table 5.2.

Then, we used the aforementioned approach to calculate the interaction energies of the PP $\pi\pi$ system ("e" and "f") using the total interaction energies of **P1** and **P1-H** in gas phase (Table 5.4). As explained above, the energies calculated in gas phase should be practically identical to those observed in solution. The total interaction energies were measured as the difference between the energy of the catalyst-substrate complexes (**14c** + **17a** + **18**) and the sum of the energies of their substrates (**14c** + **17a**) and catalyst (**18**) calculated individually: $E_{\text{int}} = (\mathbf{14c} + \mathbf{17a} + \mathbf{18}) - (\mathbf{14c} + \mathbf{17a}) - (\mathbf{18})$.

Table 5.4. Strength of the PP $\pi\pi$ system in **Int1**, **TS1** and **Int2** of **P1**.



π -interaction	Step	Energy $E_{\text{int}}(\mathbf{P1}) - E_{\text{int}}(\mathbf{P1-H})$ (kcal/mol) ^[a,b]
	Int1	-4.70
e + f	TS1	-4.13
	Int2	-2.67

[a] All the calculations were performed at the ω B97X-D/Def2QZVPP// ω B97X-D/6-31G(d)(SMD=MeNO₂) level. [b] Energy obtained from the difference in the total interaction energies of catalyst **18** and the substrates in **P1** and **P1-H**. Negative values represent stabilizing interactions.

The results indicate that the PP $\pi\pi$ system contributes importantly to lower the energy of **P1** with approximately 2.7-4.7 kcal/mol. Therefore, compared to the strength of the most important hydrogen bonds created in the catalyst-substrate complex, the energy of this system is higher than the strongest C-H--O bond (Table 5.1, interaction "a") and is only surpassed in energy by the N-H--O hydrogen bonds. The strength of the PP $\pi\pi$ system decreases progressively as the reaction goes from **Int1** to **TS1** and **Int2** (Table 5.4).

Moreover, the different reaction pathways were calculated using squaramide **35** in order to confirm that PP $\pi\pi$ system is a crucial factor in making **P1** the most favorable pathway (Figure 5.6, B). Catalyst **35** is analogous to squaramide **18** but it does not have the naphthyl group that forms the PP $\pi\pi$ system. It is worth to mention that even though **35** and the catalyst used in **P1**-

H have the same structure, the catalyst-substrate complexes are optimized in the calculations using **35** and do not maintain the same geometries observed in **P1-H**.

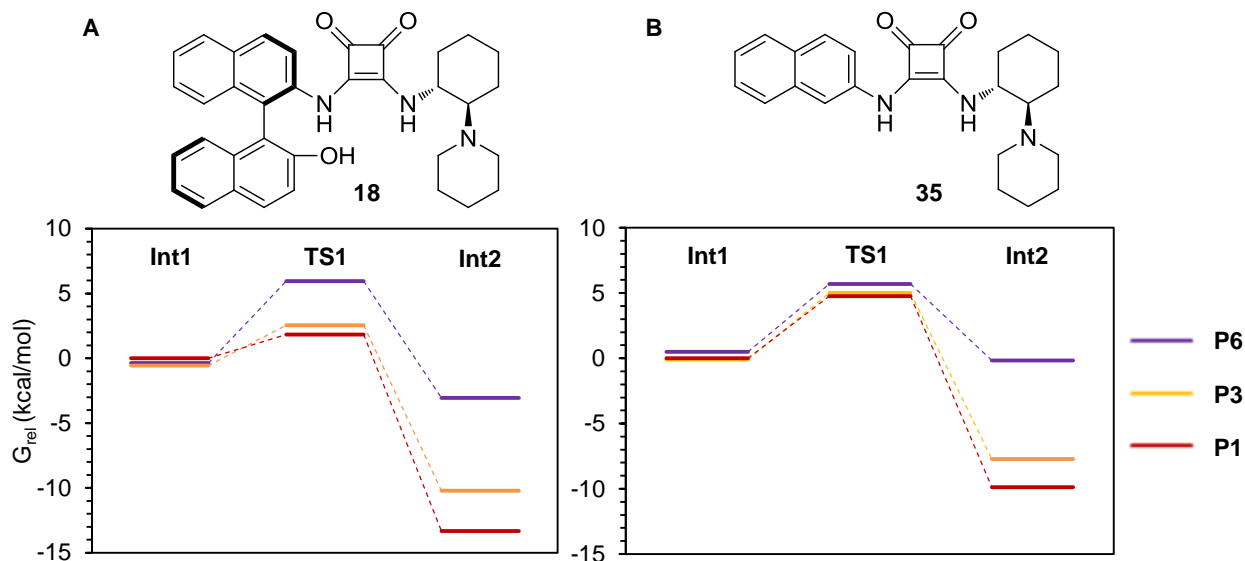
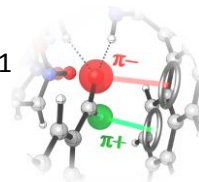


Figure 5.6. Relative G (kcal/mol) of **Int1**, **TS1** and **Int2** using different catalysts (**18** or **35**) with ω B97X-D/6-31G(d)(SMD=MeNO₂). **Int1** of **P1** was used as the reference. (A) Catalyst **18** (with the PP $\pi\pi\pi$ system in **P1**). (B) Catalyst **35** (without the PP $\pi\pi\pi$ system).

When using catalyst **35**, only pathways **P1**, **P3**, **P5** and **P6** are generated since this catalyst does not have the rotating OH group that generates pathways **P2**, **P4** and **P7**. In order to carry out reliable comparisons when measuring the energy variations caused by the PP $\pi\pi\pi$ system, the catalyst-substrate complexes must have similar geometries and spatial dispositions when using either catalyst **18** or **35**. For this reason, we discarded (1) **P5** because the structures of the complexes were different depending on the catalyst employed and (2) reaction step **Int1** because the spatial dispositions of the molecules varied significantly when changing from one catalyst to another. Therefore, we compared the G of reaction steps **TS1** and **Int2** of pathways **P1**, **P3** and **P6** because, in all these cases, the catalyst-substrate complexes showed similar structures and spatial dispositions when using either catalyst **18** or **35**.

The energy profiles of the pathways obtained with catalyst **35** showed important differences when compared to the results observed with catalyst **18**: **TS1** and **Int2** of **P1** are closer in energy to **TS1** and **Int2** of **P3** and **P6** (Figure 5.6, B). For example, the difference in the G (ΔG) of **TS1** in **P1** and **TS1** in **P6** ($G^{TS1(P6)} - G^{TS1(P1)}$) changes from 4.13 kcal/mol when using catalyst **18** to 0.93 kcal/mol when using catalyst **35**. Moreover, the ΔG between **TS1** of **P1** and **TS1** of **P3** ($G^{TS1(P3)} - G^{TS1(P1)}$), which has a great impact on the reactivity and the enantioselectivity of the reaction, changes from 0.73 to 0.24 kcal/mol when catalyst **18** is replaced with catalyst **35**.

These variations in the energy of the pathways observed when changing from catalyst **18** to **35** are mostly produced by the absence of the PP $\pi\pi\pi$ system. This determines that (1) the elimination of the PP $\pi\pi\pi$ system would lead to important changes in the outcomes of the Henry



reactions and (2) the PP $\pi\pi$ system is crucial in the energetic differentiation of **P1** over the rest of the pathways.

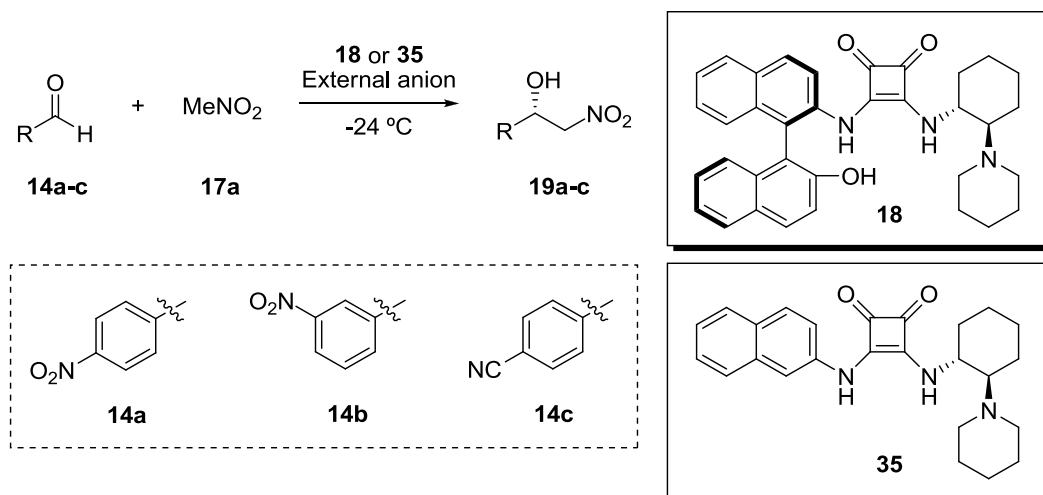
Experimental study of π -interactions.

In order to verify that the PP $\pi\pi$ system is formed during the course of the reaction, different experiments were designed using catalyst **35**. Using this catalyst, the reactivity and stereoselectivity observed in diverse Henry reactions were much lower than the corresponding values obtained when using **18** (Table 5.5, entries 1-6). This suggests that the second naphthyl group of catalyst **18** plays an important role in the mechanism and the PP $\pi\pi$ system has a significant impact on the results.

As stated above, the computational study indicated that there are $\pi-\delta^-$ atom interactions in the most favorable pathways, **P1** and **P3**, which considerably influence the outcomes of the reactions. Therefore, the addition of external anions should disrupt the formation of these interactions and cause a noticeable change in the results of the reactions.^[90] In this reaction, the external anions mainly affect the reactivity and enantioselectivity of the reaction by disrupting the $\pi-\delta^-$ atom interactions that are created in the rate-limiting step and in previous steps (**Int1** and **TS1**). The π -anion interactions formed in **Int2** are probably influenced as well, but this should not have an important effect on the outcomes of the reactions since these interactions are created after the rate-limiting step.

The choice of the external anion is a crucial factor in this study, since squaramides can form hydrogen bonds through their NH bonds with diverse anions such as halogen anions and oxoanions.^[91] In order to determine which anions could interact with the squaramide group through the NH bonds and lead to erroneous results, we used catalyst **35**, which is a modified version of catalyst **18** that can generate hydrogen bonds but cannot create any π -interactions with the substrates.

As expected, the addition of NO_3^- and Br^- anions led to significant changes in the results (Table 5.5, entries 7-8). This is probably caused by the strong coordination of these anions with the NH groups of the squaramide catalyst, which changes dramatically the reaction mechanism. However, the addition of a weakly coordinating anion, PF_6^- , and its conjugated cation, BMIM^+ , did not lead to any considerable changes in the results of the catalysis even at high concentrations. In fact, when PF_6^- and catalyst **35** were used together in the same reaction, the resulting yield corresponded to the sum of the yields of the reactions where **35** and PF_6^- were used individually (Table 5.5, entries 6 and 9-10). In addition, the enantiomeric excess observed when adding PF_6^- is only slightly lower than the analogous value obtained without PF_6^- . This slight change is produced by the reaction background promoted by PF_6^- (Table 5.5, entry 10), which indicates that the addition of PF_6^- does not noticeably alter the reaction mechanism.

Table 5.5. Results of the Henry reaction using aldehydes **14a-c**, MeNO₂ (**17a**) and catalyst **18** or **35** in the presence or absence of diverse external anions.

Entry ^[a]	Aldehyde	Squaramide	External anion ^[b]	t (h)	Yield (%)	ee (%)
1	14a	18	-	20	>95 ^[c]	82
2	14a	35	-	20	48 ^[c]	54
3	14b	18	-	19	93	94
4	14b	35	-	19	10	60
5	14c	18	-	19	56	78
6	14c	35	-	19	14	52
7	14a	35	NO ₃ ⁻	20	100 ^[c]	0
8	14a	35	Br ⁻	20	100 ^[c]	0
9	14a	35	PF ₆ ⁻	20	61 ^[c]	48
10	14a	-	PF ₆ ⁻	20	16 ^[c]	0

[a] Reaction conditions: Aldehyde **14a-c** (0.4 mmol, 0.2 M) was added to a solution of squaramide **18** (0.004 mmol, 0.002 M) or **35** (0.02 mmol, 0.01 M) and the external anion (1 mmol, 0.5 M), when used, in MeNO₂ (**17a**) (2 mL) at -24 °C. Then, after the corresponding reaction time, the products were isolated by column chromatography. [b] Salts employed: [NBu₄⁺][NO₃⁻], [NBu₄⁺][Br⁻] and [BMIM⁺][PF₆⁻] (1-butyl-3-methylimidazolium hexafluorophosphate) at a concentration of 0.5 M. [c] Yields were determined by ¹H-NMR.

After determining that PF₆⁻ is a suitable anion for the experimental study of π-δ⁻ atom interactions because this anion does not interact with the squaramides through the NH bonds, the same experiments were carried out with catalyst **18**. The results indicated that the reaction yields became lower as the amount of PF₆⁻ increased when catalyst **18** was used (Table 5.6, entries 1-4 and 5-6), which was in sharp contrast to what was observed when using squaramide **35**. This is produced by the addition of competitive anions that can form π-anion interactions with catalyst **18**, disrupting the formation of the Pπππ system between the catalyst and the aldehydes.²⁹ Therefore, these experiments suggest that there are π-δ⁻ atom interactions in **P1** and **P3**.

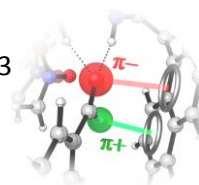
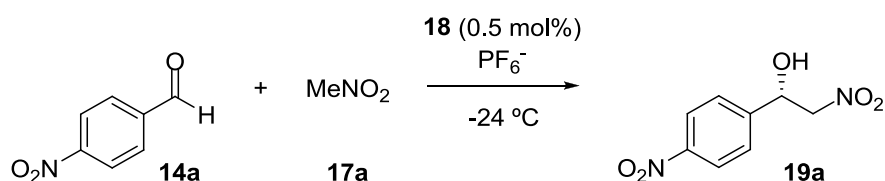


Table 5.6. Results of the Henry reaction using **14a**, MeNO₂ (**17a**) and catalyst **18** with different amounts of [BMIM⁺][PF₆⁻] as the source of external anions.

Entry ^[a]	t (h)	C of PF ₆ ⁻ (M)	Yield (%)	ee (%)
1	7	0	62	76
2	7	0.05	55	74
3	7	0.25	53	72
4	7	0.5	49	69
5	17	0	87	78
6	17	0.05	78	77
7 ^[b]	7	0.5	6	0

[a] Reaction conditions: Aldehyde **14a** (0.8 mmol, 0.2 M) was added to a solution of squaramide **18** (0.004 mmol, 0.001 M) and the external anion in MeNO₂ (**17a**) (4 mL) at -24 °C. After the reaction time showed in the table, yields were determined by ¹H-NMR and an aliquot from the reaction was used to measure the enantioselectivity after isolating the product by column chromatography. [b] Reaction performed without catalyst **18**.

5.4 Conclusions

During the study of this organocatalyzed Henry reaction, a PP $\pi\pi$ interaction system has been observed for the first time in catalysis. This system is a key factor in lowering the energy of **P1**, the most favorable pathway. The computational tests indicate that the energy of the PP $\pi\pi$ system varies from 2.7 to 4.7 kcal/mol in the reaction steps studied (**Int1**, **TS1** and **Int2**), which is crucial for the differentiation in energy of **P1** over the rest of the pathways.

The PP $\pi\pi$ system comprises two π -interactions created by a naphthyl group that interacts simultaneously with a δ^+ atom (hydrogen atom) and a δ^- atom (oxygen atom). This system shows a unique structure and mode of interaction compared to the previously discovered types of PP $\pi\pi$ systems. In fact, all the previous systems contained aromatic surfaces with two regions of different ESP values that were specifically designed to interact with cations on one part and anions on the other part. Additionally, in previous examples, the aromatic surfaces were attached covalently to at least one ion included in the PP $\pi\pi$ systems. On the contrary, in the PP $\pi\pi$ system observed in this Henry reaction, (1) the aromatic surface shows similar ESP values in all the rings and (2) the hydrogen and oxygen atoms and the aromatic surface are not part of the same molecule.

Moreover, the creation of π -interactions during the reaction was also studied experimentally. First, diverse reactions were carried out using catalyst **35**, which has the same structure of squaramide **18** except in that it does not contain the naphthyl group that produces

the P π π π system. In all the cases, the yields observed when catalyst **35** was employed were lower than the corresponding yields obtained when using catalyst **18**.

An additional test was carried out to verify that π -interactions were produced during the reaction. In this test, different amounts of an external anion were added to the reactions catalyzed by catalyst **18** in order to hinder the formation of the π - δ^- atom interactions observed in the mechanism. The results showed that the yields became progressively lower as the amount of external anion increased, which indicates that π - δ^- atom interactions are created during the course of the Henry reaction and they affect the outcomes of this reaction.

5.5 References

[76] a) Gil-Ramírez, G.; Escudero-Adán, E. C.; Benet-Buchholz, J.; Ballester, P. *Angew. Chem. Int. Ed.* **2008**, *47*, 4114; b) Schottel, B. L.; Chifotides, H. T.; Dunbar, K. R. *Chem. Soc. Rev.* **2008**, *37*, 68; c) Wang, D.-X.; Wang, M.-X. *J. Am. Chem. Soc.* **2013**, *135*, 892; d) Giese, M.; Albrecht, M.; Rissanen, K. *Chem. Rev.* **2015**, *115*, 8867; e) Biedermann, F.; Schneider, H.-J. *Chem. Rev.* **2016**, *116*, 5216.

[77] a) Robertazzi, A.; Krull, F.; Knapp, E.-W.; Gamez, P. *CrystEngComm* **2011**, *13*, 3293; b) Chifotides, H. T.; Dunbar, K. R. *Acc. Chem. Res.* **2013**, *46*, 894; c) Bishop, R. *CrystEngComm* **2015**, *17*, 7448.

[78] a) Dougherty, D. A. *Science* **1996**, *271*, 163; b) Ma, J. C.; Dougherty, D. A. *Chem. Rev.* **1997**, *97*, 1303; c) Davis, J. T. *Nat. Chem.* **2010**, *2*, 516.

[79] a) Kennedy, C. R.; Lin, S.; Jacobsen, E. N. *Angew. Chem. Int. Ed.* **2016**, *55*, 12596; b) Zhao, Y.; Cotelle, Y.; Sakai, N.; Matile, S. *J. Am. Chem. Soc.* **2016**, *138*, 4270; c) Neel, A. J.; Hilton, M. J.; Sigman, M. S.; Toste, F. D. *Nature* **2017**, *543*, 637.

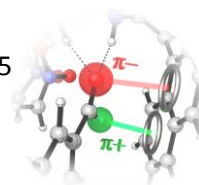
[80] a) Fujisawa, K.; Beuchat, C.; Humbert-Droz, M.; Wilson, A.; Wesolowski, T. A.; Mareda, J.; Sakai, N.; Matile, S. *Angew. Chem. Int. Ed.* **2014**, *53*, 11266; b) Fujisawa, K.; Humbert-Droz, M.; Letrun, R.; Vauthey, E.; Wesolowski, T. A.; Sakai, N.; Matile, S. *J. Am. Chem. Soc.* **2015**, *137*, 11047.

[81] Non-covalent interactions found in **P1**, **P3** and **P6** are analogous to those observed in **P2**, **P4** and **P7**, respectively (the only change between these pathways is the position of the OH group).

[82] a) Johnson, E. R.; Keinan, S.; Mori-Sánchez, P.; Contreras-García, J.; Cohen, A. J.; Yang, W. *J. Am. Chem. Soc.* **2010**, *132*, 6498; b) Lu, T.; Chen, F. *J. Comput. Chem.* **2012**, *33*, 580.

[83] Humphrey, W.; Dalke, A.; Schulten, K. *J. Molec. Graphics* **1996**, *14*, 33.

[84] a) Weigend, F.; Ahlrichs, R. *Phys. Chem. Chem. Phys.* **2005**, *7*, 3297; b) Weigend, F. *Phys. Chem. Chem. Phys.* **2006**, *8*, 1057.



[85] a) Zhao, Y.; Domoto, Y.; Orentas, E.; Beuchat, C.; Emery, D.; Mareda, J.; Sakai, N.; Matile, S. *Angew. Chem. Int. Ed.* **2013**, *52*, 9940; b) Berkessel, A.; Das, S.; Pekel, D.; Neudörfl, J. M. *Angew. Chem. Int. Ed.* **2014**, *53*, 11660; c) Zhao, Y.; Beuchat, C.; Domoto, Y.; Gajewy, J.; Wilson, A.; Mareda, J.; Sakai, N.; Matile, S. *J. Am. Chem. Soc.* **2014**, *136*, 2101; d) Zhao, Y.; Benz, S.; Sakai, N.; Matile, S. *Chem. Sci.* **2015**, *6*, 6219; e) Zhao, Y.; Cotelle, Y.; Avestro, A. J.; Sakai, N.; Matile, S. *J. Am. Chem. Soc.* **2015**, *137*, 11582; f) Cotelle, Y.; Benz, S.; Avestro, A. J.; Ward, T. R.; Sakai, N.; Matile, S. *Angew. Chem. Int. Ed.* **2016**, *55*, 4275; g) Wang, C.; Miros, F. N.; Mareda, J.; Sakai, N.; Matile, S. *Angew. Chem. Int. Ed.* **2016**, *55*, 14422; h) Miros, F. N.; Zhao, Y.; Sargsyan, G.; Pupier, M.; Besnard, C.; Beuchat, C.; Mareda, J.; Sakai, N.; Matile, S. *Chem. Eur. J.* **2016**, *22*, 2648; i) Cotelle, Y.; Lebrun, V.; Sakai, N.; Ward, T. R.; Matile, S. *ACS Cent. Sci.* **2016**, *2*, 388; j) Liu, L.; Cotelle, Y.; Klehr, J.; Sakai, N.; Ward, T. R.; Matile, S. *Chem. Sci.* **2017**, *8*, 3770; k) Akamatsu, M.; Matile, S. *Synlett* **2016**, *27*, 1041; l) Akamatsu, M.; Sakai, N.; Matile, S. *J. Am. Chem. Soc.* **2017**, *139*, 6558.

[86] Espinosa, E.; Molins, E.; Lecomte, C. *Chem. Phys. Lett.* **1998**, *285*, 170.

[87] For π -H and π -cation interactions, see: a) Cubero, E.; Orozco, M.; Luque, F. J. *J. Phys. Chem. A* **1999**, *103*, 315. For π -anion interactions, see: b) Garau, C.; Frontera, A.; Quiñonero, D.; Ballester, P.; Costa, A.; Deyà, P. M. *ChemPhysChem* **2003**, *4*, 1344. For π -cation and π -anion interactions, see: c) Lucas, X.; Quiñonero, D.; Frontera, A.; Deyà, P. M. *J. Phys. Chem. A* **2009**, *113*, 10367.

[88] We did not observe any CCPs after the study of the PP $\pi\pi$ system using diverse programs, such as Multiwfn, AIMAll and AIM-UC.

[89] Deshmukh, M. M.; Gadre, S. R.; Bartolotti, L. J. *J. Phys. Chem. A* **2006**, *110*, 12519.

[90] Liu, L.; Cotelle, Y.; Avestro, A. J.; Sakai, N.; Matile, S. *J. Am. Chem. Soc.* **2016**, *138*, 7876.

[91] a) Quiñonero, D.; Prohens, R.; Garau, C.; Frontera, A.; Ballester, P.; Costa, A.; Deyà, P. M. *Chem. Phys. Lett.* **2002**, *351*, 115; b) Amendola, V.; Bergamaschi, G.; Boiocchi, M.; Fabbrizzi, L.; Milani, M. *Chem. Eur. J.* **2010**, *16*, 4368.

5.7 Supporting Information

Computational Methods

Density functional theory (DFT) with the ω B97X-D functional and the 6-31G(d) basis set was employed to optimize the geometries of the stationary points. Vibrational frequency calculations were performed in order to (1) verify that the stationary points were either energy minima or transition states and (2) obtain the thermal corrections to Gibbs free energies at 304.05 K (30.9 °C). Additionally, intrinsic reaction coordinate (IRC) calculations were carried out to confirm that **Int1** and **Int2** of the different pathways connected to their corresponding transition states. Solvent effects (solvent=nitromethane) were also taken into account using the integral equation formalism variant of the polarizable continuum model (IEF-PCM) using the SMD solvation model. All the calculations were carried out using Gaussian 09. Quasi-harmonic entropic corrections were calculated from Gaussian frequency calculations using the script created by Dr. Robert Paton and Ignacio Funes-Ardoiz.

Graphical representations of the geometries were generated using CYLView and POV-Ray. For all the tridimensional representations of non-covalent interactions, grid data for $\text{sign}(\lambda_2)\rho$ and reduced density gradient (RDG) was generated using Multiwfn^[S21] (see the Multiwfn manual for more information) and images were created using VMD.^[S22]

The electrostatic potentials (ESP) mapped on the electronic density surfaces were represented using GaussView.^[S23] For these surfaces, isodensity values of 0.01 or 0.04 e/Bohr³ (especificed in Figure 5) were employed since similar isodensity values were shown to be suitable for this type of study.^[S24] The ESP range was adjusted to make the ESP values of the hydrogen and oxygen involved in the π interactions the maximum and minimum values, respectively, in order to be able to see the changes in polarities of the two interactions.

The bond critical points (BCPs) of all the non-covalent interactions were calculated using Multiwfn. Also, the potential energy density values at critical points of hydrogen bonds [$V(r_{\text{CP}})$] were obtained with the same software. We did not find any cage critical points (CCPs) related to π interactions using diverse programs, such as Multiwfn, AIMAll^[S25] and AIM-UC.^[S26]

Calculation of the Total Interaction Energies in **P1** and **P1-H**

Total interaction energies were measured as the difference between the energy of the catalyst-substrate complexes (**14c** + **17a** + **18**) and the sum of the energies of their substrates (**14c** + **17a**) and catalyst (**18**) calculated individually: $E_{\text{int}} = (\mathbf{14c} + \mathbf{17a} + \mathbf{18}) - (\mathbf{14c} + \mathbf{17a}) - (\mathbf{18})$. The geometries that the molecules adopt in the complexes were conserved in the single point

[S21] *Multiwfn*, v3.3.7. Lu, T. 2016.

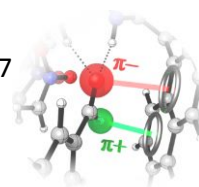
[S22] *VMD*, v1.9.2. Humphrey, W.; Dalke, A.; Schulten, K. 2012.

[S23] *GaussView*, v5.0. Dennington, R.; Keith, T.; Millam, J. Semichem Inc., Shawnee Mission KS, 2009.

[S24] Zhao, Y.; Domoto, Y.; Orentas, E.; Beuchat, C.; Emery, D.; Mareda, J.; Sakai, N.; Matile, S. *Angew. Chem. Int. Ed.* **2013**, *52*, 9940.

[S25] *AIMAll*, v17.01.25. Keith, T. A. TK Gristmill Software, Overland Park KS, 2017.

[S26] Vega, D.; Almeida, D. *J. Comp. Meth. Sci. Eng.* **2014**, *14*, 131.



energy calculations of substrates and catalyst. We employed a quadruple zeta basis set (Def2QZVPP) because it typically shows less than 2% of ΔE due to basis set superposition errors (BSSE) in combination with different DFT functionals.^[S27]

In **P1-H**, the naphthyl group involved in the PP $\pi\pi$ system observed in **P1** was replaced with a H atom conserving the same geometry of **18**. The bond length of the new C-H bond (1.0827 Å) was adjusted using the distance of the C-H bond of the same ring that is also in the *ortho* position with respect to the squaramide.

G of all the pathways with aldehyde **14c** and catalyst **35** using ω B97X-D/6-31G(d)

Table S5.1. Relative *G* at 30.9 °C of **Int1**, **TS1** and **Int2** using **35** as the catalyst with ω B97X-D/6-31G(d) (solvent = MeNO₂). **Int1** of **P1** is used as the reference.

Pathway	Reaction Step	<i>G</i> _{rel} (kcal/mol)
P1 (S)	Int1	0.00
	TS1	4.76
	Int2	-9.87
P3 (R)	Int1	-0.10
	TS1	5.00
	Int2	-7.72
P5 (R)	Int1	-8.92
	TS1	1.68
	Int2	-10.93
P7 (S)	Int1	0.50
	TS1	5.69
	Int2	-0.17

[S27] Sure, R.; Grimme, S. *J. Chem. Theory Comput.* **2015**, *11*, 3785.

6

CONCLUSIONES GENERALES

A lo largo de esta tesis doctoral, se han desarrollado varios aspectos sobre la síntesis de escuaramidas y su uso en organocatálisis. Primero, se ha diseñado una síntesis *one-pot* de escuaramidas, la cual muestra grandes ventajas respecto a las síntesis tradicionales de dos pasos usadas anteriormente. Este nuevo procedimiento sintético para producir escuaramidas se lleva a cabo de una manera más sencilla que las síntesis anteriores puesto que no requiere de la purificación de los intermedios generados en el primer paso de reacción. Además, el método *one-pot* muestra generalmente mejores rendimientos puesto que no hay pérdidas de reactivos en los procesos de purificación de los intermedios formados. Por último, también presenta algunas características que son muy atractivas tanto para sintetizar escuaramidas a nivel de laboratorio como para hacerlo a nivel industrial, como son el importante ahorro de energía, tiempo, residuos y coste que el método *one-pot* muestra en comparación con sus predecesores. Con este método se han conseguido obtener una gran cantidad de escuaramidas con sustituyentes de diferente naturaleza.

También se ha estudiado una versión de la reacción de Henry catalizada por escuaramidas. Esta reacción resultó ser muy interesante, puesto que el catalizador que se usó nunca antes se había utilizado y se consiguió bajar hasta una carga catalítica de tan sólo 0.25 mol%, superando el límite de carga catalítica que anteriormente se había establecido en organocatálisis. Con este método se sintetizaron una amplia variedad de β -nitro alcoholes con rendimientos que llegaron a ser superiores al 95% y excesos enantioméricos de hasta el 94%.

En vista de los prometedores resultados observados en la reacción anterior, se decidió llevar a cabo un estudio mecanístico acerca de la misma. Primero, se exploraron los posibles complejos catalizador-sustratos que se podían dar con las distintas formas de interaccionar entre el catalizador y los sustratos de la reacción, así como se investigó cuáles de estos complejos podían dar lugar a caminos de reacción que llevaban a la formación de los productos deseados. Después, se realizaron distintos experimentos que ayudaron a descartar algunos de los caminos que inicialmente se vieron, reduciendo drásticamente el número de posibilidades a siete caminos y facilitando el estudio mecanístico.

Una vez conocidos los caminos de reacción, se llevó a cabo su estudio computacional con distintas combinaciones de funcionales, conjuntos de bases y distintas correcciones para así encontrar una forma precisa de abordar este tipo de reacción. En el área de la catálisis con escuaramidas, nunca antes se había desarrollado un estudio similar y, por tanto, nuestro trabajo puede ser de gran ayuda como punto de partida para aquellos que busquen investigar mecanismos de reacciones catalizadas por escuaramidas. Estas catálisis son bastante complejas de analizar, puesto que normalmente incluyen una gran cantidad de átomos y una

compleja red de interacciones no covalentes. La aproximación ω B97X-D/6-311G(d) en combinación con mallas ultrafinas y aproximaciones cuasi-armónicas fue la que presentó mejores resultados, llevando a errores inferiores a 1 kcal/mol en nueve reacciones que usaban aldehídos con distintos sustituyentes.

Durante este estudio computacional, se observó que el catalizador y el aldehído formaban un sistema de interacciones bastante peculiar basado en dos interacciones π . Nuestra investigación representó el primer caso donde este sistema, llamado sistema “push-pull π +/ π -” (PP $\pi\pi$), mostró una aplicación concreta en una de las áreas de la química. Hasta entonces, sólo se habían estudiado sus propiedades y cómo variaban sus espectros de absorción en función de los componentes involucrados en las interacciones π . Los resultados obtenidos en este trabajo sugirieron que el sistema PP $\pi\pi$ contribuye a disminuir la energía de la etapa limitante de la reacción (**TS1**) del camino más favorecido (**P1**) con aproximadamente 2.7-4.7 kcal/mol, lo cual está directamente relacionado con los rendimientos y excesos enantioméricos obtenidos.

El sistema encontrado contenía dos interacciones π : una estaba formada por el átomo de oxígeno del aldehído y uno de los anillos del segundo grupo naftilo del catalizador; mientras que la otra la componían el átomo de hidrógeno del aldehído con el otro anillo del mismo grupo naftilo. Tras estudiar los mapas de potencial electrostático se determinó que este par de interacciones cumplían los requisitos para ser considerados sistemas PP $\pi\pi$, puesto que en una interacción el átomo era δ^- (O-- π) respecto al sistema aromático y en la otra era δ^+ (H-- π). Además, se realizaron diversas pruebas experimentales que también apoyaron la formación de interacciones π durante la reacción.

Annex 1

PUBLICATIONS AND CONFERENCES

A1.1 Publications That Are Related to the Content of this Thesis

The following articles and patents are related to the chapters presented in this thesis:

Articles

1. Alegre-Requena, J. V.; Marqués-López, E.; Herrera, R. P. "Push-Pull $\pi+\pi$ -" (PP $\pi\pi$) Systems in Catalysis. *ACS Catal.* **2017**, *7*, 6430-6439.
IF(2016) = 10.614. Q1 (11/145 in Chemistry, Physical).
Main cover.
Chapter 5.
2. Alegre-Requena, J. V.; Marqués-López, E.; Herrera, R. P. Optimizing Accuracy and Computational Cost in Theoretical Squaramide Catalysis: the Henry Reaction. *Chem. Eur. J.* **2017**, DOI: 10.1002/chem.201702841.
IF(2016) = 5.317. Q1 (29/166 in Chemistry, Multidisciplinary).
Frontispiece cover, hot paper.
Chapter 4.
3. Schiller, J.; Alegre-Requena, J. V.; Marqués-López, E.; Herrera, R. P.; Casanovas, J.; Alemán, C.; Díaz, D. D. Self-assembled Fibrillar Networks of a Multifaceted Chiral Squaramide: Supramolecular Multistimuli-responsive Alcohols. *Soft Matter* **2016**, *12*, 4361-4374.
IF(2016) = 3.889. Q1 (52/275 in Material Science, Multidisciplinary).
Related to **Chapter 2.**
4. Alegre-Requena, J. V.; Marqués-López, E.; Herrera, R. P. Trifunctional Squaramide Catalyst for Efficient Enantioselective Henry Reaction Activation. *Adv. Synth. Catal.* **2016**, *358*, 1801-1809.
IF(2016) = 5.646. Q1 (2/72 in Chemistry, Applied).
Highlighted in *Synfacts* **2016**, *12*, 743.
Chapter 3.

5. Quintana, M.; Alegre-Requena, J. V. (*co-first author*); Marqués-López, E.; Herrera, R. P.; Triola, G. Squaramides with Cytotoxic Activity against Human Gastric Carcinoma Cells HGC-27: Synthesis and Mechanism of Action. *MedChemComm* **2016**, *7*, 550-561.
IF(2016) = 2.608. Q2 (28/60 in Chemistry, Medicinal).
Related to **Chapter 2**.
6. Fernández-Moreira, V.; Alegre-Requena, J. V.; Herrera, R. P.; Marzo, I.; Gimeno, M. C. Synthesis of Luminescent Squaramide Monoesters: Cytotoxicity and Cell Imaging Studies in HeLa Cells. *RSC Adv.* **2016**, *6*, 14171-14177.
IF(2016) = 3.108. Q2 (59/166 in Chemistry, Multidisciplinary).
Related to **Chapter 2**.
7. Alegre-Requena, J. V.; Marqués-López, E.; Herrera, R. P.; Díaz, D. D. Metal-organic Frameworks (MOFs) Bring New Life to Hydrogen-bonding Organocatalysts in Confined Spaces. *CrystEngComm* **2016**, *18*, 3985-3995.
IF(2016) = 3.474. Q2 (49/166 in Chemistry, Multidisciplinary).
Related to **Chapter 2**.
8. Alegre-Requena, J. V.; Marqués-López, E.; Herrera, R. P. One-Pot Synthesis of Unsymmetrical Squaramides. *RSC Adv.* **2015**, *5*, 33450-33462.
IF(2015) = 3.289. Q2 (49/163 in Chemistry, Multidisciplinary).
Chapter 2.
9. Alegre-Requena, J. V. Squaramides, Discovering a New Crucial Scaffold. *Synlett* **2014**, 298-299.
IF(2014) = 2.419. Q2 (21/58 in Chemistry, Organic).
Related to **Chapter 2**.
10. Alegre-Requena, J. V.; Marqués-López, E.; Miguel, P. J. S.; Herrera, R. P. Organocatalytic Enantioselective Hydrophosphonylation of Aldehydes. *Org. Biomol. Chem.* **2014**, *12*, 1258-1264.
IF(2014) = 3.562. Q1 (12/58 in Chemistry, Organic).
Related to **Chapters 2 and 3**.

Patents

1. Alegre-Requena, J. V.; Marqués-López, E.; Herrera, R. P. One-Pot Synthesis of Squaramides. WO2016005407 A1, January 14, 2016.
International (PCT) patent.

A1.2 Complete List of Publications

1. Alegre-Requena, J. V.; Marqués-López, E.; Herrera, R. P. "Push-Pull π +/ π -" (PP π π) Systems in Catalysis. *ACS Catal.* **2017**, *7*, 6430-6439.
IF(2016) = 10.614. Q1 (11/145 in Chemistry, Physical).
Main cover of the issue.
2. Alegre-Requena, J. V.; Marqués-López, E.; Herrera, R. P. Optimizing Accuracy and Computational Cost in Theoretical Squaramide Catalysis: the Henry Reaction. *Chem. Eur. J.* **2017**, DOI: 10.1002/chem.201702841.
IF(2016) = 5.317. Q1 (29/166 in Chemistry, Multidisciplinary).
Frontispiece cover of the issue, hot paper.
3. Alegre-Requena, J. V.; Häring, M.; Herrera, R. P.; Díaz, D. D. Regulatory Parameters of Self-healing Alginate Hydrogel Networks Prepared *via* Mussel-Inspired Dynamic Chemistry. *New J. Chem.* **2016**, *40*, 8493-8501.
IF(2016) = 3.269. Q2 (52/166 in Chemistry, Multidisciplinary).
4. Schiller, J.; Alegre-Requena, J. V.; Marqués-López, E.; Herrera, R. P.; Casanovas, J.; Alemán, C.; Díaz, D. D. Self-assembled Fibrillar Networks of a Multifaceted Chiral Squaramide: Supramolecular Multistimuli-responsive Alkogels. *Soft Matter* **2016**, *12*, 4361-4374.
IF(2016) = 3.889. Q1 (52/275 in Material Science, Multidisciplinary).
5. Alegre-Requena, J. V.; Marqués-López, E.; Herrera, R. P. Trifunctional Squaramide Catalyst for Efficient Enantioselective Henry Reaction Activation. *Adv. Synth. Catal.* **2016**, *358*, 1801-1809.
IF(2016) = 5.646. Q1 (2/72 in Chemistry, Applied).
Highlighted in *Synfacts* **2016**, *12*, 743.
6. Quintana, M.; Alegre-Requena, J. V. (*co-first author*); Marqués-López, E.; Herrera, R. P.; Triola, G. Squaramides with Cytotoxic Activity against Human Gastric Carcinoma Cells HGC-27: Synthesis and Mechanism of Action. *MedChemComm* **2016**, *7*, 550-561.
IF(2016) = 2.608. Q2 (28/60 in Chemistry, Medicinal).
7. Fernández-Moreira, V.; Alegre-Requena, J. V.; Herrera, R. P.; Marzo, I.; Gimeno, M. C. Synthesis of Luminescent Squaramide Monoesters: Cytotoxicity and Cell Imaging Studies in HeLa Cells. *RSC Adv.* **2016**, *6*, 14171-14177.
IF(2016) = 3.108. Q2 (59/166 in Chemistry, Multidisciplinary).

8. Alegre-Requena, J. V.; Marqués-López, E.; Herrera, R. P.; Díaz, D. D. Metal-organic Frameworks (MOFs) Bring New Life to Hydrogen-bonding Organocatalysts in Confined Spaces. *CrystEngComm* **2016**, *18*, 3985-3995.
IF(2016) = 3.474. Q2 (49/166 in Chemistry, Multidisciplinary).
9. Alegre-Requena, J. V.; Marqués-López, E.; Herrera, R. P. One-Pot Synthesis of Unsymmetrical Squaramides. *RSC Adv.* **2015**, *5*, 33450-33462.
IF(2015) = 3.289. Q2 (49/163 in Chemistry, Multidisciplinary).
10. Alegre-Requena, J. V.; Marqués-López, E.; Herrera, R. P. Introduction: Multicomponent Strategies in *Multicomponent Reactions. Concepts and Applications for Design and Synthesis*. Marqués-López, E.; Herrera, R. P. (Eds.). J. Wiley & Sons, Inc. Hoboken, NJ, **2015**, pp 1-15.
Book Chapter
11. Alegre-Requena, J. V.; Marqués-López, E.; Herrera, R. P. Guanidine Motif in Biologically Active Peptides. *Aust. J. Chem.* **2014**, *67*, 965-971.
IF(2014) = 1.558. Q2 (73/157 in Chemistry, Multidisciplinary).
12. Alegre-Requena, J. V. Squaramides, Discovering a New Crucial Scaffold. *Synlett* **2014**, 298-299.
IF(2014) = 2.419. Q2 (21/58 in Chemistry, Organic).
13. Alegre-Requena, J. V.; Marqués-López, E.; Miguel, P. J. S.; Herrera, R. P. Organocatalytic Enantioselective Hydrophosphonylation of Aldehydes. *Org. Biomol. Chem.* **2014**, *12*, 1258-1264.
IF(2014) = 3.562. Q1 (12/58 in Chemistry, Organic).

A1.3 Complete List of Patents

1. Alegre-Requena, J. V.; Marqués-López, E.; Herrera, R. P. One-Pot Synthesis of Squaramides. WO2016005407 A1, January 14, 2016.
International (PCT) patent

A1.4 Complete List of Conferences

1. Alegre-Requena, J. V.; Marqués-López, E.; Herrera, R. P. Squaramides, Key Structures in Diverse Fields of Chemistry. **V G-9 Doctoral Conference**. Palma de Mallorca, Spain, February 2017.
Oral presentation.
2. Alegre-Requena, J. V.; Marqués-López, E.; Herrera, R. P. Studying Computationally Anion- π Interactions for the First Time in Asymmetric Catalysis: Squaramide-Catalyzed Henry Reactions. **8th European Symposium on Computing π -Conjugated Compounds**. Malaga, Spain, January 2017.
Oral presentation.
3. Alegre-Requena, J. V.; Marqués-López, E.; Herrera, R. P. Expanding the Boundaries of Asymmetric Squaramide Organocatalysis: Henry Reactions Driven by Anion- π Interactions. **VII Conference of Young Aragonese Researchers**. Zaragoza, Spain, November 2016.
Poster presentation.
4. Alegre-Requena, J. V.; Marqués-López, E.; Herrera, R. P. Expanding the Boundaries of Asymmetric Squaramide Organocatalysis: Henry Reactions Driven by Anion- π Interactions. **XIII Young Researchers Symposium of the Spanish Royal Society of Chemistry-Sigma Aldrich**. Logroño, Spain, November 2016.
Oral presentation.
5. Schiller, J.; Herrera, R. P.; Alegre-Requena, J. V.; Marqués-López, E.; Casanovas, J.; Alemán, C.; Díaz, D. D. Squaramide-Based Supramolecular Multi-stimuli-Responsive Alcolgels. **6th EuCheMS Chemistry Congress**. Seville, Spain, September 2016.
6. Alegre-Requena, J. V.; Marqués-López, E.; Herrera, R. P. One-pot Synthesis of Unsymmetrical Squaramides and their Application in Organocatalytic Henry Reactions. **XII Young Researchers Symposium of the Spanish Royal Society of Chemistry-Sigma Aldrich**. Barcelona, Spain, November 2015.
Oral presentation.
7. Alegre-Requena, J. V.; Izaga, A.; Marqués-López, E.; Gimeno, M. C.; Herrera, R. P. New Trends in Hydrogen Bond Based Catalysts. **XXXV Biannual Reunion of the Spanish Royal Society of Chemistry**. A Coruña, Spain, July 2015.
8. Alegre-Requena, J. V.; Marqués-López, E.; Herrera, R. P. Efficient Organocatalytic Henry Reaction. **7th Spanish-Portuguese-Japanese Organic Chemistry Symposium**. Seville, Spain, June 2015.

9. Alegre-Requena, J. V.; Marqués-López, E.; Herrera, R. P. Hydrogen Bonds that Stand Out: Squaramides in Organocatalysis. **VI Conference of Young Aragonese Researchers**. Zaragoza, Spain, November 2014.
Oral presentation.
10. Alegre-Requena, J. V.; Marqués-López, E.; Herrera, R. P. Squaramides: a New Piece in the Puzzle of Organocatalysis. **XI Young Researchers Symposium of the Spanish Royal Society of Chemistry-Sigma Aldrich**. Bilbao, Spain, November 2014.
Oral presentation.
11. Alegre-Requena, J. V. Catalysis in Daily Life. **Researchers' Night**. Zaragoza, Spain, November 2014.
Oral presentation.
12. Alegre-Requena, J. V.; Marqués-López, E.; Herrera, R. P. Organocatalytic Hydrophosphonylation Promoted by a Hydrogen Bond Based Catalyst. **X Young Researchers Symposium of the Spanish Royal Society of Chemistry-Sigma Aldrich**. Madrid, Spain, November 2013.
13. Alegre-Requena, J. V.; Marqués-López, E.; Herrera, R. P. Organocatalytic Hydrophosphonylation Promoted by a Hydrogen Bond Based Catalyst. **5th ORCA Meeting**. Alicante, Spain, October 2013.
Poster presentation.
14. Alegre-Requena, J. V.; Marqués-López, E.; Herrera, R. P. Organocatalytic Hydrophosphonylation Promoted by a Hydrogen Bond Based Catalyst. **XXXIV Biannual Reunion of the Spanish Royal Society of Chemistry**. Santander, Spain, September 2013.
15. Alegre-Requena, J. V.; Verdú, C. R.; Vicente, N. E.; Conejero, A. C. Lithium Ion Batteries. **I Conference of Chemistry Students of the University of Alicante**. Alicante, Spain, November 2010.
Oral presentation.
16. **II Nanomediterranean Workshop**. Alicante, Spain, June 2010.